Studies on the magnetoelectric coupling in transition-metal oxides

AYATO IYAMA

MARCH 2014

Studies on the magnetoelectric coupling in transition-metal oxides

A dissertation submitted to
THE GRADUATE SCHOOL OF ENGINEERING SCIENCE
OSAKA UNIVERSITY
in partial fulfillment of the requirements for the degree of
DOCTOR OF PHILOSOPHY IN ENGINEERING

BY

AYATO IYAMA

MARCH 2014

Abstract

Coupling between electric and magnetic properties has been a major subject in solid state physics since the discovery of the linear magnetoelectric (ME) effect in which an electric polarization (magnetization) is linearly induced by an applied magnetic (electric) field. Research for decades on the linear ME effect has revealed that a number of materials show this effect because once the inversion and time-reversal symmetries are broken in a material, the linear ME effect can be observed regardless of microscopic parameters like sign of an exchange constant, which makes this effect universal. In terms of the coupling between them, ME multiferroics have recently been another hot topic where ferroelectricity and magnetism coexist in the same phase. In some ME multiferroic materials, more remarkable ME effect can be expected than the linear ME compounds, and indeed has been observed.

For the sake of deeper understanding of these two ME phenomena, it is beneficial to comprehensively discuss these phenomena in a single framework. Towards this end, it is taken into account that electric or magnetic property is not only electric polarization or magnetization but also dielectric constant or magnetic susceptibility. Based on this strategy, the linear ME effect in Cr_2O_3 and $FeSb_2O_4$ are reinvestigated in this thesis. The former material is the most famous linear ME material, and the experimental results on the latter material is the first report on the single-crystalline samples. From the experimental results and symmetry considerations, it is in fact clarified that the linear ME effect and some ME multiferroics can be comprehensively understood.

Coupling between dielectric constant and magnetism has been observed and called the magnetodielectric (MD) effect even in the absence of a macroscopic electric polarization in a material. The known MD effect originates from spin-lattice coupling, and change in the dielectric constant is proportional to the square of an applied magnetic field. However, a distinct MD effect in $SmMnO_3$ has been found by a former colleague of the author which cannot simply be understood by existing phenomenological theory. To further obtain the insights, high-magnetic-field and neutron scattering experiments are carried out. The aim is to clarify how the MD effect behaves in a high magnetic field, and to resolve what happens to the Sm and Mn magnetic moments when the MD effect is observed. It is revealed that interaction between the Sm and Mn moments is a key to understand the MD effect in this compound.

Contents

“Studies on the magnetoeletric coupling in transition-metal oxides”

Chapter 1 Introduction

Electrons play a major role in condensed matter physics, and have three degrees of freedom – charge, spin, and orbital. An electron in a matter interacts with a lot of electrons in it, which gives rise to a variety of phenomena. Of those many-body effects in solids, ferromagnetism has been one of the hot topics which is induced by spin degree of freedom. Magnetization in a ferromagnet is naturally controlled by a magnetic field. What if, however, magnetization is controlled by other parameters such as an electric field or pressure through charge or orbital degree of freedom? Such combination of some of the degrees of freedom has attracted much attention as well as ferromagnetism itself, and opened various possibilities for new functions solids would have.

The main subject of this thesis is coupling between electric and magnetic properties in insulating transition-metal oxides. Usually, coupling between them is thorough electric current known as Faraday's law and Ampere's law. However, the coupling has also been observed in insulators where no electric current flows, in which electricity and magnetism are correlated in a non-trivial way.

The first example of this coupling is the linear magnetoelectric (ME) effect in which an electric polarization (magnetization) is linearly induced by a magnetic field (electric field). This unusual coupling can be observed in a system with broken inversion and time-reversal symmetries, and was indeed observed in such a material Cr_2O_3 in 1960 for the first time. The linear ME effect is still under investigation and is an interesting topic to be examined.

The second example of this coupling is ME multiferroics where ferroelectricity and magnetism coexist in the same phase. In a multiferroic material, large ME coupling can be expected, and was indeed observed in $TbMnO_3$ in 2003. In this material, a spin spiral order breaks the inversion symmetry, and induces the ferroelectric polarization. A flop by 90° of this electric polarization by application of a magnetic field is a large ME effect, and this discovery has triggered intense research on this coupling.

The third example of this coupling is the magnetodielectric effect. It is the effect that the dielectric constant is affected by a magnetic field or a magnetic ordering. Not only the electric polarization but also the dielectric constant is one of the fundamental electric property, and it is sometimes controlled by magnetism through ME coupling. The dielectric constant is rather difficult to intuitively understand, compared with electric

polarization, however, it is significant by itself, and it is an important clue to clarify the ME properties.

In this chapter, these ME couplings are introduced in some detail. After the explanations of these couplings, the purpose of this thesis is mentioned.

1.1 The linear magnetoelectric effect

The linear magnetoelectric (ME) effect has attracted much attention over 50 years since the first discovery of the effect in 1960, in which an electric polarization P (magnetization M) is linearly induced by an applied magnetic field H (electric field E) [1,2]. The proportional constant is α which is a 3 × 3 matrix, reflecting a magnetic symmetry of a material [3]. The linear ME effect can be observed in a system where both inversion and time-reversal symmetries are broken because E is a polar vector and H is an axial one [4]. Then, soon after a prediction that Cr_2O_3 is a promising candidate for the linear ME effect to occur [5], the first discovery of the linear ME effect was made in Cr_2O_3 in 1960 [6]. In this experiment, ac E was applied to the sample, around which a detection coil was set in order to observe a change in the magnetic flux as an electric voltage. After the publication of ref. 6, the inverse effect, namely an induction of P by H, was measured in Cr_2O_3 which is consistent with the former experiment [7].

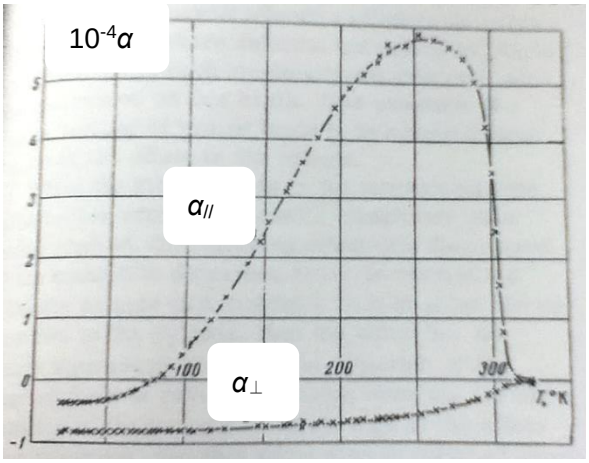

Figure 1-1: The first measurement of the linear ME effect in Cr_2O_3 [6].

In the early stage of the ME history, several theories were proposed to explain the microscopic origin of the linear ME effect [8-11], in which the inverse effect of the super-exchange interaction [9] or the inverse effect of the Dzyaloshinskii-Moriya (DM) interaction [11] is still an important concept to understand the ME coupling beyond the linear ME effect. The microscopic origin is still under debate which has been tried to figure out mainly by the first-principles calculations [12-16]. Note that the microscopic origin has to explain not only the induction of M by E but also the induction of P by H

because the linear ME effect is totally symmetric between electricity and magnetism. Besides, some important phenomenological theories have been provided on the linear ME effect about the upper bound of the ME susceptibility [17] or Lyddane-Sachs-Teller relation [18, 19]. Here, ref. 17 showed that the upper bound is $\alpha^2 < \chi_e\chi_m$ where χ_e and χ_m are electric and magnetic susceptibilities, respectively. From this relation, it seems to be expected that ferroelectric and ferromagnetic material in which large χ_e and χ_m are expected has large ME tensor. However, it is not always true because the relation determines only the upper bound [16]. The important point is to increase coupling between electricity and magnetism.

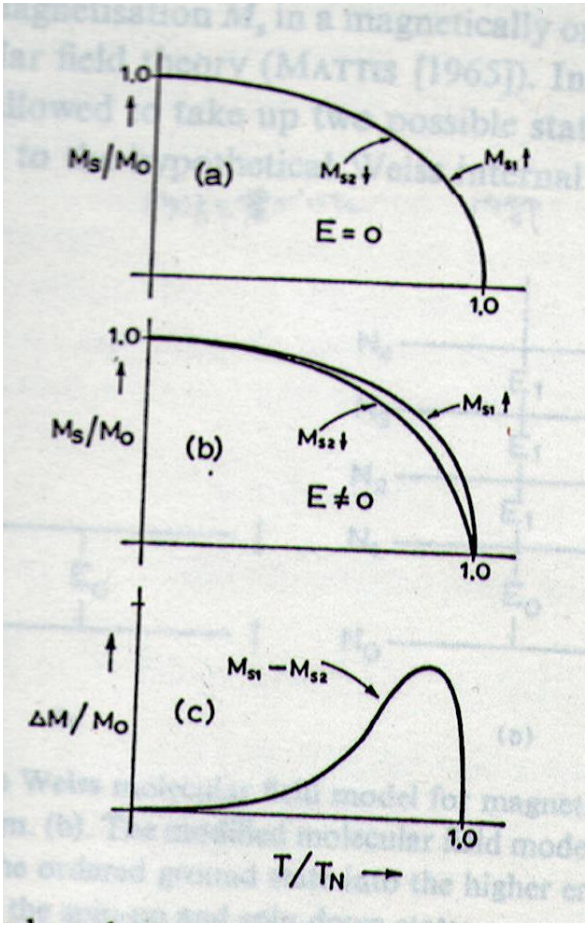

Figure 1-2: A model to explain the overall temperature dependence of the ME tensor in Cr_2O_3 [1].

It is still difficult to understand the microscopic origin of the linear ME effect. However, it is rather simple to roughly understand the overall feature of the temperature T dependence of the ME tensor $\alpha_{//}$ by considering a model as in Figure 1-2 [1]. Consider that E changes the T dependence of the sublattice magnetization oppositely. Then, the observed ME tensor is the difference between the two sublattice magnetization which is largely consistent with the experimental result on Cr_2O_3. In an atomic level, the applied E changes the energy levels of the excited states in each sublattice oppositely, which results in the change in the effective magnitude of spins in each site at $T > 0$. In this way, ref. 11 explained the overall feature of $\alpha_{//}$, and concluded that the inverse super-exchange interaction [9] seems to be the microscopic origin except at low temperature by dealing with spins in a statistical-mechanical way. The alternative view of the above scenario is that the overall T dependence is a result of combination of the magnetic susceptibility $\chi_{//}$ and the order parameter (= staggered magnetization) G_c, which is ultimately the same with the former argument because $\chi_{//}$ represents T-induced fluctuation of the sublattice magnetization [11, 13].

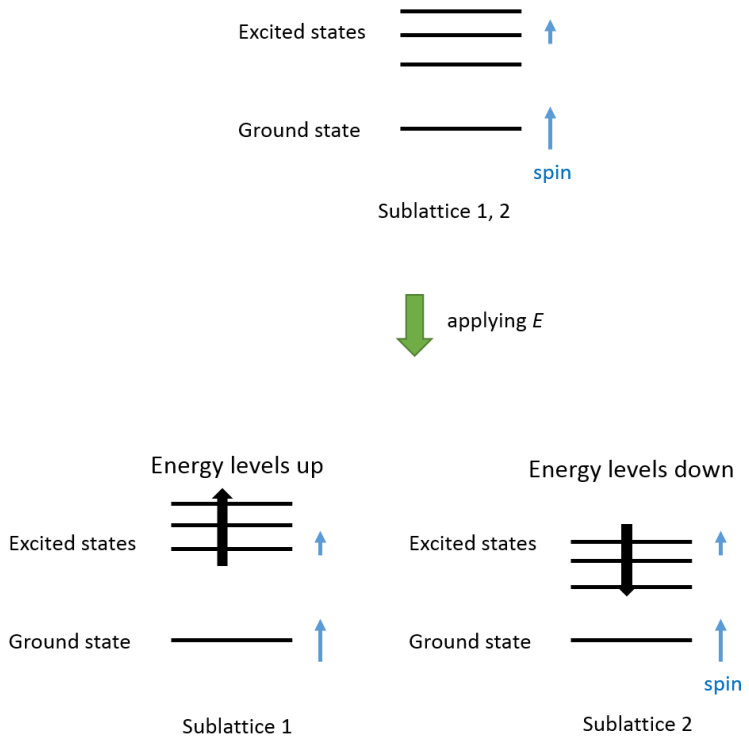

Figure 1-3: Electric field changes energy of the excited levels in each sublattice.

Several new concepts have been proposed which enrich physics on the linear ME effect. One of them is a toroidal moment which is defined as a sum of $r \times S$ where r represents position of a magnetic ion and S is its spin [20-23], which can be observed by means of the second harmonic generations [24, 25], the resonant x-ray diffraction [26-28], or the asymmetric ME tensor [29, 30]. The ferrotoroidic order is odd for both the inversion and time-reversal operations which can be thought as the fourth-ferroic order after ferroelastic, ferroelectric, and ferromagnetic. With the same symmetry condition, another concept has recently been proposed, which is a 'monopolarization' [31, 32], describing the isotropic ME effect. This 'monopole' can be observed via the resonant x-ray diffraction as well [33] in a cubic ME material [34].

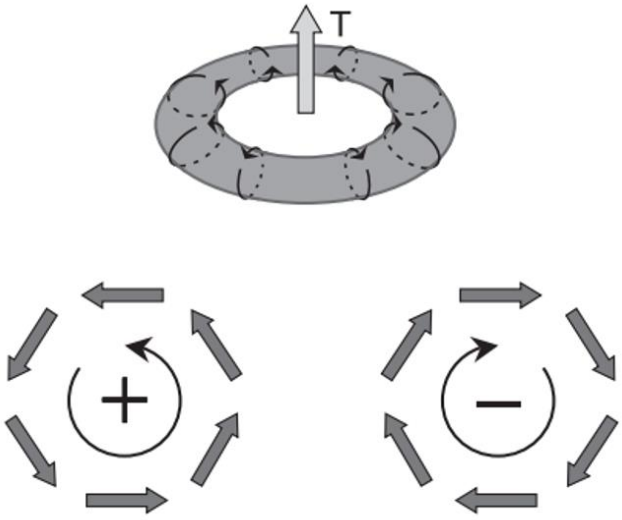

Figure 1-4: Toroidal moment [22].

The ME coupling is not only static but also dynamic, which can be observed as a result of interaction between an ME material and light. Optical ME effect [35], the non-reciprocal optical rotation [36, 37], and the second harmonic generations [38] were observed. Their optical effects can be useful to carry out the domain mapping [39, 40] or to investigate the ME dynamics [41].

The interesting aspects of the linear ME effect is an unusual coupling between electricity and magnetism. The usual way of the coupling is through electric current which is absent in the ME materials otherwise E cannot be applied or P cannot be measured. Thus, the ME coupling is unnatural to intuitively understand, which becomes clearer by considering the following situation.

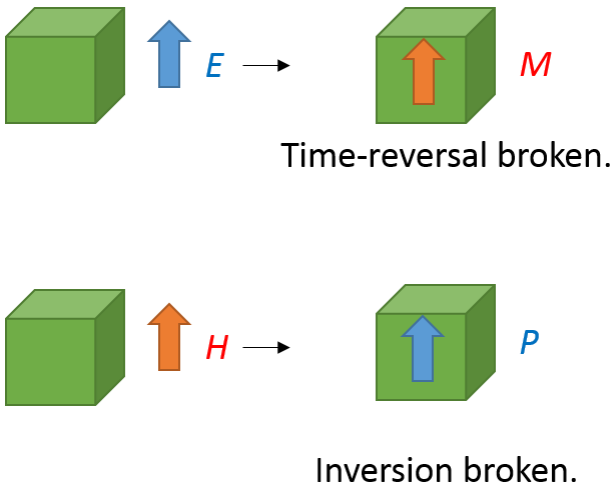

Figure 1-5: Considering a naive situation when E or H is applied to a sample.

Imagine that there is a sample, and E is applied. If the linear ME effect occurs, that is M appears in the sample, time-reversal symmetry must be broken via applying E. This is not likely, and this argument is also applied to the inverse situation. The only answer to this apparent paradox is that both the inversion and time-reversal symmetries must be broken even in the absence of the applied field. Therefore, the breaking of the two symmetries is essential for the linear ME effect. *Once the two symmetries are broken, the linear ME effect can be observed regardless of microscopic parameters such as sign of exchange interaction in a system etc., which makes the ME effect universal.*

1.2 Magnetoelectric multiferroics

In a ‘multiferroic’ material, some ferroic orders coexist in the same phase such as ferroelastic, ferroelectric, or ferromagnetic [42-51]. In this thesis, the magnetoelectric multiferroics are mentioned. There are two types in the magnetoelectric multiferroics. A so-called type 1 is a material in which ferroelectric order occurs at a temperature and magnetic order occurs at another temperature [49]. Hence, coupling between the two properties is usually small. In a type 2 material, on the other hand, these orders occur simultaneously at the same temperature. Thus, the coupling is large. Here, only the type 2 is focused on.

In the type 2 materials, a spin order induces a ferroelectric polarization. The most famous one is $TbMnO_3$, which has triggered intense research on this field [52].

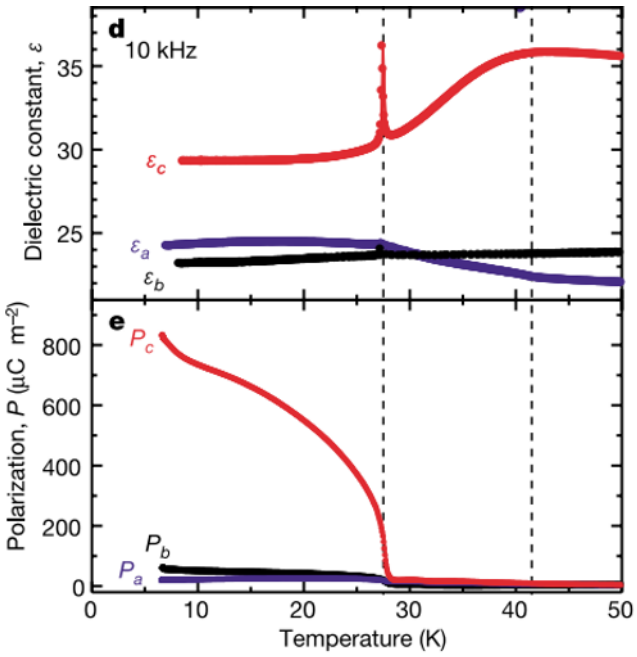

Figure 1-6: Ferroelectricity induced by the cycloidal spin ordering in $TbMnO_3$ [52].

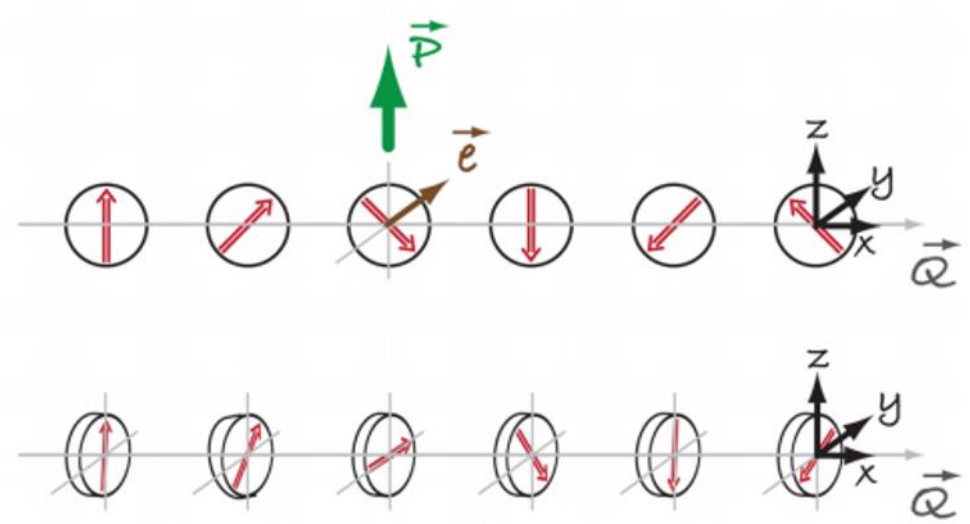

Figure 1-7: The upper panel is a cycloidal spiral order, and the lower one is a screw spiral order [49].

This compound shows a cycloidal spin order at low temperature, which breaks the inversion symmetry and induces the ferroelectric polarization [53]. A more interesting point is that an applied *H* flops the ferroelectric polarization by 90°, which is a large magnetoelectric effect [52]. The microscopic origin which induces the polarization has been explained by a 'spin-current model' or an 'inverse DM interaction mechanism' [54-65].

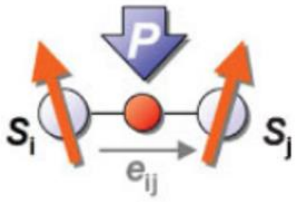

$$\mathbf{P}_{ij} = A_0 \cdot \mathbf{e}_{ij} \times (\mathbf{S}_i \times \mathbf{S}_j)$$

Figure 1-8: A cluster of an anion and two cations which have canted spins with each other. *S* is a spin and *e* is a vector connecting the two cations at site *i* and *j*. *A* is a constant including the spin-orbit interaction [50].

Consider a model as Figure 1-8. This cluster consists of an anion and two cations which have canted magnetic moments with each other. In the spin-current model, it is considered that when there is a noncollinear spin structure, in other words there is non-zero $S_i \times S_j$, spin current exists between the spins. This can be understood as follows. There is Heisenberg exchange interaction between the two spins so that the spins tend to align in a parallel or antiparallel way although the spins are canted with each other in fact. Then,

the tendency can be thought in a different way in which spin current permanently flows between the two spins and the spins are affected by the spin current via a spin-transfer torque. In this way of understanding, spin current is always flowing from the 1 to 2 site and the direction of the spin of the spin current is $S_i \times S_j$.

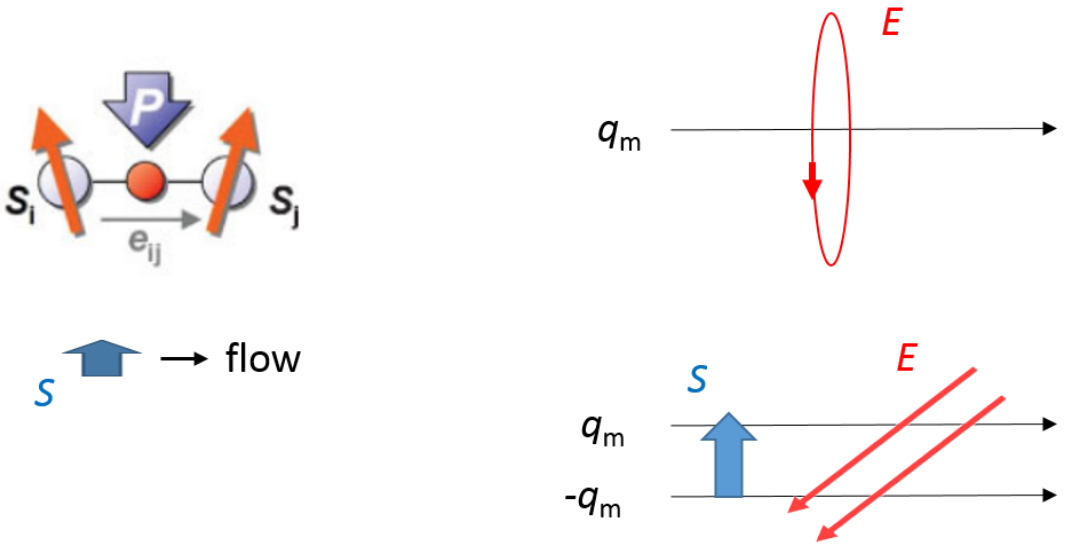

Figure 1-9: Spin current model. Flow of a magnetic charge is accompanied by a rotation of an electric field.

Here, flow of the spin current involves an electric field in the direction of perpendicular to its spin and its flow because flow of a magnetic charge generate a rotation of an electric field and a spin is combination of positive and negative magnetic charges. In this way, an electric polarization appears from purely electronic contribution between the two canted spins.

On the other hand, the inverse DM interaction is an effect of spin-lattice coupling, not an electronic contribution. The DM interaction makes two spins canting when no inversion center exists between the two spins [66, 67]. Then, the inverse DM interaction makes an anion between the two spins shift to break the inversion symmetry when the two spins are canting by an effect such as frustration. From the first-principles calculations which investigated the electric polarization in $TbMnO_3$ revealed that the dominant contribution is the inverse DM interaction and the electric polarization by the spin-current contribution is actually small and opposite in direction [64, 65].

Until now, a number of such materials have been found (e.g., RMnO$_3$ (R = Tb, Dy, etc.) [68-72], $CoCr_2O_4$ [73, 74], or CuO [75]). In RMnO$_3$, an applied H flops the macroscopic electric polarization, and in $CoCr_2O_4$, an applied H reverses the electric polarization.

These are the intriguing examples in type 2 multiferroics. These interesting magnetic-field effects are possible because spins are the primary order parameter in the ferroelectric phase, not the electric polarization itself. Note that not only the cycloidal order but also other magnetic orders can yield a ferroelectric polarization such as an E-type spin order [72, 76], or a screw spiral [59, 77-79], however, the symmetry of the crystal structure is limited in this case because as Figure 1-10 depicts, symmetry of a cycloid is *2m'm'* which is polar by itself, but, that of a screw is *22'2'* which is not polar.

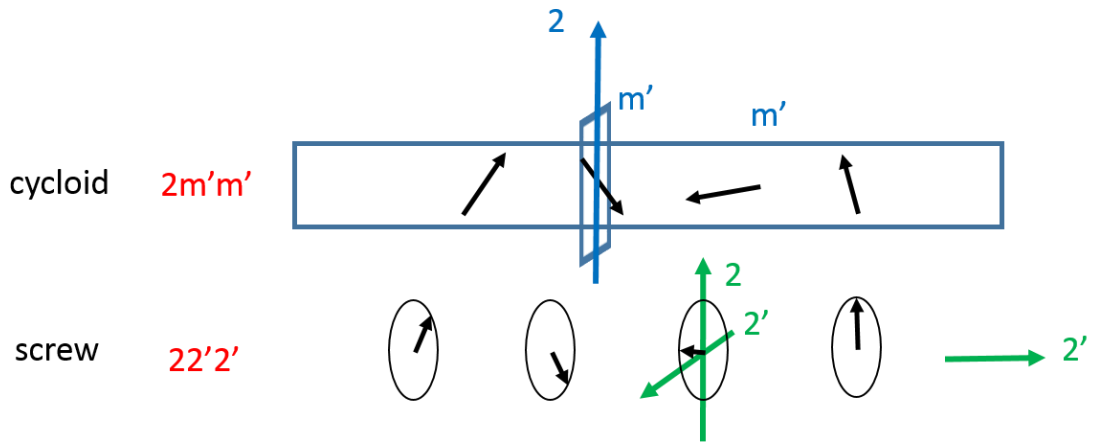

Figure 1-10: Symmetry of a cycloid and a screw spin structures. *2* is a two-fold axis, *m* is a mirror, and prime means time-reversal.

One of the outstanding achievements of the magnetoelectric multiferroics is the concept that other orders can induce ferroelectricity such as charge-, orbital-, and spin-ordering or combination of these orders. Thus, research on ferroelectricity has been spread into many systems. Ferroelectrics induced by such other orders are called 'improper' ferroelectrics [80, 81]. Recent famous example is coupling between ferroelectric displacement and oxygen octahedral (or bypyramid-) rotations [82-86]. Such coupling and combination of the coupling with spins will open new possibilities for generating and controlling ferroelectricity in various ways such as magnetic field, uniaxial pressure, and strain.

1.3 The magnetodielectric effect

Dielectric constant ε is an electric property which reflects the extent how an electric polarization is induced by an applied electric field in a material. In some magnetic materials, this electric property is affected by magnetism, and it is called the magnetodielectric effect or magnetocapacitance effect. The most typical magnetodielectric effect is that relative change in ε is proportional to square of an applied magnetic field H^2 because the smallest order term of the magnetoelectric coupling in free energy is $\gamma P^2 M^2$ by symmetry where γ is a constant, concerning the magnetodielectric effect [87]. (Note, however, that $\gamma P^2 M$ is also allowed in a system with broken time-reversal symmetry.) This coupling term originates from spin-lattice coupling, namely coupling of spins with optical phonons, and expressed as

$$\omega = \omega_{\mathrm{PM}} + \lambda \langle \mathbf{S}_i \cdot \mathbf{S}_j \rangle$$

where ω is frequency of an optical phonon, ω_{PM} is the freqnency in paramagnetic state, and λ is a constant, depending on the sign of exchange interaction [88]. To apply H modulates the spin state, changes ω, and causes the magnetodielectric effect. This can simply be understood by the fact that exchange constant J depends on positions of the spins, therefore, the positions change when the spin state is modulated by H or a magnetic ordering occurs. This type of the magnetodielectric effect has indeed been observed in $EuTiO_3$ in which λ is tuned by strain [89, 90], and other materials [91-95].

Another magnetodielectric effect has been observed via multiferroic phase transition as critical phenomena [52, 69, 96, 97]. In a multiferroic $TbMn_2O_5$, for example, successive phase transitions occur, say, at T_{high} and T_{low}. At T_{high}, the dielectric constant shows a divergence-type anomaly, however, at T_{low}, it shows a step-like anomaly, although the spin ordering induces the ferroelectric polarization in both phases [96]. This difference originates from different numbers of the order parameters involved [98]. At T_{high}, the ferroelectric polarization is effectively proportional to one spin order parameter, therefore, the polarization behaves in the same way with proper ferroelectrics, and the dielectric constant shows a divergence-type anomaly. On the other hand, at T_{low}, the ferroelectric

polarization is proportional to two spin order parameters, hence, the polarization behaves differently from proper ferroelectrics, and the dielectric constant shows a step-like anomaly. In this way, the behavior of the dielectric constant near the transition point is a clue to clarify what is the nature of the phase transition, the symmetry of the order parameters, or the microscopic origin of the ferroelectric polarization.

Finally, the dielectric constant can probe dynamics. In a multiferroic $DyMnO_3$, the ferroelectric polarization along the *c* axis flops to the *a* axis by applying *H*. At this phase transition, the dielectric constant shows a frequency-dependent divergence-type anomaly [97]. This frequency dependence was ascribed to the motions of the domain walls. The fast relaxation rate even at low temperature suggests that the domain walls are mobile and indicates that these domain walls are thick, not atomically thin. Another example is the dielectric relaxation in RMnO$_3$ [99]. In orthorhombic RMnO$_3$, the dielectric relaxation has widely been observed regardless of its spin structure. The characteristic feature is that it is a general property in RMnO$_3$, and it seems that the relaxation rate is the same in most RMnO$_3$ perovskites at high *T*. The relaxation rate at low *T* is affected by the magnetic ordering and an applied magnetic field. This is an interesting property to be investigated because the microscopic origin is still unknown. Note that the dielectric relaxation has also been observed at the paramagnetic phases, indicating that the microscopic origin comes from its lattice or orbital properties and the properties are somewhat related to the magnetism.

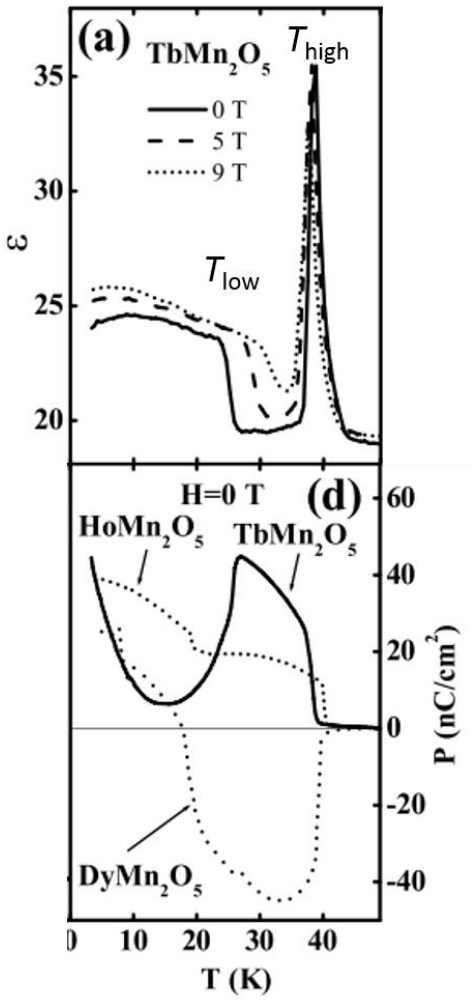

Figure 1-11: Dielectric constant and electric polarization in $TbMn_2O_5$ [96].

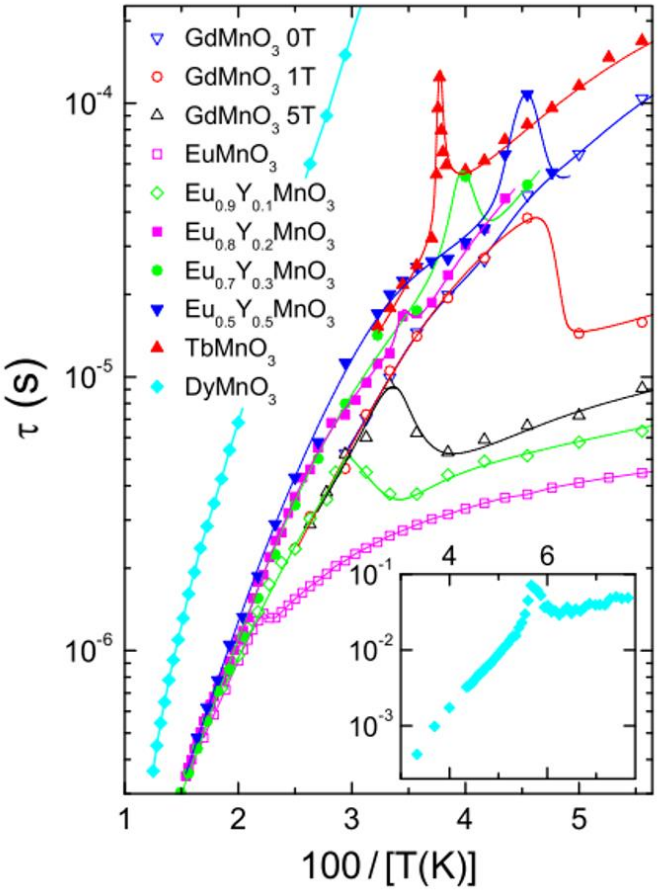

Figure 1-12: Dielectric relaxation in orthorhombic *R*MnO_3 [94].

One should be careful about the dielectric relaxation because the relaxation sometimes comes from extrinsic effect, called the Maxwell-Wagner effect [100]. In this case, the frequency dependence originates from buildups of charges inside the sample or its interface with the electrodes.

1.4 Motivation and purpose

From the history of the ME research, one interesting point is more or less missing. That is, electric property or magnetic property is not only electric polarization or magnetization but also dielectric constant or magnetic susceptibility. It is beneficial to comprehensively understand all these properties as it is in part clear from the section 1.3.

Therefore, the purpose of this thesis is to clarify how these properties behave in the linear ME compounds. To this end, the linear ME Cr_2O_3 and $FeSb_2O_4$ are investigated and described in chapters 3 and 4, respectively. The former material is the most famous linear ME compound, and the experimental results on the latter material is the first report on the single-crystalline samples. The ultimate goal is to elucidate the relation between the similar physical phenomena – the linear ME effect and ME multiferroics – through the investigation of the above-mentioned properties.

The other purpose of this thesis is to further study the unusual magnetodielectric effect in $SmMnO_3$ which has been found for the first time by a former colleague of the author. The magnetodielectric effect in this compound cannot be simply understood by the existing phenomenological way as described in the section 1.3. Thus, further studies are carried out by high-magnetic-field and neutron scattering experiments as described in chapters 5 and 6, respectively. The aim is to clarify how the magnetodielectric effect behaves in a high magnetic field and what happens to the Sm and Mn magnetic moments when the magnetodielectric effect is observed.

1.5 Outline of this dissertation

This thesis is organized as follows. In chapter 2, experimental details are explained, including single crystal growth and measurement techniques. In chapter 3, reinvestigation of the linear ME effect in Cr_2O_3 is discussed in terms of ME multiferroics. It will be shown that the linear ME Cr_2O_3 can be understood as a ferroelectric in a magnetic field and as a ferromagnet in an electric field. In chapter 4, one of the linear ME $FeSb_2O_4$ is investigated with its single-crystalline samples. This is the first experiment with the single crystals, and it will be discussed that the experimental results can be understood by considering the peculiar quasi-1 dimensional crystal structure of this material. In chapters 5 and 6, experimental results on $SmMnO_3$ which is known to have a large magnetodielectric effect are given, on high-magnetic-field physical properties and neutron scattering experiment, respectively. It will be discussed that the magnetodielectric effect comes from interaction between the Sm and Mn magnetic moments.

Appendix

Table 1-1: List of representative magnetoelectric materials [114, 115]

Material	Neel temperature (K)	Magnetic point symmetry	Observed ME tensor	Max. value of ME tensor (CGS)	Reference
Cr_2O_3	307	-3'm'	α_{11} α_{33}	1.5×10^{-6} 1.0×10^{-4}	6, 7
$Nb_2Mn_4O_9$	110	-3'm'	α_{poly}	1.7×10^{-6}	101
$Nb_2Co_4O_9$	27	-3'm'	α_{poly}	11×10^{-5}	101
$Ta_2Co_4O_9$	20.6	-3'm'	α_{poly}	6.4×10^{-5}	101
$GaFeO_3$	280	m'm2'	α_{23}	4.1×10^{-4}	102
$Ni_3B_7O_{13}I$	64	m'm2'	α_{32}	3.3×10^{-4}	103
$FeSb_2O_4$	46	mm2	α_{poly}	none	104
$MnNb_2O_6$	4.4	m'mm	α_{23} α_{32}	$< 10^{-7}$ 2.1×10^{-6}	105
$MnGeO_3$	11	m'mm	α_{23} $\fallingdotseq\alpha_{32}$	2×10^{-6}	106
$LiFePO_4$	50	m'mm	α_{23} α_{32}	0.82×10^{-4} 1.0×10^{-4}	107
$LiCoPO_4$	23	m'mm	α_{23} α_{32}	none	107
$DyAlO_3$	3.5	m'm'm'	α_{33}	1.5×10^{-3}	108
$TbAlO_3$	3.95	m'm'm'	α_{11}	2.2×10^{-3}	109
$DyPO_4$	3.4	4'/m'mm'	α_{11}	1.2×10^{-3}	110
Fe_2TeO_6	219	4'/m'm'm'	α_{33}	3×10^{-5}	111
$GdVO_4$	2.4	4'/m'm'm	α_{11}	2.8×10^{-4}	112
Gd_2CuO_4	6.5	mmm'	α_{13}	1×10^{-4}	113

Note that multiplying $(4\pi/c)$ converts the ME tensor (CGS) into the SI unit (s/m) where c is speed of light (3×10^8 m/s).

References

[1] T. H. O'Dell, *The Electrodynamics of Magneto-Electric Media* (1970).

[2] M. Fiebig, J. Phys. D: Appl. Phys. **38**, R123 (2005).

[3] H. Schmid, J. Phys.: Condens. Matter **20**, 434201 (2008).

[4] L. D. Landau and E. M. Lifshitz, *Electrodynamics of Continuous Media* (1956).

[5] I. E. Dzyaloshinskii, Sov. Phys. JETP **10**, 628 (1960).

[6] D. N. Astrov, Sov. Phys. JETP **11**, 708 (1960).

[7] G. T. Rado and V. J. Folen, Phys. Rev. Lett. **7**, 310 (1961).

[8] G. T. Rado, Phys. Rev. Lett. **6**, 609 (1961).

[9] M. Date, J. Kanamori, and M. Tachiki, J. Phys. Soc. Jpn. **16**, 2589 (1961).

[10] S. Alexander and S. Shtrikman, Solid State Commun. **4**, 115 (1966).

[11] R. Hornreich and S. Shtrikman, Phys. Rev. **161**, 506 (1967).

[12] J. Íñiguez, Phys. Rev. Lett. **101**, 117201 (2008).

[13] M. Mostovoy, A. Scaramucci, N. A. Spaldin, and K. T. Delaney, Phys. Rev. Lett. **105**, 087202 (2010).

[14] E. Bousquet, N. A. Spaldin, and K. T. Delaney, Phys. Rev. Lett. **106**, 107202 (2011).

[15] A. Malashevich, S. Coh, I. Souza, and D. Vanderbilt, Phys. Rev. B **86**, 094430 (2012).

[16] T. Birol, N. A. Benedek, H. Das, A. L. Wysocki, A. T. Mulder, B. M. Abbett, E. H. Smith, S. Ghosh, and C. J. Fennie, Solid State Mater. Sci. **16**, 227 (2012).

[17] W. F. Brown Jr., R. M. Hornreich, and S. Shtrikman, Phys. Rev. **168**, 574 (1968).

[18] R. Resta, Phys. Rev. Lett. **106**, 047202 (2011).

[19] R. Resta, Phys. Rev. B **84**, 214428 (2011).

[20] H. Schmid, Ferroelectrics **252**, 41 (2001).

[21] C. Ederer and N. A. Spaldin, Phys. Rev. B **76**, 214404 (2007).

[22] N. A. Spaldin, M. Fiebig, and M. Mostovoy, J. Phys.: Condens. Matter **20**, 434203 (2008).

[23] K. T. Delaney, M. Mostovoy, and N. A. Spaldin, Phys. Rev. Lett. **102**, 157203 (2009).

[24] B. B. Van Aken, J.-P. Rivera, H. Schmid, and M. Fiebig, Nature **449**, 702 (2007).

[25] M. Fiebig, V. V. Pavlov, and R. V. Pisarev, J. Opt. Soc. Am. B **22**, 96 (2005).

[26] S. W. Lovesey and V. Scagnoli, J. Phys.: Condens. Matter **21**, 474214 (2009).

[27] V. Scagnoli, U. Staub, Y. Bodenthin, R. A. de Souza, M. G.-Fernández, M. Garganourakis, A. T. Boothroyd, D. Prabhakaran, and S. W. Lovesey, Science **332**, 696 (2011).
[28] S. Di Matteo and M. R. Norman, Phys. Rev. B **85**, 235143 (2012).
[29] Y. F. Popov, A. M. Kadomtseva, G. P. Vorob'ev, V. A. Timofeeva, D. M. Ustinin, A. K. Zvezdin, and M. M. Tegeranchi, JETP **87**, 146 (1998).
[30] Y. F. Popov, A. M. Kadomtseva, D. V. Belov, G. P. Vorob'ev, and A. K. Zvezdin, JETP Lett. **69**, 330 (1999).
[31] N. A. Spaldin, M. Fechner, E. Bousquet, A. Balatsky, and L. Nordstorm, Phys. Rev. B **88**, 094429 (2013).
[32] D. I. Khomskii, arXiv: 1307.2327 (2013).
[33] S. W. Lovesey and D. D. Khalyavin, J. Phys. Soc. Jpn. **82**, 103703 (2013).
[34] S. Coh and D. Vanderbilt, Phys. Rev. B **88**, 121106(R) (2013).
[35] J. H. Jung, M. Matsubara, T. Arima, J. P. He, Y. Kaneko, and Y. Tokura, Phys. Rev. Lett. **93**, 037403 (2004).
[36] I. Dzyaloshinskii and E. V. Papamichail, Phys. Rev. Lett. **75**, 3004 (1995).
[37] B. B. Krichevtsov, V. V. Pavlov, R. V. Pisarev, and V. N. Grindnev, Phys. Rev. Lett. **76**, 4628 (1996).
[38] M. Fiebig, D. Fröhlich, B. B. Krichevtsov, and R. V. Pisarev, Phys. Rev. Lett. **73**, 2127 (1994).
[39] M. Fiebig, D. Fröhlich, G. Sluyterman v. L., and R. V. Pisarev, Appl. Phys. Lett. **66**, 2906 (1995).
[40] M. Fiebig, D. Fröhlich, and H.-J. Thiele, Phys. Rev. B **54**, 12681(R) (1996).
[41] T. Satoh, B. B. Van Aken, N. P. Duong, T. Lottermoser, and M. Fiebig, Phys. Rev. B **75**, 155406 (2007).
[42] G. A. Smolenskiĭ and I. E. Chupis, Sov. Phys. Usp. **25**, 475 (1983).
[43] H. Schmid, Ferroelectrics **162**, 317 (1994).
[44] N. A. Hill, J. Phys. Chem. B **104**, 6694 (2000).
[45] D. I. Khomskii, J. Magn. Magn. Mater. **306**, 1 (2006).
[46] T. Kimura, Annu. Rev. Matter. Res. **37**, 387 (2007).
[47] S.-W. Cheong and M. Mostovoy, Nat. Mater. **6**, 13 (2007).
[48] T. Kimura and Y. Tokura, J. Phys.: Condens. Matter **20**, 434204 (2008).
[49] D. I. Khomskii, Physics **2**, 20 (2009).
[50] Y. Tokura and S. Seki, Adv. Mater. **22**, 1554 (2009).
[51] T. Arima, J. Phys. Soc. Jpn. **80**, 052001 (2011).

[52] T. Kimura, T. Goto, H. Shintani, K. Ishizuka, T. Arima, and Y. Tokura, Nature **426**, 55 (2003).
[53] M. Kenzelmann, A. B. Harris, S. Jonas, C. Broholm, J. Schefer, S. B. Kim, C. L. Zhang, S.-W. Cheong, O. P. Vajk, and J. W. Lynn, Phys. Rev. Lett. **95**, 087206 (2005).
[54] H. Katsura, N. Nagaosa, and A. V. Balatsky, Phys. Rev. Lett. **95**, 057205 (2005).
[55] M. Mostovoy, Phys. Rev. Lett. **96**, 067601 (2006).
[56] I. A. Sergienko, C. Sen, and E. Dagotto, Phys. Rev. B **73**, 094434 (2006).
[57] T. A. Kaplan and S. D. Mahanti, arXiv: 0608227 (2006).
[58] H. J. Xiang, E. J. Kan, Y. Zhang, M.-H. Whangbo, and X. G. Gong, Phys. Rev. Lett. **107**, 157202 (2011).
[59] T. A. Kaplan and M. D. Mahanti, Phys. Rev. B **83**, 174432 (2011).
[60] H. J. Xiang, P. S. Wang, M.-H. Whangbho, and X. G. Gong, Phys. Rev. B **88**, 054404 (2013).
[61] A. B. Harris, Phys. Rev. B **76**, 054447 (2007).
[62] P. G. Radaelli and L. C. Chapon, Phys. Rev. B **76**, 054428 (2007).
[63] A. Raeliarijaona, S. Singh, H. Fu, and L. Bellaiche, Phys. Rev. Lett. **110**, 137205 (2013).
[64] H. J. Xiang, S.-H. Wei, M.-H. Whangbo, and J. L. F. Da Silva, Phys. Rev. Lett. **101**, 037209 (2008).
[65] A. Malashevich and D. Vanderbilt, Phys. Rev. Lett. **101**, 037210 (2008).
[66] I. Dzyaloshinsky, J. Phys. Chem. Solids **4**, 241 (1958).
[67] T. Moriya, Phys. Rev. **120**, 91 (1960).
[68] T. Goto, T. Kimura, G. Lawes, A. P. Ramirez, and Y. Tokura, Phys. Rev. Lett. **92**, 257201 (2004).
[69] T. Kimura, G. Lawes, T. Goto, Y. Tokura, and A. P. Ramirez, Phys. Rev. B **71**, 224425 (2005).
[70] Y. J. Choi, C. L. Zhang, N. Lee, and S.-W. Cheong, Phys. Rev. Lett. **105**, 097201 (2010).
[71] M. Mochizuki and N. Furukawa, Phys. Rev. B **80**, 134416 (2009).
[72] M. Mochizuki, N. Furukawa, and N. Nagaosa, Phys. Rev. B **84**, 144409 (2011).
[73] Y. Yamasaki, S. Miyasaka, Y. Kaneko, J.-P. He, T. Arima, and Y. Tokura, Phys. Rev. Lett. **96**, 207204 (2006).
[74] Y. J. Choi, J. Okamoto, D. J. Huang, K. S. Chao, H. J. Lin, C. T. Chen, M. van Veenendaal, T. A. Kaplan, and S.-W. Cheong, Phys. Rev. Lett. **102**, 067601 (2009).

[75] T. Kimura, Y. Sekio, H. Nakamura, T. Siegrist, and A. P. Ramirez, Nat. Mater. **7**, 291 (2008).
[76] I. A. Sergienko, C. Şen, and E. Dagotto, Phys. Rev. Lett. **97**, 227204 (2006).
[77] T. Arima, J. Phys. Soc. Jpn. **76**, 073702 (2007).
[78] C. Jia, S. Onoda, N. Nagaosa, and J. H. Han, Phys. Rev. B **74**, 224444 (2006).
[79] C. Jia, S. Onoda, N. Nagaosa, and J. H. Han, Phys. Rev. B **76**, 144424 (2007).
[80] A. P. Levanyuk and D. G. Sannikov, Sov. Phys. Usp. **17**, 199 (1974).
[81] J. C. Tolédano and P. Tolédano, *The Landau theory of phase transitions*, World Scientific (1987).
[82] E. Bousquet, M. Dawber, N. Stucki, C. Lichtensteiger, P. Hermet, S. Gariglio, J.-M. Triscone, and P. Ghosez, Nature **452**, 732 (2008).
[83] N. A. Benedek and C. J. Fennie, Phys. Rev. Lett. **106**, 107204 (2011).
[84] B. B. Van Aken, T. T. M. Palstra, A. Filippetti, and N. A. Spaldin, Nat. Mater. **3**, 164 (2004).
[85] C. J. Fennie and K. M. Rabe, Phys. Rev. B **72**, 100103(R) (2005).
[86] V. Gopalan and D. B. Litvin, Nat. Mater. **10**, 376 (2011).
[87] T. Kimura, S. Kawamoto, I. Yamada, M. Azuma, M. Takano, and Y. Tokura, Phys. Rev. B **67**, 180401(R) (2003).
[88] C. J. Fennie and K. M. Rabe, Phys. Rev. Lett. **97**, 267602 (2006).
[89] J. H. Lee, L. Fang, E. Vlahos, X. Ke, Y. W. Jung, L. F. Kourkoutis, J.-W. Kim, P. J. Ryan, T. Heeg, M. Roeckerath, V. Goian, M. Bernhagen, R. Uecker, P. C. Hammel, K. M. Rabe, S. Kamba, J. Schubert, J. W. Freeland, D. A. Muller, C. J. Fennie, P. Schiffer, V. Gopalan, E. J.-Halperin, and D. G. Schlom, Nature **466**, 954 (2010).
[90] T. Birol and C. J. Fennie, Phys. Rev. B **88**, 094103 (2013).
[91] G. Lawes, A. P. Ramirez, C. M. Varma, and M. A. Subramanian, Phys. Rev. Lett. **91**, 257208 (2003).
[92] M. S. Seehra and R. E. Helmick, Phys. Rev. B **24**, 5098 (1981).
[93] M. S. Seehra and R. E. Helmick, J. Appl. Phys. **55**, 2330 (1984).
[94] N. Hur, S. Park, S. Guha, A. Borissov, V. Kiryukhin, and S.-W. Cheong, Appl. Phys. Lett. **87**, 042901 (2005).
[95] R. Muralidharan, T.-H. Jang, C.-H. Yang, Y. H. Jeong, and T. Y. Koo, Appl. Phys. Lett. **90**, 012506 (2007).
[96] N. Hur, S. Park, P. A. Sharma, G. Guha, and S.-W. Cheong, Phys. Rev. Lett. **93**, 107207 (2004).
[97] F. Kagawa, M. Mochizuki, Y. Onose, H. Murakawa, Y. Kaneko, N. Furukawa, and Y. Tokura, Phys. Rev. Lett. **102**, 057604 (2009).

[98] P. Tolédano, W. Schranz, and G. Krexner, Phys. Rev. B **79**, 144103 (2009).
[99] F. Schrettle, P. Lunkenheimer, J. Hemberger, V. Yu Ivanov, A. A. Mukhin, A. M. Balbashov, and A. Loidl, Phys. Rev. Lett. **102**, 207208 (2009).
[100] H. Fricke, J. Phys. Chem. **57**, 934 (1953).
[101] E. Fischer, G. Gorodetsky, and R. M. Hornreich, Solid State Comm. **10**, 1127 (1972).
[102] G. T. Rado, Phys. Rev. Lett. **13**, 335 (1964).
[103] E. Ascher, H. Rieder, H. Schmid, and H. Stössel, J. Appl. Phys. **37**, 1404 (1966).
[104] G. Gorodetsky, M. Sayar, and S. Shtrikman, Mat. Res. Bull. **5**, 253 (1970).
[105] L. M. Holmes, A. A. Ballman, and R. R. Hecker, Solid State Comm. **11**, 409 (1972).
[106] G. Gorodetsky, Phys. Lett. A **39**, 155 (1972).
[107] M. Mercier, P. Bauer, and B. Fouilleu, Comptes Rendus B **267**, 1345 (1968).
[108] L. M. Holmes, L. G. van Uitert, and G. W. Hull, Solid State Comm. **9**, 1373 (1971).
[109] M. Mercier and B. Cursoux, Solid State Comm. **6**, 207 (1968).
[110] G. T. Rado, Phys. Rev. Lett. **23**, 644 (1969).
[111] S. Buksphan, Solid State Comm. **10**, 657 (1972).
[112] G. Gorodetsky, R. M. Hornreich, and B. M. Wanklyn, Phys. Rev. B **8**, 2263 (1973).
[113] H. Wiegelmann, I. M. Vitebsky, A. A. Stepanov, A. G. M. Jansen, and P. Wyder, Phys. Rev. B **55**, 15304 (1997).
[114] H. Schmid, '*Magnetoelectric Effects in Insulating Magnetic Materials*' SPIE Press, Bellingham (2003).
[115] S. Chikazumi, K. Ohta, K. Adachi, N. Tsuya, and Y. Ishikawa, 'Handbook of Magnets' Asakura Shoten, (2006). [in Japansese]

Chapter 2 Experimental Details

2.1 Single crystal growth

Growth of $SmMnO_3$ and $EuMnO_3$

$SmMnO_3$ and $EuMnO_3$ single crystals were grown by the floating-zone method [1, 2]. The detail on the growth is as follows. First, polycrystalline feed rods were prepared by solid state reaction. Stoichiometric amount of Sm_2O_3 (Eu_2O_3) and Mn_2O_3 powders with 99.9 % purity (purchased from Kojundo Chemical Lab. Co., Ltd) were mixed and heated at 1000 °C for 12 h in air. The polycrystalline samples were ground, and pressed into a rod with the typical dimension of 6 mm in diameter and 12 cm in length. The rods were heated again at 1300 °C for 40 h in air. The single crystals were grown with the use of the resulting rod by a halogen-lamp image furnace in Ar flow. The growth rate was 6 – 8 mm/h. The single crystals with a clear facet were successfully obtained, checked by a powder x-ray diffraction, and confirmed to be a single phase. Then, obtained single crystals were oriented by Laue x-ray patterns, and cut into plates with the largest planes perpendicular to the *c* axis (*Pbnm* setting) for the dielectric measurements.

Figure 2-1: Obtained single crystal of $SmMnO_3$ by the floating-zone method.

Growth of Cr_2O_3

Cr_2O_3 single crystals were grown by the flux method [3]. The detail on the growth is as follows. 10.2 g of Cr_2O_3 powders with 99.9 % purity and 45 g of Bi_2O_3 powders with 99.9 % purity were put into a Pt crucible. The powders were purchased from Kojundo Chemical Lab. Co., Ltd. The sample was heated up to 1345 °C for 24 h and cooled down to 850 °C with the rate of 1.3 °C/h. The grown samples were in a plate shape (~ 2 × 1 × 0.1 mm^3), and the largest plane was the *c* plane (in the hexagonal setting). The flux was removed by HCl aq. The obtained samples were checked by x-ray diffraction and confirmed to be a single phase.

Figure 2-2: Obtained single crystals of Cr_2O_3 by the flux method.

Growth of $FeSb_2O_4$

$FeSb_2O_4$ single crystals were grown by the hydrothermal method [4]. The detail on the growth is as follows. Appropriate amount of $FeC_2O_4 \cdot 2H_2O$ powders with 99.9 % purity (purchased from Rare Metallic Co., Ltd) and Sb_2O_3 powders with 99.9 % purity (purchased from Kojundo Chemical Lab. Co., Ltd.) were put into a silver tube with 5 % NaOH as a solvent. The growth condition was 500 °C and 1000 kg/cm^2, and the reaction time was 96 h. The frequently obtained samples were dark-reddish-brown-colored needle-shaped with bottom faces, and the typical dimension was 80 μm × 80 μm × 1 mm. By-product materials were transparent yellow-colored Sb_2O_3 with needle-shaped as well. Quality of the samples was checked by single-crystalline x-ray diffraction which confirmed that obtained samples were single crystals (space group $P4_2/mbc$) with the lattice constants of $a = b = 8.619(10)$ Å, and $c = 5.884(11)$ Å. The crystallographic axes were determined by using a four-circle diffractometer. The long direction of the crystals was along the *c* axis.

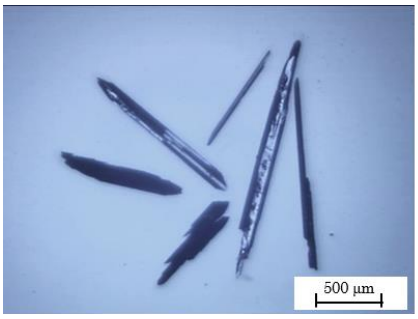

Figure 2-3: Obtained single crystals of $FeSb_2O_4$ by the hydrothermal method.

2.2 Magnetization measurement

DC magnetization measurement was done with using a commercial magnetometer (MPMS SQUID VSMRK2), which can reach a magnetic field up to 7 T and temperature from 1.8 K to 400 K. The sensitivity was ~ 10^{-7} emu. DC magnetization at high-field measurement on $SmMnO_3$ was measured by a vibrating sample magnetometer at National High Magnetic Field Laboratory, Florida, USA.

For the measurement of the magnetoelectric effect in Cr_2O_3, a home-made probe was inserted into the SQUID magnetometer in order to apply an electric field during the measurements. Silver electrodes were vacuum deposited to the largest plane of a Cr_2O_3 single crystal (*c* plane), set in order to apply an electric field and measure a magnetization parallel to each other, and connected to a voltage generator with Cu wires.

2.3 Dielectric measurement

Dielectric constant

Dielectric constant was measured with using an LCR meter (Agilent E4980A) at frequency of 100 – 100k Hz. By measuring a capacitance C of a sample, dielectric constant is obtained from an equation as

$$C = \varepsilon\varepsilon_0\left(\frac{S}{d}\right)$$

where ε, ε_0, S, d are relative dielectric constant, dielectric constant at vacuum, area of electrodes of the sample, thickness of the sample, respectively. The capacitance of $SmMnO_3$ at high magnetic fields was measured with using capacitance bridges at National High Magnetic Field Laboratory, Florida, USA.

To measure the temperature and magnetic-field dependences of the dielectric constant, a home-made probe was inserted into a superconducting magnet PPMS. Terminals at sample space of the probe is connected to BCN connectors at the top of the probe with stainless steel coaxial cables. Silver was vacuum deposited or silver paste was put as electrodes. The electrodes were connected to the terminal of the probe by Cu and Au wires.

Electric polarization

Electric polarization was measured with using an electrometer (Keithley 6517A). The sample setting was the same with the measurement for the dielectric constant.

One can measure not an electric polarization itself but change in an electric polarization according to modern theories [5–7]. Change in an electric polarization is electric current, thus, electric current was measured with sweeping temperature (called pyroelectric current) or an external field (called magnetoelectric current in the case of a magnetic field). This is expressed as

$$I_P = S\frac{dP}{dT}\frac{dT}{dt}$$

$$I_{ME} = S\frac{dP}{dH}\frac{dH}{dt}$$

where P, T, H, I, S, t are electric polarization, temperature, magnetic field, electric current, area of the electrodes of the sample, and time, respectively. Then, P is obtained by an integration of the electric current.

$$P = \frac{1}{S}\int dt I_P$$

$$P = \frac{1}{S}\int dt I_{ME}$$

Before each measurement, magnetoelectric (ME) poling was done in order to make a single domain unless a net P is zero. At $T > T_N$ (Néel temperature), E (electric field) and H were applied. Then the sample was cooled down. After this procedure, P was measured.

For the *P-E* hysteresis measurements, an electric circuit as Figure 2-4 was employed in order to smooth the applied voltage to the sample because a voltage supply generates an electric voltage as a step-like manner. A capacitor with the capacitance of 0.47 μF and a resistor with the resistance of 100 kΩ were used.

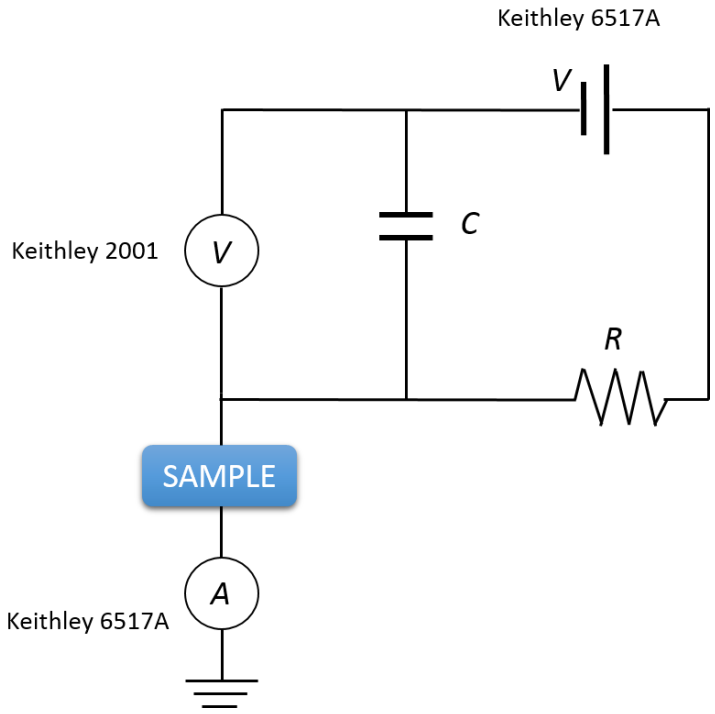

Figure 2-4: A circuit for the *P-E* hysteresis measurement.

2.4 Neutron diffraction

Neutron scattering experiment is a powerful tool to study a magnetic structure as well as a crystal structure because neutrons have spin degree of freedom. In order to survey a magnetic structure of $SmMnO_3$, single crystal neutron scattering experiment is, thus, a natural way to carry out. However, natural isotope of Sm has a large cross section for neutrons [8-10], and thus neutron scattering experiment is difficult in a usual way. A solution to this problem is to use a single crystal with a special isotope of Sm [11], but it costs appreciably and hence it is not a versatile way. Another solution is to use 'hot neutrons' [12-14]. Usually, neutron scattering experiment uses 'thermal neutrons' with the wavelength of ~ 1 – 2 Å, however, the wavelength of hot neutrons is ~ 0.5 Å which is shorter than thermal neutrons. Neutron absorption can be suppressed with hot neutrons because cross sections for neutrons depend on the wavelength of neutrons as described in Figures 2-5 and 2-6.

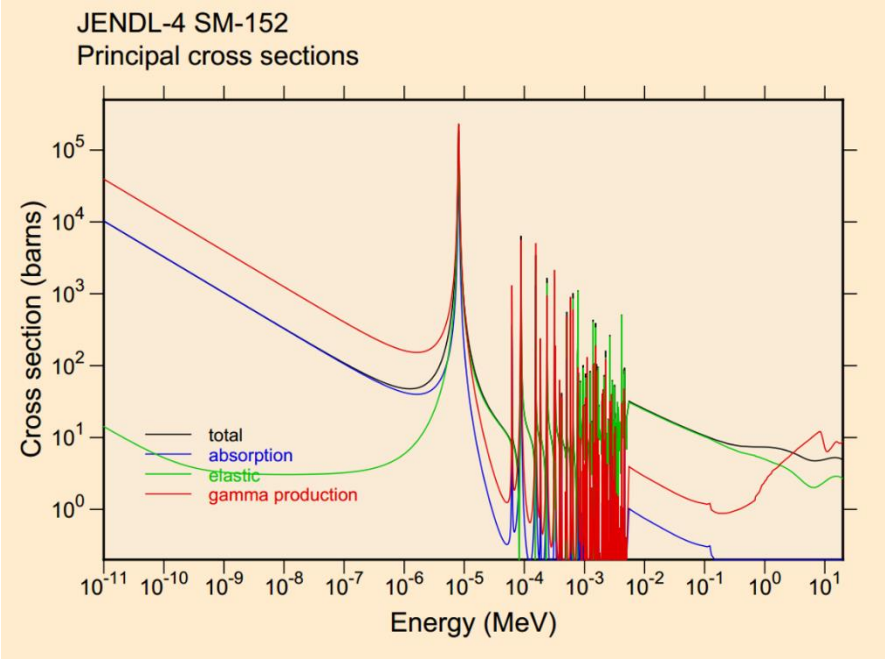

Figure 2-5: Neutron cross sections of ^{152}Sm [15]. Concentration of ^{152}Sm is 26.6 % which is the largest among the isotopes.

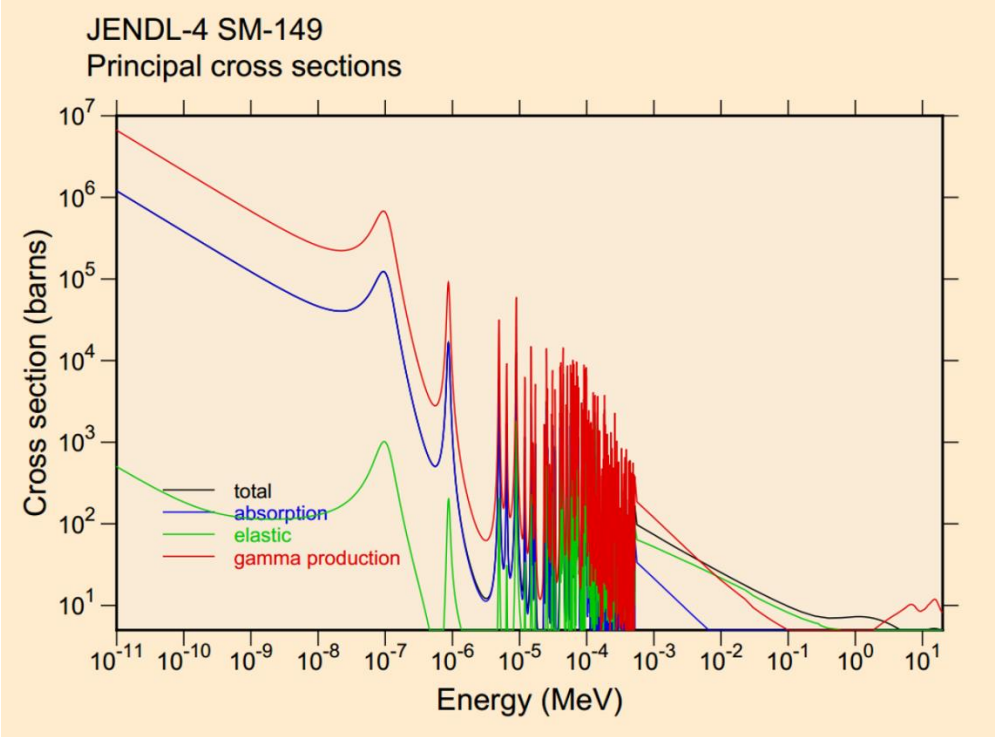

Figure 2-6: Neutron cross sections of ^{149}Sm [15]. Concentration of ^{149}Sm is 13.9 % which has the largest cross sections among the isotopes.

Here, the following equation is useful.

$$\lambda(\text{Å}) = \frac{9.044}{\sqrt{E(meV)}}$$

where λ and E are the wavelength and energy of a neutron, respectively. Then, E = 20 meV when λ = 2 Å, and E = 327 meV when λ = 0.5 Å. Thus, cross sections for hot neutrons are 1-2 orders smaller than those for thermal neutrons.

Neutron scattering experiment with hot neutrons was carried out at D9 in Institute Laue-Langevin, Grenoble, France. Monochromic neutron beam from a reactor was irradiated to a single crystal $SmMnO_3$ set to a four-circle diffractometer, and was detected by a 2-dimensional detector as Figure 2-6.

First, Bragg reflections corresponding to *Pmmm* (at small-*q* regions) and *Pbnm* (at large-*q* regions) space groups were collected in order to check the crystal structure of $SmMnO_3$ (space group *Pbnm*) at 40 K (below T_N).Then, temperature dependence of intensity at some Bragg peaks was measured to extract information on the canting angles of the Mn magnetic moments which determine the weakly ferromagnetic component of this material

especially just below T_N where the Sm magnetic moments are nearly zero. Note that magnetic Bragg peaks corresponding to the 'ferromagnetic component' always overlap to the nuclear Bragg peaks, thus, measuring T dependence of the intensity is necessary to separate the magnetic contribution from the nucleus contribution.

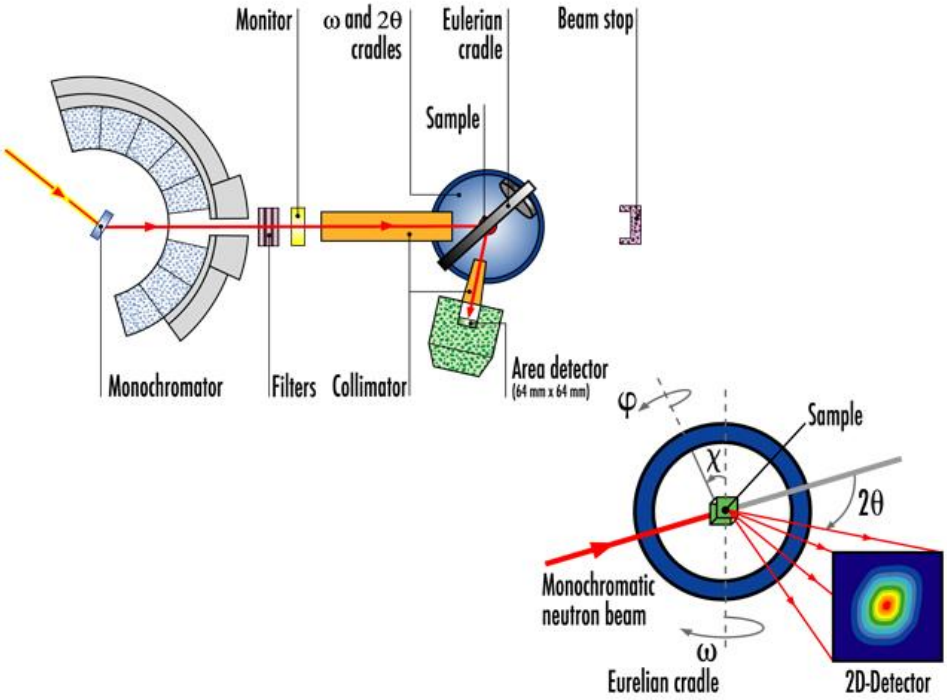

Figure 2-7: Instrument layout at D9 in Institute Laue-Langevin (from the website).

References

[1] S. M. Koohpayeh, D. Fort, and J. S. Abell, Prog. Cryst. Growth Charact. Mater. **54**, 121 (2008).

[2] T. Mori, N. Kamegashira, K. Aoki, T. Shishido, and T. Fukuda, Mater. Lett. **54**, 238 (2002).

[3] G. Garton, S. H. Smith, and B. M. Wanklyn, J. Cryst. Growth **13-14**, 588 (1972).

[4] E. Koyama, I. Nakai, and K. Nagashima, Nippon Kagaku Kaishi **6**, 793 (1979) [in Japanese].

[5] R. D. King-Smith and D. Vanderbilt, Phys. Rev. B **47**, 1651(R) (1993).

[6] R. Resta, Rev. Mod. Phys. **66**, 899 (1994).

[7] N. A. Spaldin, J. Solid State Chem. **195**, 2 (2012).

[8] V. F. Sears, Neutron News **3**, 26 (1992).

[9] R. E. Lapp, J. R. VanHorn, and A. J. Dempster, Phys. Rev. **71**, 745 (1947).

[10] A. J. Dempster, Phys. Rev. **74**, 505 (1948).

[11] D. O'Flynn, C. V. Tomy, M. R. Lees, A. D.-Aladine, and G. Balakrishnan, Phys. Rev. B **83**, 174426 (2011).

[12] K. Wisshak, K. Guber, F. Voss, F. Käppeler, and G. Reffo, Phys. Rev. C **48**, 1401 (1993).

[13] K. A. Toukan, K. Debus, K. Käppeler, and G. Reffo, Phys. Rev. C **51**, 1540 (1995).

[14] J. Pospíšil, G. Nénert, S. Miyashita, H. Kitazawa, Y. Skourski, M. Diviš, J. Prokleška, and V. Sechovský, Phys. Rev. B **87**, 214405 (2013).

[15] JENDL-4 Incident-Neutron Data [http://t2.lanl.gov/nis/data/jendl/neutronJ4.html]

Chapter 3

In-field ferroic nature in the linear magnetoelectric Cr_2O_3

3.1 Introduction

This chapter describes that the most famous linear magnetoelectric (ME) compound Cr_2O_3 actually shows ferroelectric (FE) behaviors in a magnetic field H and ferromagnetic (FM) behaviors in an electric field E. This chapter is organized as follows. First, previous studies on Cr_2O_3 are introduced, in which the crystal structure and the magnetism are also included. Second, experimental results on the reinvestigation of the linear ME effect on Cr_2O_3 are given. Third, the results are discussed by focusing on the relation between the linear ME effect and spin-driven multiferroics. Finally, perspectives on the linear ME effect are discussed.

3.2 Previous studies on Cr_2O_3

Cr_2O_3 has a corundum structure with the space group $R\bar{3}c$, possessing the inversion center. Cr ions are located at 12*c* sites with the site symmetry 3, and O ions are at 18*e* sites with the site symmetry 2. This compound shows a simple antiferromagnetic ordering below the Néel temperature T_N ~ 307 K [1]. The Cr spins are aligned almost parallel to the *c* axis in the hexagonal notation [2, 3]. It was theoretically predicted that by the spin ordering, inversion and time-reversal symmetries are broken,

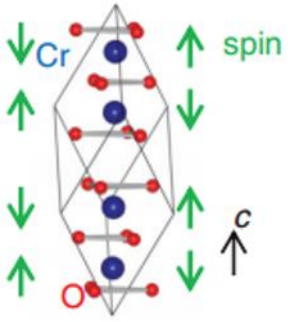

Figure 3-1: Crystal structure of Cr_2O_3. The notation is the hexagonal setting.

allowing the linear ME effect [4]. According to the magnetic symmetry, the ME tensor is expressed as [4, 5]

$$\alpha = \begin{pmatrix} \alpha_{\perp} & 0 & 0 \\ 0 & \alpha_{\perp} & 0 \\ 0 & 0 & \alpha_{//} \end{pmatrix}$$

Soon after the prediction, the linear ME effect was experimentally confirmed [6-8]. Several papers were published for discussing the microscopic origin of the linear ME effect after the experimental confirmation [9-12], however, the origin is still under debate. This is why theoreticians have still tried to explain the origin by the first principles calculations [13-18].

Concerning the experiments, the ME and magneto-optical properties have been investigated [19-23]. The ME tensor can be accurately measured by using SQUID with applying an electric voltage [19, 21]. The results show that $\alpha_{//}$ appears below T_N and has a peak around 260 K, and then decreases as depicted in Figure 3-2. This behavior has been understood by the combination between temperature dependence of the order parameter (staggered magnetization) and the magnetic susceptibility along the *c* axis [12, 14]. At lower temperature below ~ 100 K, $\alpha_{//}$ changes the sign to minus. This cannot be explained by the above scenario, and for now, the origin of this behavior and the absolute value of $\alpha_{//}$ have not been explained so far.

The dielectric constant ε was measured in the early stage of the ME research [24-26]. However, as Figure 3-3 shows, only rough temperature profiles of ε at a few magnetic fields have been reported to date. Hence details of dielectric property and its magnetic field effect is still unclear.

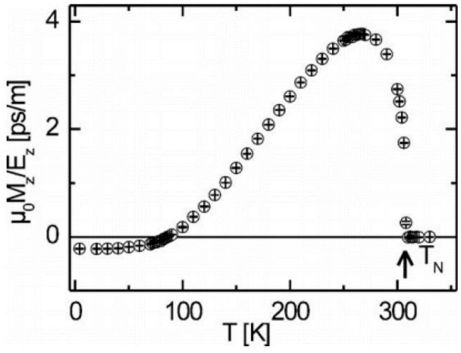

Figure 3-2:
Temperature dependence of $\alpha_{//}$ [21].

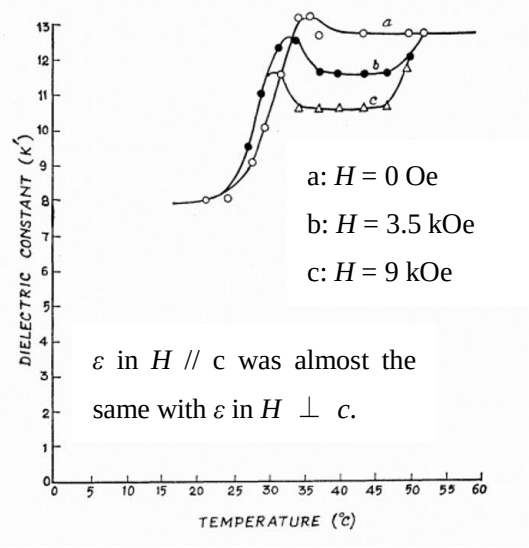

Figure 3-3: Temperature dependence of the dielectric constant [25].

3.3 The purpose of this study

Until now, almost all researches on the linear ME effect have been concerned in temperature dependence of the ME tensor, and the absolute values, because P (M) is linearly induced by H (E), and then, a specific parameter of each material is only the ME tensor. But here, the linear ME effect is similar to ME multiferroics because both the phenomena are the coupling between electric and magnetic properties in a substance. Then, it is expected that both effects can be understood in a coherent way. Therefore, it is interesting to measure ε, P, and M in H and E again, concerning how the induced P (M) by H (E) is understood in terms of multiferroics. Thus, the purpose of this study is to show how both the effects can be explained simultaneously by measuring electric and magnetic properties in the linear ME compound.

To this end, Cr_2O_3 was chosen as an example because this compound is the first ME material and it is the most investigated one, and it is a rare example showing the ME effect at room temperature. The latter characteristic feature leads to researches for future application such as exchange bias effect [27, 28]. Thus, this study mostly focuses on the properties around T_N. Note that there is no literature which reports detailed data on ε and $\alpha_{//}$ around T_N.

3.4 Experimental results

Here the experimental results are shown [29]. The experiments focus on $\alpha_{//}$ around T_N. Single crystals were grown by the flux method with Bi_2O_3 [30]. 10.2 g of Cr_2O_3 and 45 g of Bi_2O_3 were put into a Pt crucible. The sample were heated up to 1345 °C and cooled down to 850 °C with the rate of 1.3 °C/h. The grown samples were in a plate shape, and the largest plane was the *c* plane (in the hexagonal setting). Silver electrodes were vacuum deposited. The measured properties and external fields were only along the *c* axis, which corresponds to measurements of $a_{//}$. Before measurements of *P* and *M*, the ME poling was done in order to make the system with the single domain.

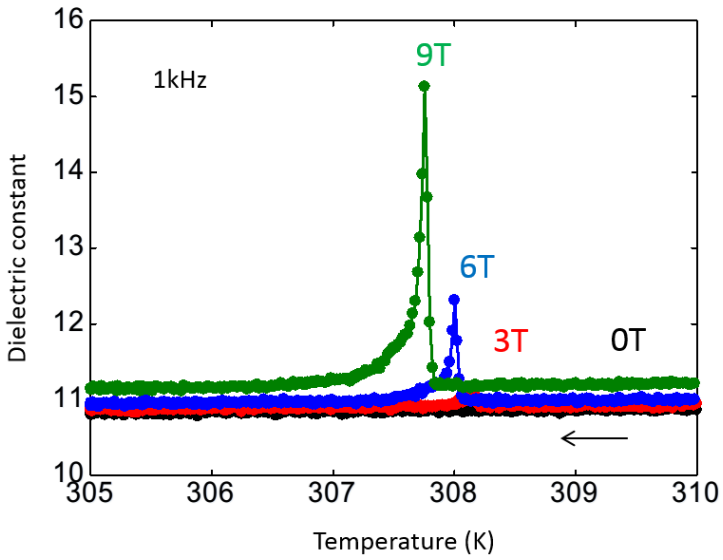

Figure 3-4: Temperature dependence of the dielectric constant along the *c* axis. The frequency is 1 kHz.

First, the dielectric constant was measured around T_N. Figure 3-4 shows temperature dependence of ε in selected *H*. In 0 T, ε has no anomalies and is almost flat in this temperature range. The modulus is consistent with previous studies [24, 25]. Then, a λ-type peak appears in *H* at T_N. These anomalies originate from the linear ME effect because there is no anomaly in 0 T. This type of the peak is reminiscent of a second order ferroelectric phase transition. The temperature at which a peak appears in ε decreases in a high *H*, which corresponds to the decrease of T_N in a high *H*.

The peak top becomes larger in a higher H as shown in Figure 3-5: , and is proportional to H^2, which is a common behavior [31] except that this H dependence of ε is just on the transition point. The amount of change is about 80 % at 100 Hz between the peak top in 9 T and 0 T (corresponding to the modulus without anomalies), which can be said to be the large magnetocapacitance effect above room temperature.

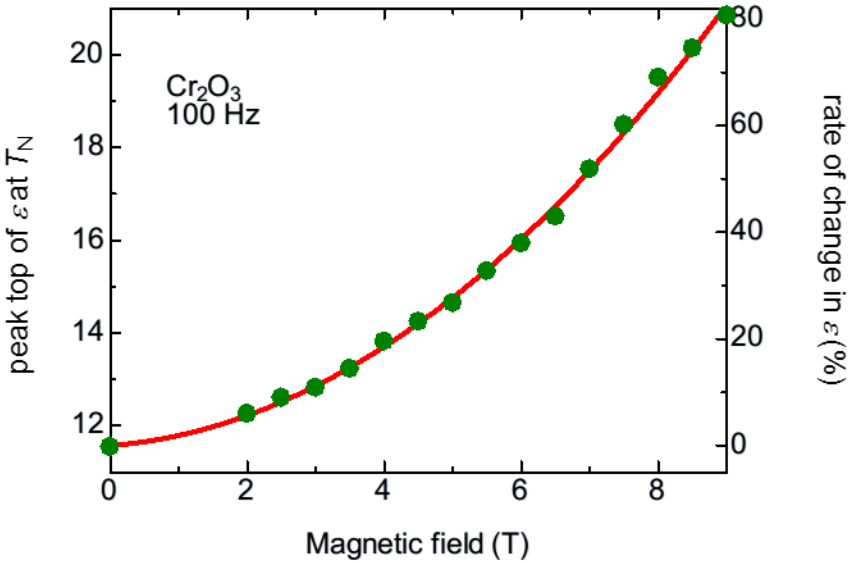

Figure 3-5: Magnetic field dependence of the peak top of the dielectric constant. The solid line is the fit by a bilinear function.

The magnetocapacitance effect is remarkable around T_N as represented in Figure 3-6. The amount of change is about 22 %, and this effect reflects the fluctuation of P at this temperature.

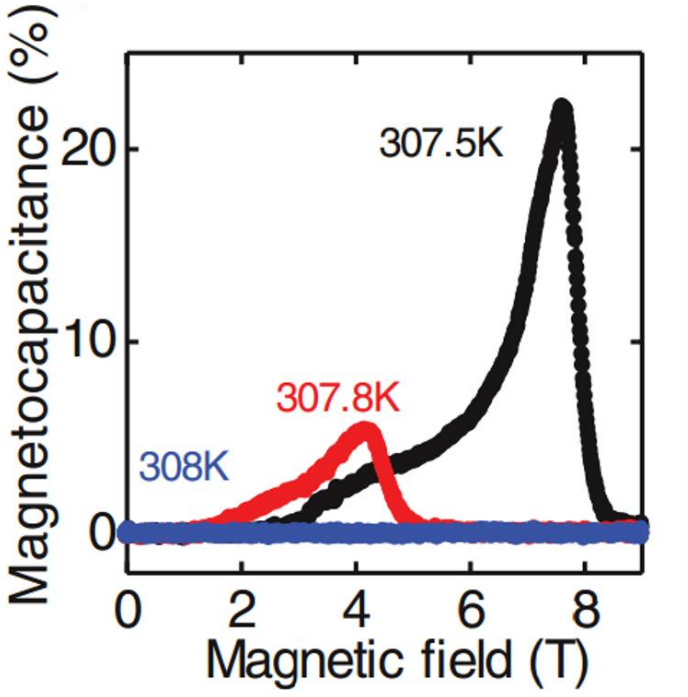

Figure 3-6: The magnetocapacitance effect near T_N.

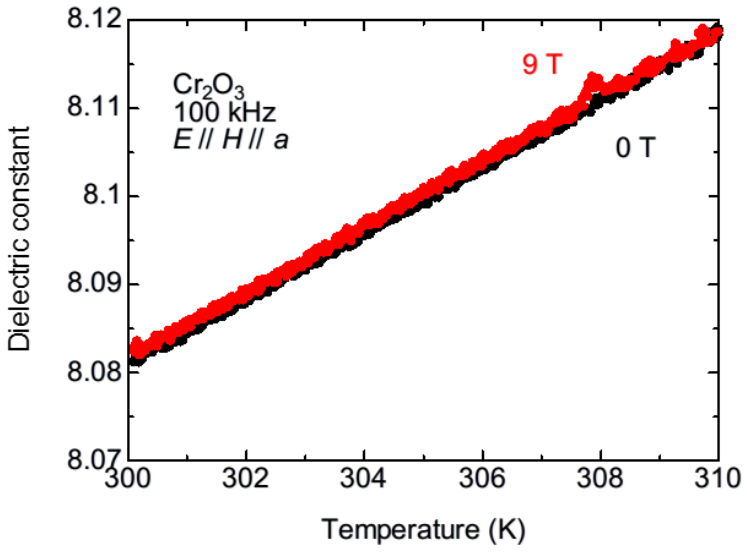

Figure 3-7: Dielectric constant along the *a* axis. A magnetic field is parallel to the electric field.

Figure 3-7 shows the dielectric constant along the *a* axis, although all other data are along the *c* axis. *H* is also parallel to the *a* axis, hence, the dielectric constant reflects $\alpha_{\perp}$. The absolute value is slightly smaller than the previous study [24]. A distinct difference of this alignment from that of the *c* axis is that an anomaly at T_N is small even in an applied *H* of ~ 9 T, although the shape of the anomaly is similar. This difference can be ascribed to the different microscopic origin of the induced electric polarization between along the *c* axis and perpendicular to the *c* axis, and also can be attributed to the fact that spins in the antiferromagnetic phase is parallel to the *c* axis because the fluctuation of *P* comes from the fluctuation of the antiferromagnetic spins. The electric polarization along the *a* axis was not detectable due to the smallness of the sample and $\alpha_{\perp}$.

Next, the electric polarization was measured in selected magnetic fields. Substantial *P* is not observed in 0 T. On the other hand, *P* is finite in *H* below T_N. This *P* comes from the linear ME effect because *P* is linearly induced by an applied *H*. The curvature of the temperature dependence of the induced *P* is reminiscent of that of the staggered magnetization G_c measured by neutron scattering experiment [32]. This is consistent with the theory that $\alpha_{//}$ is proportional to G_c times the magnetic susceptibility along the *c* axis χ_c because χ_c is almost constant in this temperature range. From the *H* dependence of *P* at 300 K, $\alpha_{//}$ is estimated to be 2.8 ps/m which is comparable to that reported in the latest experiment [21].

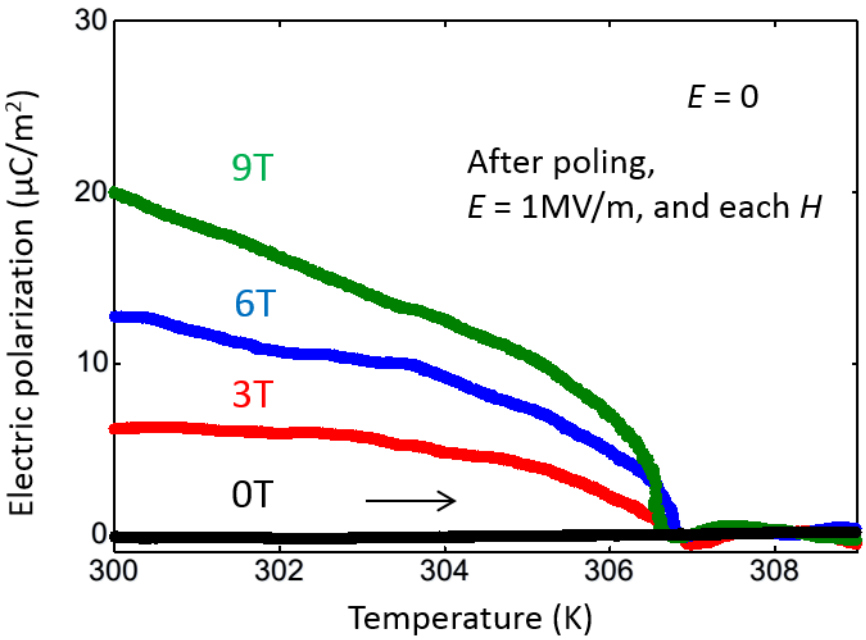

Figure 3-8: Temperature dependence of the electric polarization in selected magnetic fields.

Here the interest is how the induced P by H is understood from the view point of multiferroics. Therefore, electric field dependence of the induced P was measured below and above T_N. The results are shown in Figure 3-9. The induced P reverses by sweeping E at 300 K. That is to say, P–E hysteresis curve is obtained at room temperature. This hysteresis loop disappears above T_N, thus this hysteresis curve clearly originates from the linear ME effect. This ferroelectric behavior is ascribed to a switching of the antiferromagnetic domains because a reversal of G_c leads to a reversal of P [33, 34].

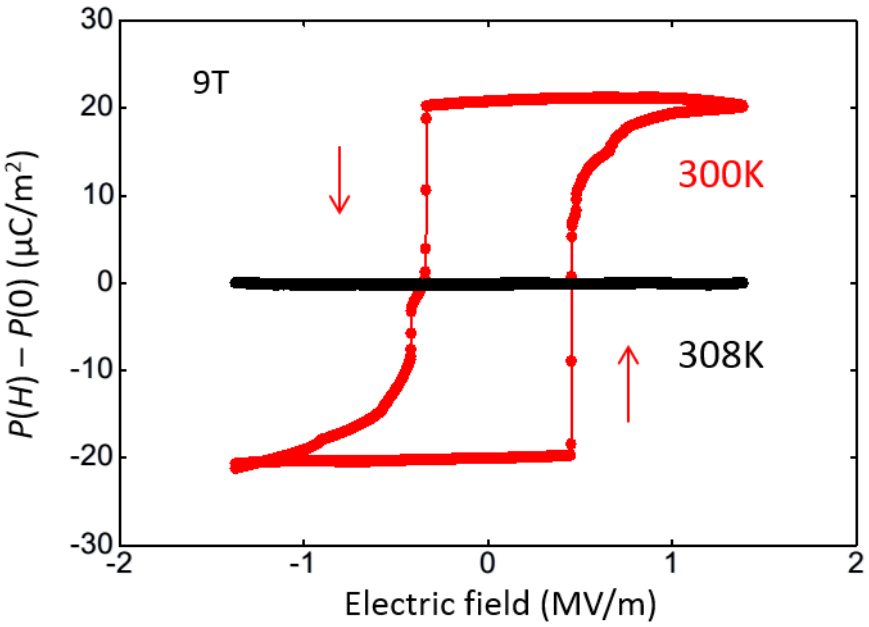

Figure 3-9: Electric field dependence of the induced electric polarization below and above T_N.

The *P*-*E* hysteresis curves depend on *H*, temperature, and poling *E*. Figure 3-10 shows *E*-dependence of the induced *P* at 300 K in *H* of 5 T and 9 T after poling procedures of *E* = -1.3 MV/m and *H* = 5 T and 9 T, respectively. (The data of 9 T is the same with that of Figure 3-9.) As free energy of the magnetoelectric term is proportional to *EH*, it is expected that the coercive *E* becomes larger for smaller *H*, assuming that at some *EH* the magnetoelectric energy overcomes the magnetic anisotropy energy in order to reverse the antiferromagnetic vector, and it was indeed observed.

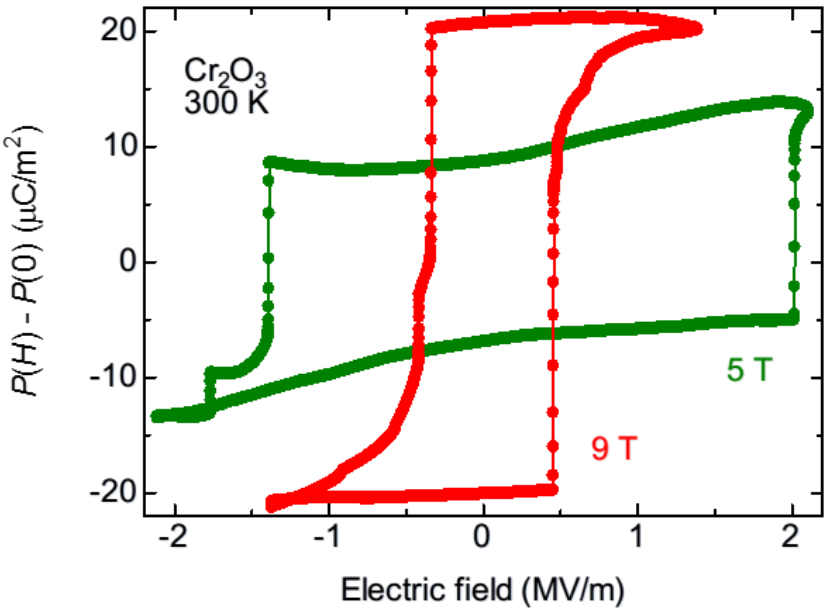

Figure 3-10: Electric field dependence of the induced electric polarization by a magnetic field of 5 T and 9 T at 300 K.

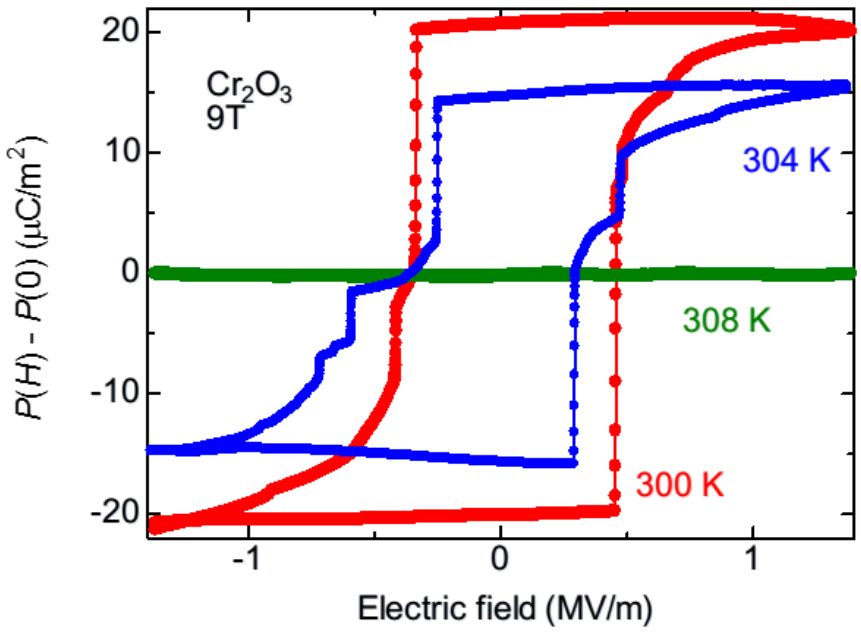

Figure 3-11: Electric field dependence of the induced electric polarization by a magnetic field of 9 T at 300, 304, and 308 K.

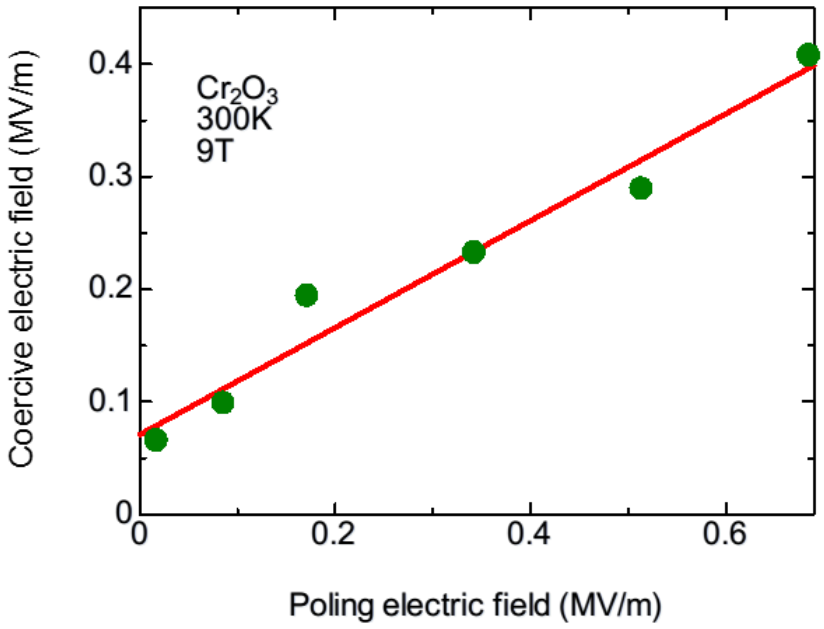

Figure 3-12: Relation between poling electric field and coercive electric field at 300 K under application of a magnetic field of 9 T. The red solid line is the fit by a linear function.

Figure 3-11 depicts *E*-dependence of the induced *P* by *H* of 9 T at 300, 304, and 308 K. The remanent *P* at 304 K is smaller than that at 300 K is consistent with the *P*-*T* curve in Figure 3-8. The corecive *E* at 304 K seems to be smaller than that at 300 K, but it is subtle. Accorging to the previous study [33], the corecive *E* dependes on temprrature as ~ exp (1/*T*), thus, the change in the coercive *E* at 300 and 304 K is estimated to be ~ 5 % which is indeed subtle. Almost reactangular shape and sometimes with a few steps of the *P*-*E* hysteresis curve is also consistent with the previous study [33]. Figure 3-12 describes a relation between a poling *E* and a coercive *E* at 300 K in 9 T. From this relation, it is clear that the higher the poling *E* is applied, the higher the coercive *E* becomes, and the relation is roughly linear. This relation was observed as well in the previous study [33], but the origin of this relation is unclear. One possibility is that a seed domain around defects or something triggers an antiferromagnetic switching, and a larger poling *E* decreases the seed domains. This is for the future investigation.

Next, the inverse ME effect, namely *M* induced by *E*, was investigated. Figure 3-13 shows time dependence of an applied *E* and measured *M* at 300 K after + *EH* or – *EH* poling procedure, with *E* = 1 MV/m, *H* = 7 T. As *E* = -1, 0, 1 MV/m was periodically applied, the induced *M* also changes. In Figure 3-14, the induced *M* as a function of an applied *E* is represented. From the *E* dependence of *M*, it is clear that *M* is proportional to *E*, and the coefficient (ME tensor) was estimated to be 2.9 ps/m, which is also consistent with the previous study and the *P* measurement in *H*. Therefore, it is obvious that the home-made probe to measure *M* with applying *E* properly works.

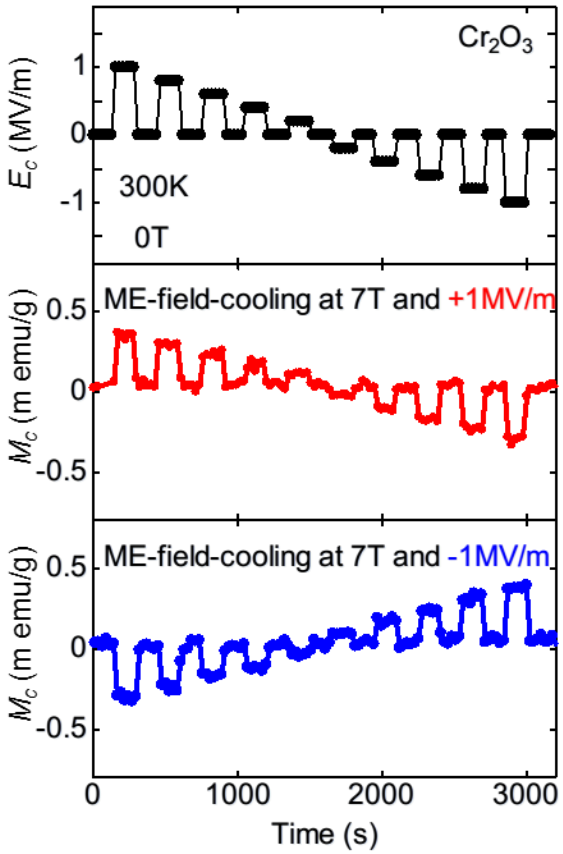

Figure 3-13: An applied electric field (the upper panel) and the measured magnetization (the middle and lower panels) at room temperature after a poling procedure.

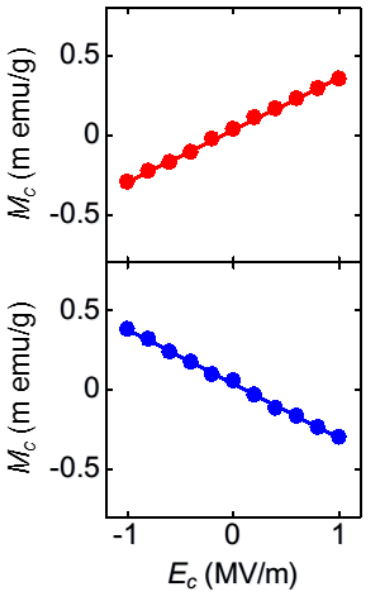

Figure 3-14: An electric field dependence of the measured magnetization in Figure 3-13.

Furthermore, an experimental demonstration was done as shown in Figure 3-15 that *M* switches by reversing the applied *E* at 300 K. This is the first realization of *M* reversal only by *E* in a single compound at room temperature. This experimental demonstration is based on the fact that Cr_2O_3 shows the linear ME effect even at room temperature which is a characteristic feature of this material.

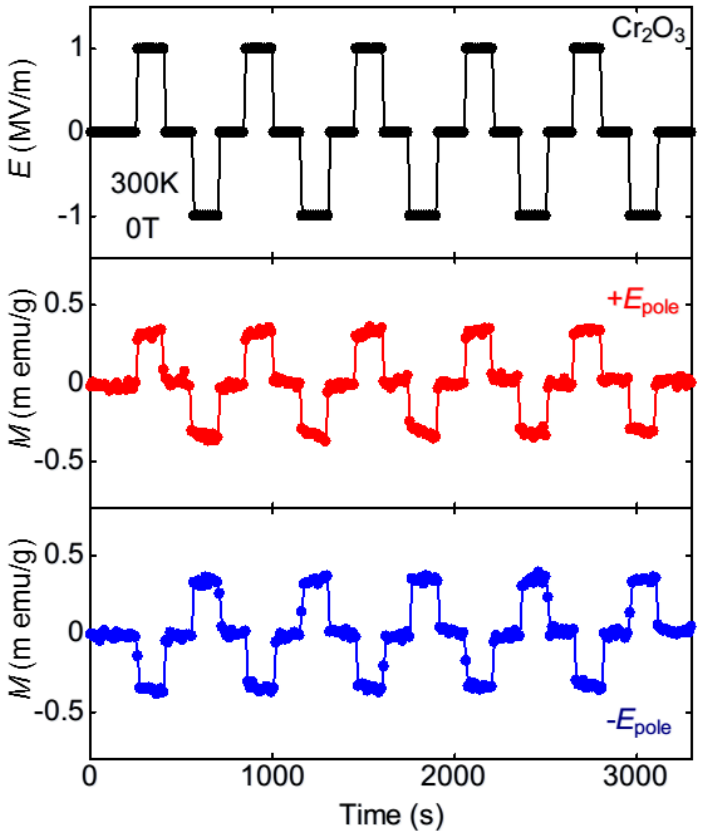

Figure 3-15: A magnetization switching by means of an electric field alone at room temperature.

Then, because the ME tensor is totally symmetric between electric and magnetic properties, ferromagnetic behaviors can be expected in the presence of *E*. Figure 3-16 describes temperature dependence of the magnetization in selected *E*. Although *M* is zero without applied *E*, *M* is finite in *E* below T_N, and the temperature dependence is similar to *P*-*T* curve in Figure 3-8.

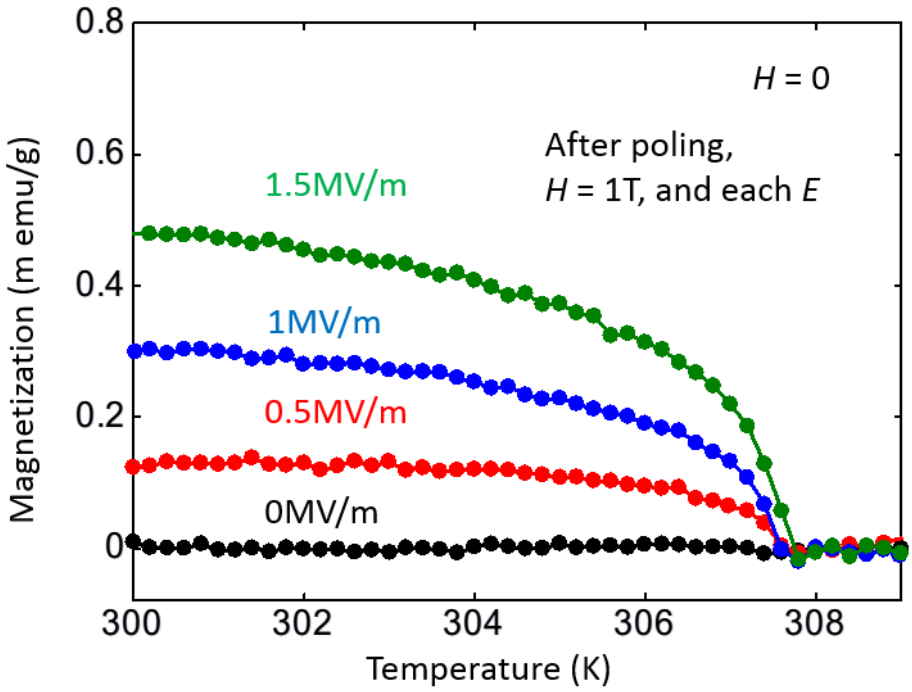

Figure 3-16: Temperature dependence of the magnetization in selected electric fields.

Here, the interest is how the induced *M* by *E* is interpreted in terms of multiferroics. Consequently, *H* dependence of the induced *M* was measured below and above T_N. The results are given in Figure 3-17. In the right panel, it is clear that the induced *M* reverses by sweeping *H* at 290 K, while the behavior disappears above T_N. Obvisouly, it is a ferromagnetic behavior, originating from the linear ME effect. The measurement protocol is follwing. First, the sample was cooled with E = 2.3 MV/m and m_0H = 1 T. Second, *M* was measured with applying *E* as a function of time. After 2 min, *E* was turned off, and subsequently, *M* was measured for the following 2 min. Here, the average and the standard deviation of *M* were obtained. The representative data are depicted in the left panels of Figure 3-17. Then, *E* was turned on again, and *H* was changed to the next point. In this way, the *M*-*H* hysteresis loop at room temperature was obtained.

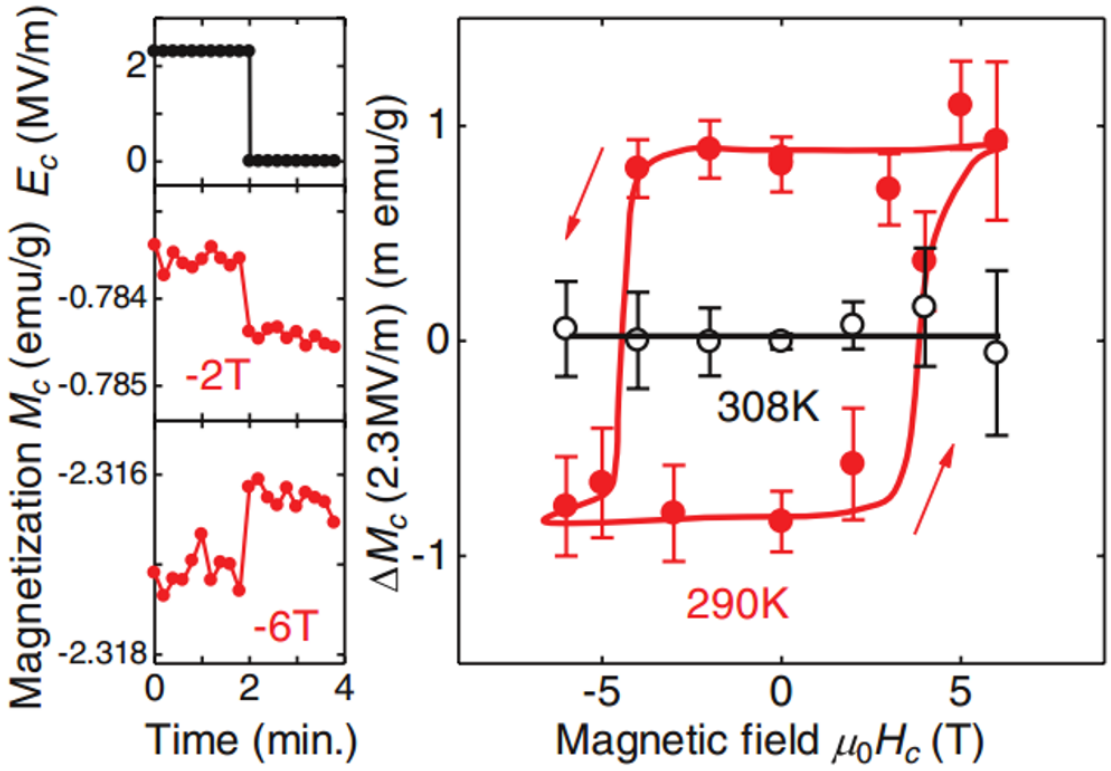

Figure 3-17: Magnetic field dependence of the induced magnetization by an electric field. The left panel is the raw data.

3.5 Discussion

From the experimental results, it has become evident that the linear ME compound Cr_2O_3 shows a ferroelectric behavior in H and a ferromagnetic behavior in E at room temperature.

First, the ferroelectric behavior is discussed in the context of that in a spin-driven multiferroic material in which the appearance of the ferroelectric polarization is ascribed to a development of the complex magnetic ordering such as spiral one. For example, the order parameter in one of the most famous spin-driven ferroelectric compounds, $TbMnO_3$, is the so-called vector spin chirality which resides in a noncollinear spin spiral order [35, 36]. That is to say, in spin-driven ferroelectrics, the order parameters inside the materials make them polar. On the other hand, in the linear ME compound Cr_2O_3, the order parameter inside the system G plus an external field H make it polar [14]. Based on the symmetry argument, this is the only difference between spin-driven ferroelectrics and the linear ME Cr_2O_3. As a consequence, in H, Cr_2O_3 shows a similar ferroelectric behavior to spin-driven ferroelectrics such as $TbMnO_3$ (pseudo-proper ferroelectricity in this case [37]). This is probably because H corresponds to the frozen order parameter S_3 which has been already ordered at high temperature, and G corresponds to the order parameter S_2 at the multiferroics phase transition (For the detail, see appendix 2) described in Ref. 37 which explains that ferroelectric P in $TbMnO_3$ is proportional to the order parameters S_2S_3. Indeed, temperature dependence of P in Cr_2O_3 behaves in a similar way to the pseudo-proper ferroelectricity in $TbMnO_3$ (not like an improper ferroelectricity in which P arises linearly with decreasing T, and ε has a step-type anomaly at the transition point because of the simultaneous activation of the two order parameters, contrary to the activation of only one order parameter of the two parameters in a pseudo-proper ferroelectricity [38]). In this way, the linear ME effect (and the behavior of ε near the phase transition point) is naturally and comprehensively understood. Note that it is difficult to naturally understand such behaviors (especially those of ε) in the context of a historical way in which the order parameter in the linear ME compound is α and the conjugate field is EH. Thus, it can be said that the new point of view is more versatile in order to understand the electric and magnetic properties in the linear ME materials.

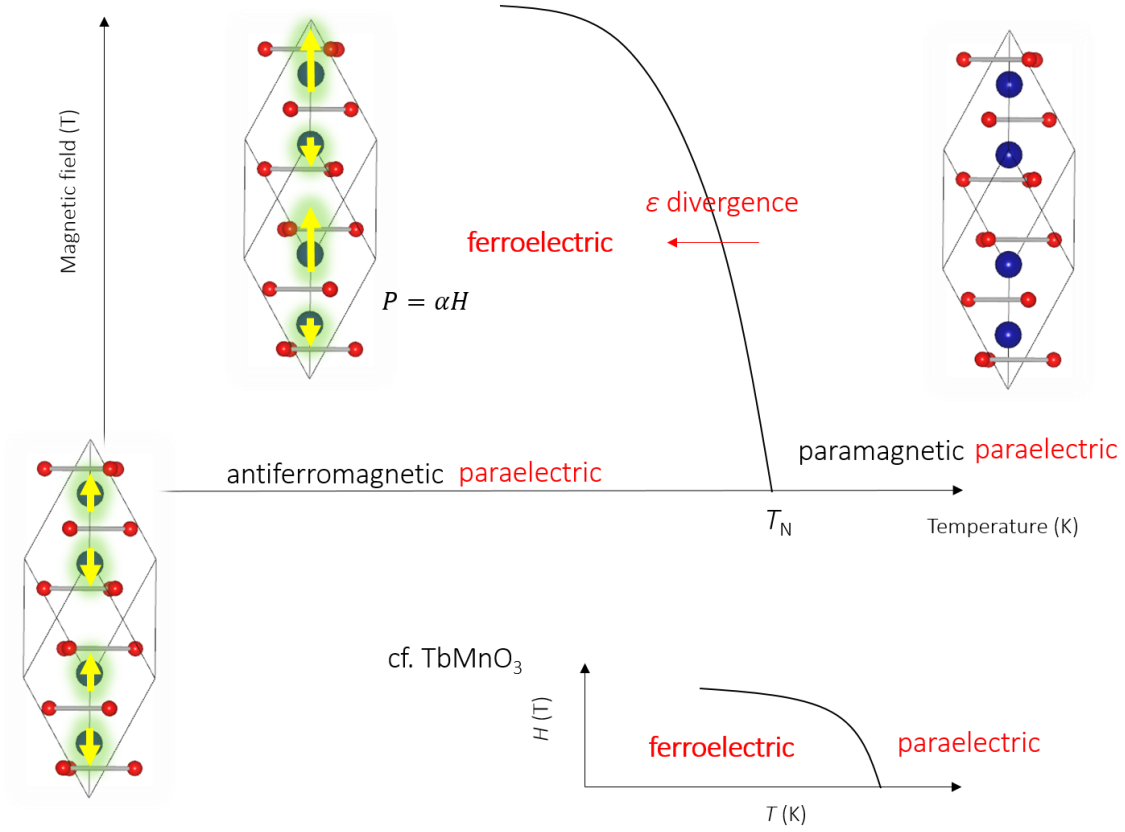

Figure 3-18: *H-T* phase diagram in Cr_2O_3 and in $TbMnO_3$. Each symmetry is given by Ref. 39.

In Figure 3-18, the *H-T* phase diagram in Cr_2O_3 is given. Above T_N, Cr_2O_3 is paraelectric and paramagnetic. In 0 T below T_N, Cr_2O_3 becomes antiferromagnetic but is still paraelectric (piezoelectric, strictly speaking). In contrast, in *H*, Cr_2O_3 becomes ferroelectric as clarified by the experiments. Therefore, in *H*, paraelectric-ferroelectric phase transition occurs at the transition point. Thus, a divergence of ε is observed near T_N. On the other hand, a phase diagram of multiferroic $TbMnO_3$ is described at the bottom panel, and there is no 'paraelectric' phase below the transition temperature. Note that, in this manner, it is expected that ε of other linear ME compounds such as $GaFeO_3$ whose crystal structure is polar [40] behaves in a different way compared with Cr_2O_3.

Next, the origin of the hysteresis loops is briefly discussed. In $TbMnO_3$, the sign of vector spin chirality determines the sign of ferroelectric *P*. On the other hand, in Cr_2O_3, the signs of *G* and *H* determine the sign of *P*. In the *P*-*E* measurement in Figure 3-9, *H* was applied and *E* was swept. When *P* is reversed, it should be accompanied by a reversal of *G*, as mentioned earlier, because *H* was fixed during the measurement. Consequently, the reversal of *G* induces a hysteresis, and the situation is the same in the *M*-*H* hysteresis measurement. This is, in fact, consistent with previous studies [33, 34] because ME domains are identical with antiferromagnetic domains in Cr_2O_3.

3.6 Perspectives

Perspectives on the linear ME effect are mentioned. Very recently, a ‘monopole’ scenario in the linear ME effect has been proposed in which the ME tensor is totally symmetric and diagonal [41, 42]. Cr_2O_3 is not suitable for this investigation because $\alpha_{\perp} \neq \alpha_{//}$ [43]. For the realization of such a material, it is predicted that a pyrochlore compound with an all-in-all-out magnetic order would be the candidate [44]. If such a material can be synthesized, it is possible to detect the ‘monopole’ with a resonant x-ray diffraction technique [45]. This ‘monopole’ physics is interesting in association with topological insulators [46, 47].

In terms of symmetry consideration of the linear ME effect, the linear ME compounds belong to a ‘secondary ferroic’ class [48, 49], contrary to a ‘primary ferroic’ class such as ferroelectric or ferromagnetic. For example, an order parameter of a ferroelectric is *P* and the conjugated field is *E*. On the other hand, an order parameter of a ferroelectromagnet (= the linear ME compound) is α and the conjugated field is *EH*. From experiments of this research, it has been revealed that the linear ME compound Cr_2O_3 shows ferromagnetic behaviors in *E*, and ferroelectric behaviors in *H*. Therefore, it is expected that other secondary ferroic classes such as piezoelectric and piezomagnetic should show the same physics with the linear ME compound. Thus, it is interesting to examine whether ferroelectric (ferromagnetic) behaviors are observed in piezoelectric (piezomagnetic) materials under uniaxial pressure (shear stress can be applied with a piston cylinder pressure cell by considering the direction of the uniaxial pressure). Furthermore, it would be more interesting that the same effect with pressure can be obtained by using a lattice mismatch in a thin-film sample. As a consequence, a thin-film piezoelectric material might become ferroelectric just by depositing to a substance with a different lattice constant.

3.7 Summary

The classical linear magnetoelectric (ME) effect in Cr_2O_3 was revisited by measuring its magnetocapacitance, electric polarization *P* induced by a magnetic field *H*, and magnetization *M* induced by an electric field *E*. The experiments reveal that the first ME material shows ferromagnetic behaviors in *E*, and ferroelectric behaviors in *H*, by properly confirming a λ-type anomaly in the dielectric constant at the Néel temperature and the hysteresis loops in *M*-*H* and *P*-*E* curves. The observed in-field ferroic nature in the linear ME compound is similar to that in some multiferroics such as spin-driven ferroelectrics, and can provide an appropriate contribution to a comprehensive understanding of the classical linear ME effect and recent studies on multiferroics.

Acknowledgements

The author thanks Y. Yamaguchi for his help in experiments. This work was supported by KAKENHI (Grant No. 24244058) and the Global COE Program (Program No. G10), MEXT, Japan.

Appendix

1 The microscopic origin of the linear ME effect in Cr_2O_3 at high temperature [10, 12, 14].

The microscopic origin of the linear ME effect in Cr_2O_3 is still under debate, however, the origin at high temperature has been almost clarified by the theoretical studies [10, 12, 14]. In this appendix, the origin is reviewed because current investigation on this thesis has focused on the high-temperature region.

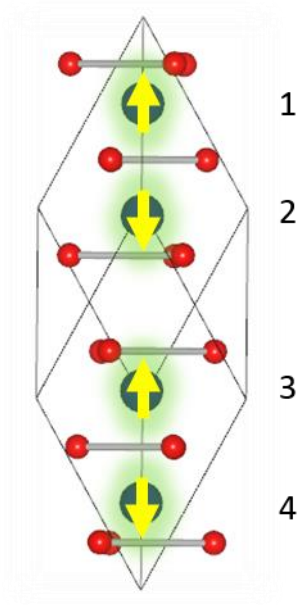

Figure 3-19: Crystal and magnetic structure of Cr_2O_3.

Figure 3-19 depicts the crystal and magnetic structure of Cr_2O_3 in the antiferromagnetic phase. When no H is applied, the magnetic symmetry is not polar, thus, no P exists. Then, let us consider the situation when H is applied. From the symmetry consideration [14], the symmetry of the induced P is described by coupling term of the spins as $S_1 \cdot S_3$ and $S_2 \cdot S_4$, not $S_1 \cdot S_2$ ($S_3 \cdot S_4$). Therefore, the intra-sublattice coupling is the source for inducing

P. In order to consider the intra-sublattice coupling, detailed crystal structure is described in Figure 3-20.

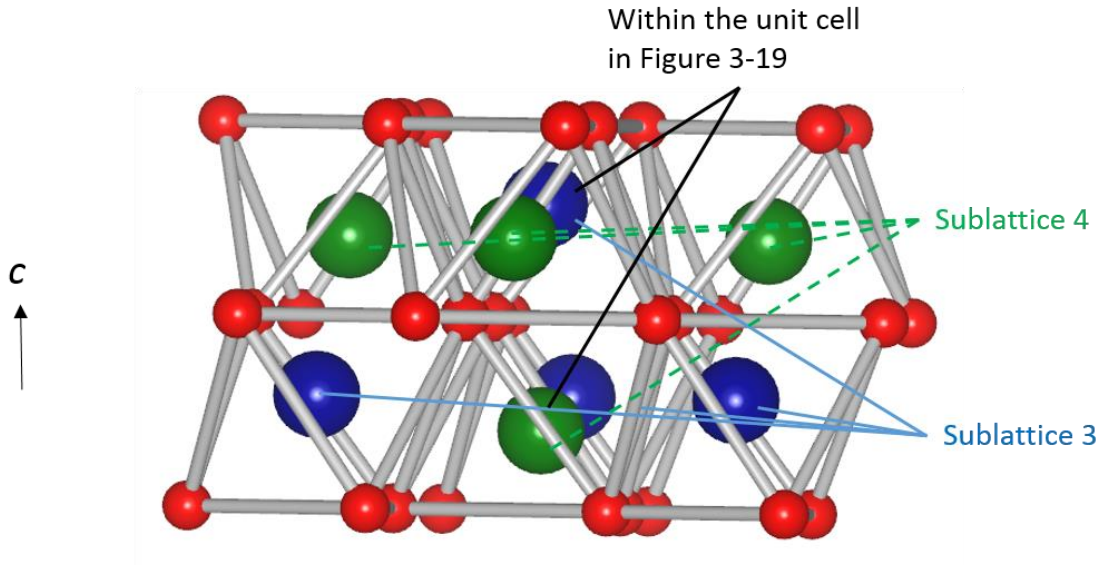

Figure 3-20: Crystal structure of Cr_2O_3 including next unit cells.

Each Cr^{3+} ion is surrounded by a distorted oxygen ocrahedron, and these octahedra are connected with shearing their faces along the *c* axis, and shearing their corners within each sublattice.

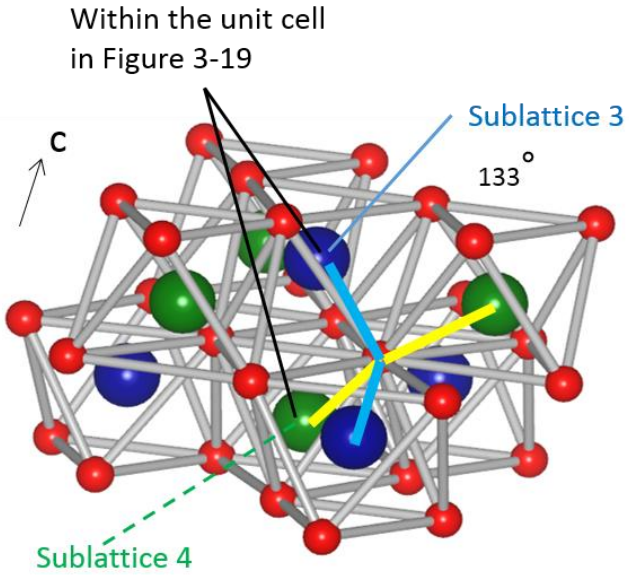

Figure 3-21: Slightly different angle view of Figure 3-20.

Then, the bond angle θ of intra-sublattice coupling is 133°, and the distance is 3.65 Å. Thus, the intra-sublattice coupling is via super-exchange interaction, and the interaction causes the ferromagnetic coupling. The point is that this intra-sublattice coupling is through the same oxygen as clearly seen in Figure 3-21. When *H* is applied, magnetic moments of one sublattice (sublattice 3, for instance) elongate via thermal fluctuation of the spins, and magnetic moments of the other sublattice (sublattice 4) shrink. In this stage, there is more energy gain if the oxygen moves to one direction in order to increase the overlap of the sublattice 3 coupling and decrease the overlap of the sublattice 4 coupling because sublattice 3 coupling with elongated moments is more important than sublattice 4 coupling with shrunk moments. In this way, oxygen layers eventually move to the *c* axis relative to the Cr layers, and this results in the macroscopic electric polarization parallel to *H* along the *c* axis.

Importantly, this explanation can also be applied to the inverse effect because when *E* is applied along the *c* axis, the oxygen layers shift relative to the Cr layers. Then, as the overlap of the sublattice 3 increases and the overlap of the sublattice 4 decreases, the magnetic moments in sublattice 3 elongate and the magnetic moments in sublattice 4 shrink via the thermal fluctuation. Thus, the macroscopic magnetization appears parallel to *E* along the *c* axis. This mutual explanation has not clearly mentioned in the previous studies, however, this mechanism naturally explains the microscopic origin of the linear ME effect in Cr_2O_3 except at low temperature because the thermal fluctuation plays an important role.

2 The pseudo-proper ferroelectricity in $TbMnO_3$ and its relation with Cr_2O_3 [37].

In the discussion session, similarity of the order parameters in $TbMnO_3$ and those in Cr_2O_3 was discussed. In this appendix, the details are explained.

$TbMnO_3$ shows successive phase transitions at 41 K and 27 K, and 7K [50]. At 41 K, a sinusoidal order of the Mn moments occurs, and at 27 K, a cycloidal spin order occurs and a ferroelectric polarization appears [50, 51].

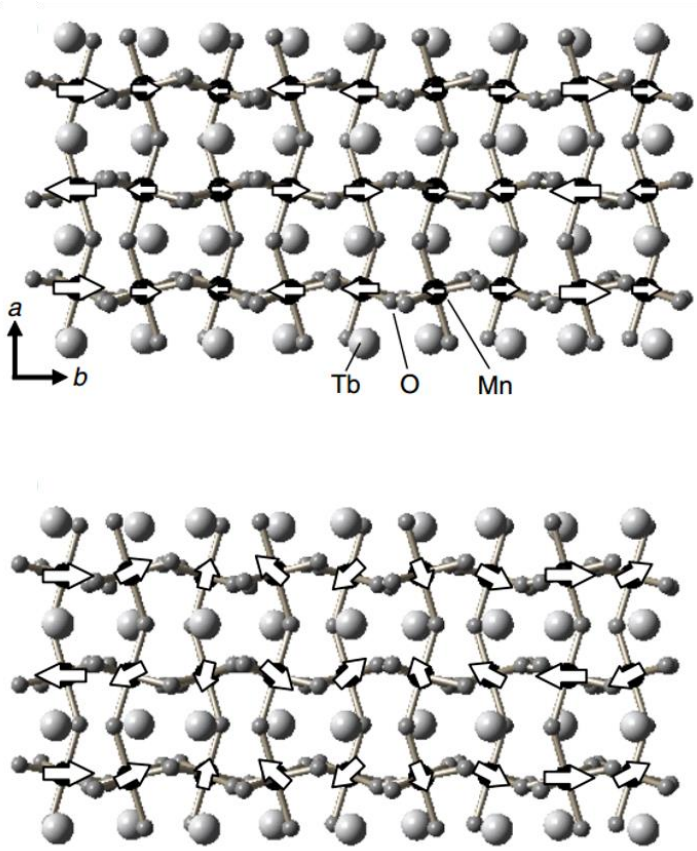

Figure 3-22: A sinusoidal (the upper) and a cycloidal (the lower) spin ordering in $TbMnO_3$ [52].

According to the symmetry consideration [37], one spin order parameter S_3 orders at 41 K. At 27 K, another spin order parameter S_2 orders. Then, the ferroelectric polarization P is proportional to S_2S_3. Naively, because $P \propto S_2S_3$, improper ferroelectric behavior is expected where P depends on temperature as $P \propto (T_{\mathrm{order}} - T)^{-1}$, rather than $(T_{\mathrm{order}} - T)^{-1/2}$, and the dielectric constant shows a step-like anomaly, rather than a divergence. However, this picture is inconsistent with experiments [50]. This discrepancy is revised by considering that S_3 is not an active order parameter at 27 K, but it is almost frozen because S_3 has already ordered at 41 K. Thus, P is effectively proportional to S_2, and S_3 is like a constant. Hence, P depends on temperature as $(T_{\mathrm{order}} - T)^{-1/2}$, and the dielectric constant shows a divergence-type anomaly. This is called 'pseudo-proper' ferroelectric, and consistent with the experiments.

As for Cr_2O_3, P is proportional to M_cG_c where M_c is a magnetization induced by H and G_c is staggered magnetization which is the order parameter of an antiferromagnet [14]. Comparing $P \propto M_cG_c$ in Cr_2O_3 with $P \propto S_2S_3$ in $TbMnO_3$, it can be considered that G_c corresponds to S_2 which is an active order parameter, and M_c corresponds to S_3 which is a frozen order parameter. In this way, it is expected that Cr_2O_3 behaves as a pseudo-proper ferroelectric in the presence of H, and because this picture is consistent with experiments on this thesis, it is concluded that multiferroic $TbMnO_3$ and the linear ME Cr_2O_3 can be comprehensively understood.

3 Magnetization measurement

The results of the magnetization measurement are shown in Figure 3-23. The temperature dependence of the magnetization of the investigated sample is typical for an antiferromagnet with its spin parallel to the *c* axis. The ordering temperature is ~ 307 K which is consistent with previous studies. Curie-like tail at low temperature is probably originating from a small amount of isolated Cr^{3+} spins in the sample.

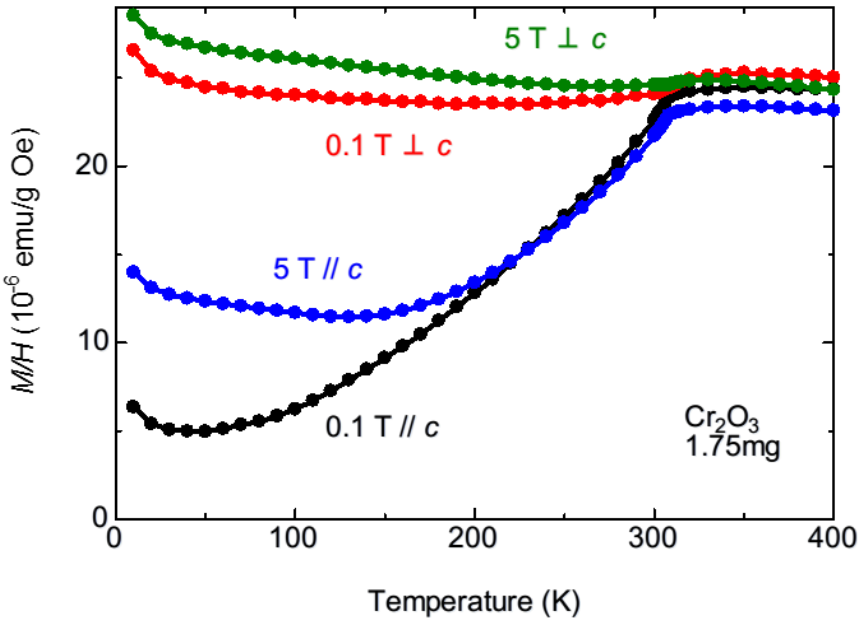

Figure 3-23: Magnetization versus temperature in Cr_2O_3.

References

[1] B. N. Brockhouse, J. Chem. Phys. **21**, 961 (1953).

[2] T. R. McGuire, E. J. Scott, and F. H. Grannis, Phys. Rev. **102**, 1000 (1956).

[3] I. Dzyaloshinsky, J. Phys. Chem. Solids **4**, 241 (1958).

[4] I. E. Dzyaloshinskii, Sov. Phys. JETP **10**, 628 (1960).

[5] H. Schmid, J. Phys.: Condens. Matter **20**, 434201 (2008).

[6] D. N. Astrov, Sov. Phys. JETP **11**, 708 (1960).

[7] D. N. Astrov, Sov. Phys. JETP **13**, 729 (1961).

[8] V. J. Folen, G. T. Rado, and E. W. Stalder, Phys. Rev. Lett. **6**, 607 (1961).

[9] G. T. Rado, Phys. Rev. Lett. **6**, 609 (1961).

[10] M. Date, J. Kanamori, and M. Tachiki, J. Phys. Soc. Jpn. **16**, 2589 (1961).

[11] S. Alexander and S. Shtrikman, Solid State Commun, **4**, 115 (1966).

[12] R. Hornreich and S. Shtrikman, Phys. Rev. **161**, 506 (1967).

[13] J. Íñiguez, Phys. Rev. Lett. **101**, 117201 (2008).

[14] M. Mostovoy, A. Scaramucci, N. A. Spaldin, and K. T. Delaney, Phys. Rev. Lett. **105**, 087202 (2010).

[15] E. Bousquet, N. A. Spaldin, and K. T. Delaney, Phys. Rev. Lett. **106**, 107202 (2011).

[16] A. Malashevich, S. Coh, I. Souza, and D. Vanderbilt, Phys. Rev. B **86**, 094430 (2012).

[17] A. Scaramucci, E. Bousquet, M. Fechner, M. Mostovoy, and N. A. Spaldin, Phys. Rev. Lett. **109**, 197203 (2012).

[18] T. Birol, N. A. Benedek, H. Das, A. L. Wysocki, A. T. Mulder, B. M. Abbett, E. H. Smith, S. Ghosh, and C. J. Fennie, Curr. Opin. Solid State Mater Sci. **16**, 227 (2012).

[19] E. Kita, A. Tasaki, and K. Siratori, Jpn. J. Appl. Phys. **18**, 1361 (1979).

[20] Y. F. Popov, A. M. Kadomtseva, D. V. Belov, G. P. Vorob'ev, and A. V. Zvezdin, JETP Lett. **69**, 330 (1999).

[21] P. Borisov, A. Hochstrat, V. V. Shvartsman, and W. Kleeman, Rev. Sci. Instrum. **78**, 106105 (2007).

[22] M. Fiebig, D. Frohlich, B. B. Krichevtsov, and R. V. Pisarev, Phys. Rev. Lett. **73**, 2127 (1994).

[23] B. B. Krichevtsov, V. V. Pavlov, R. V. Pisarev, and V. N. Gridnev, Phys. Rev. Lett. **76**, 4628 (1996).
[24] P. H. Fang and W. S. Brower, Phys. Rev. **129**, 1561 (1963).
[25] H. B. Lal, R. Srivastava, and K. G. Srivastava, Phys. Rev. **154**, 505 (1967).
[26] A. A. Samokhvalov, Sov. Phys. Solid State **3**, 2613 (1962).
[27] X. He, Y. Wang, N. Wu, A. N. Caruso, E. Vescovo, K. D. Belashchenko, P. A. Dowben, and C. Binek, Nat. Mater. **9**, 579 (2010).
[28] W. Echtenkamp and Ch. Binek, Phys. Rev. Lett. **111**, 187204 (2013).
[29] A. Iyama and T. Kimura, Phys. Rev. B **87**, 180408 (R) (2013).
[30] G. Garton, S. H. Smith, and B. M. Wanklyn, J. Cryst. Growth **13-14**, 588 (1972).
[31] T. Kimura, S. Kawamoto, I. Yamada, M. Azuma, M. Takano, and Y. Tokura, Phys. Rev. B **67**, 180401(R) (2003).
[32] E. J. Samuelsen, M. T. Hutchings, and G. Shirane, Physica **48**, 13 (1970).
[33] T. J. Martin and J. C. Anderson, IEEE Trans. Magn. **2**, 446 (1966).
[34] C. A. Brown and T. H. O'Dell, IEEE Trans. Magn. **5**, 964 (1969).
[35] M. Mostovoy, Phys. Rev. Lett. **96**, 067601 (2006).
[36] A. Raeliarijaona, S. Singh, H. Fu, and L. Bellaiche, Phys. Rev. Lett. **110**, 137205 (2013).
[37] P. Tolédano, Phys. Rev. B **79**, 094416 (2009).
[38] J. C. Tolédano and P. Tolédano, *The Landau theory of phase transitions*, World Scientific (1987).
[39] I. M. Vitebskii, Sov. J. Low Temp. Phys. **7**, 686 (1981).
[40] G. T. Rado, Phys. Rev. Lett. **13**, 335 (1964).
[41] N. A. Spaldin, M. Fechner, E. Bouaquet, A. Balatsky, and L. Nordström, Phys. Rev. B **88**, 094429 (2013).
[42] D. Khomskii, arXiv:1307.2327 (2013).
[43] F. W. Hehl, Y. N. Obukhov, J.-P. Rivera, and H. Schmid, Phys. Lett. A **372**, 1141 (2008).
[44] S. Coh and D. Vanderbilt, Phys. Rev. B **88**, 121106(R) (2013).
[45] S. W. Lovesey and D. D. Khalyavin, J. Phys. Soc. Jpn. **82**, 103703 (2013).
[46] M. Z. Hasan and C. L. Kane, Rev. Mod. Phys. **82**, 3045 (2010).
[47] Y. Ando, J. Phys. Soc. Jpn. **82**, 102001 (2013).
[48] R. E. Newnham and L. E. Cross, Mat. Res. Bull. **9**, 927 (1974).
[49] R. E. Newnham and L. E. Cross, Mat. Res. Bull. **9**, 1021 (1974).
[50] T. Kimura, T. Goto, H. Shintani, K. Ishizuka, T. Arima, and Y. Tokura, Nature **426**, 55 (2003).

[51] M. Kenzelmann, A. B. Harris, S. Jonas, C. Broholm, J. Schefer, S. B. Kim, C. L. Zhang, S.-W. Cheong, O. P. Vajk, and J. W. Lynn, Phys. Rev. Lett. **95**, 087206 (2005).

[52] T. Kimura and Y. Tokura, J. Phys.: Condens. Matter **20**, 434204 (2008).

Chapter 4

The magnetoelectric effect in $FeSb_2O_4$ single crystals

4.1 Introduction

This chapter describes that $FeSb_2O_4$ shows the linear ME effect contrary to an expectation from the magnetic symmetry which indicates that this material is spin-driven ferroelectric. This chapter is organized as follows. First, previous studies in $FeSb_2O_4$ are introduced in which the crystal and magnetic structures are also explained. After denoting the purpose of this study, the experimental results are provided. Then, validity of the results is discussed. Finally, perspectives on this material are given.

4.2 Previous studies on $FeSb_2O_4$

$FeSb_2O_4$ has a tetragonal crystal structure with the space group $P4_2/mbc$. Fe^{2+} ions are surrounded by distorted oxygen octahedra. This oxygen octahedron is connected along the *c* axis, shearing its edge and the distance between Fe^{2+} ions is about 3 Å. On the contrary, this oxygen octahedron is not directly connected in the *ab*

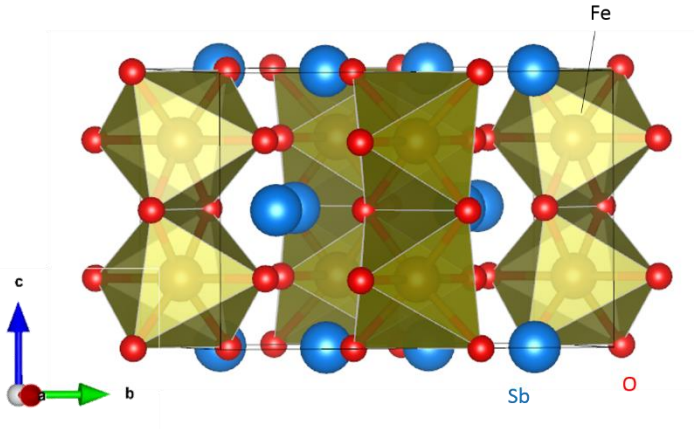

Figure 4-1: Crystal structure of $FeSb_2O_4$. The axes are in the tetragonal notation.

plane, and the distance between the nearest Fe^{2+} ions in the plane is approximately 6 Å. Thus, it can be said that this crystal structure is quasi-1 dimensional. As for the magnetism, the magnetic structure was proposed by means of neutron scattering with powder samples [1]. According to the results, the magnetic symmetry is $Pmc2_1$ with the spin component of $A_aG_bC_c$ (in the tetragonal setting) in complete analogy with the perovskites. Therefore, the linear magnetoelectric (ME) effect is expected [2]. After the neutron experiment, the linear ME effect was observed with powder samples as well [3]. This experiment revealed that below the Néel temperature $T_N \sim 46$ K, the ME tensor α becomes finite, as expected by the magnetic symmetry. There was no investigation with single crystals.

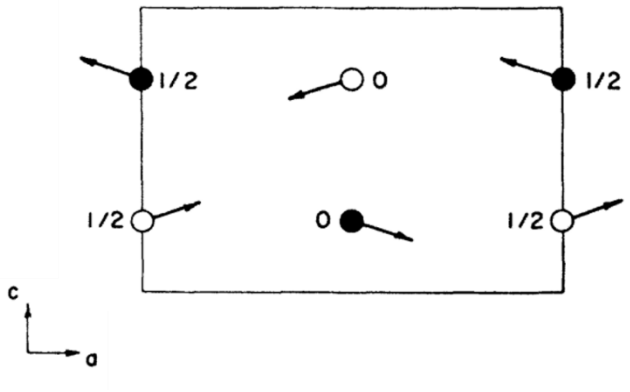

Figure 4-2: Proposed magnetic structure of $FeSb_2O_4$ [1].

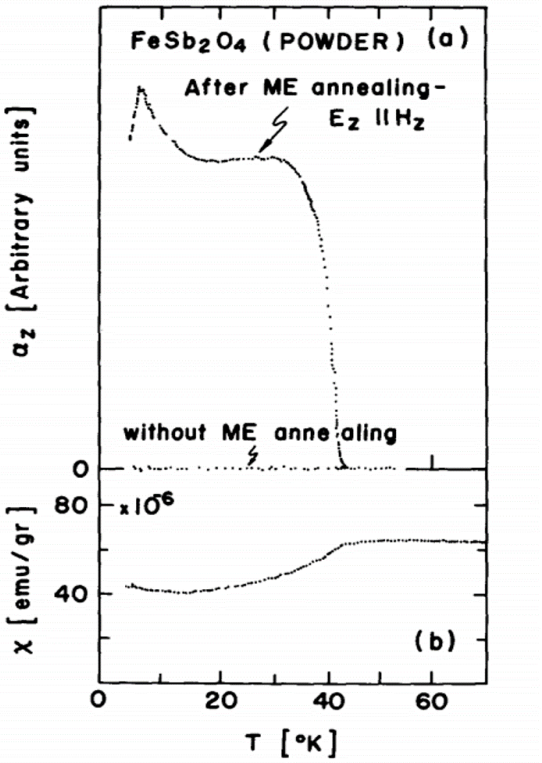

Figure 4-3: Temperature dependence of the ME tensor [3].

4.3 The purpose of this study

From the current standpoint, this material is a spin-driven ferroelectric because $P4_2/mbc$ is centrosymmetric and $Pmc2_1$ is polar. In this sense, its magnetism should lead to ferroelectricity in this compound [4,5]. Therefore, it is expected that a spontaneous electric polarization P is observed along the b axis in the tetragonal setting. Furthermore, the investigation of the linear ME effect in single-crystalline samples is beneficial for checking whether the proposed magnetic structure is correct because the ME tensor is determined by the magnetic symmetry. Hence, the purpose of this study is to measure the linear ME effect of this material with single crystals, and to check whether the above scenario is correct or not.

4.4 Experimental results

The experimental results of this study are given in this section [6]. $FeSb_2O_4$ single crystals were grown by the hydrothermal method [7]. Appropriate amount of $FeC_2O_4 \cdot 2H_2O$ and Sb_2O_3 were put into a silver tube with 5 % NaOH as a solvent. The growth condition was 500 °C and 1000 kg/cm^2, and the reaction time was 96 h. The frequently obtained samples were dark-reddish-brown-colored needle-shaped with bottom faces, and the typical dimension was 80 μm × 80 μm × 1 mm, as shown in Figure 4-4. By-product materials were transparent yellow-colored Sb_2O_3 with needle-shaped as well. Quality of the samples was checked by single-crystalline x-ray diffraction which confirmed that obtained samples were single crystals with the lattice constants of $a = b = 8.619(10)$ Å, and $c = 5.884(11)$ Å. The crystallographic axes were determined by using a four-circle diffractometer. The long direction of the crystals was along the c axis. For measurements of the dielectric properties, silver paint was put as electrodes. The dielectric constant ε was measured with an LCR meter, and P was obtained by integrating pyroelectric current with sweeping temperature. Magnetization M was measured with a commercial vibrating sample magnetometer. The notation of the axes is tetragonal setting through this chapter.

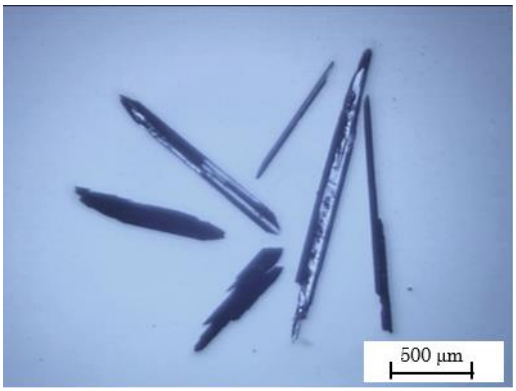

Figure 4-4: Obtained single crystals of $FeSb_2O_4$.

First, in order to check whether the obtained single crystals were $FeSb_2O_4$, M was measured along and perpendicular to the c axis as shown in Figure 4-5. As previously reported, an antiferromagnetic ordering occurs at $T_N \approx 43$ K with a cusp of M both along the a and c axes. The cusp of M_a was more significant than that of M_c, which is consistent with the proposed magnetic structure with the Bertaut notation $A_aG_bC_c$ with a major component of A_a [1, 8]. As lowering temperature, M turned into upward approximately below 20 K, indicating the presence of small amount of magnetic impurity. In fact, a ferromagnetic-like behavior was seen around 0 T in the M-H curve at 30 K (not shown). This magnetic impurity is likely to be Fe_3O_4, as observed in powder and single-crystalline samples in the previous studies [1, 7], and to adhere to the surface of this sample.

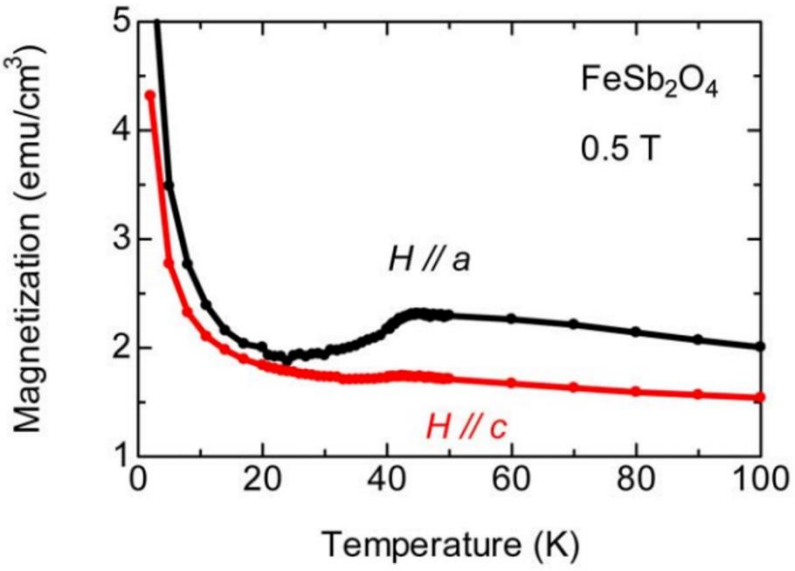

Figure 4-5: Temperature dependence of the magnetization along and perpendicular to the c axis.

The upturn of the magnetization at low temperature is likely originating from isolated spins of Fe^{2+} and Fe^{3+} ions. In order to roughly estimate the amount of such spin contributions, fitting was done by the Curie law below 20 K, and the result is described in Figure 4-6. As a consequence, the amount of the isolated spins is a few percent of the total spins in this sample. Such amount seems to be related to the instability of Fe^{2+} ions in this compound, as Fe_3O_4 was clearly seen in powder and single-crystalline samples.

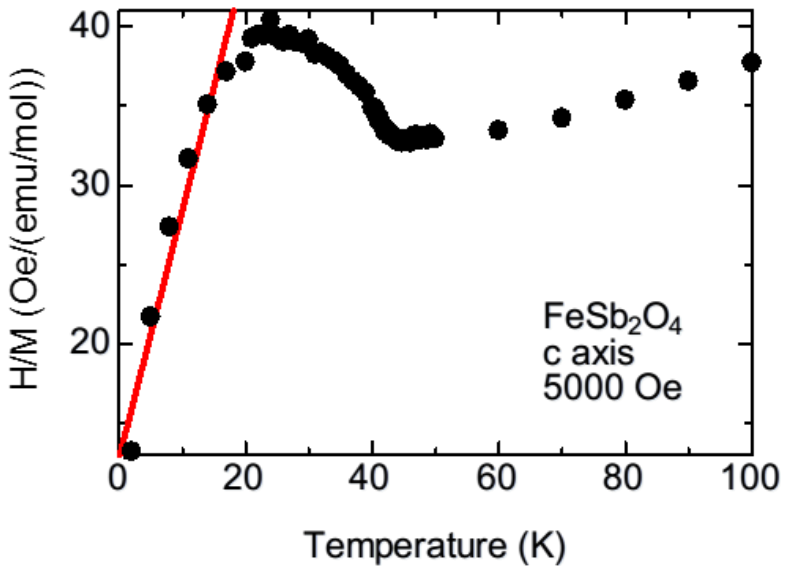

Figure 4-6: Fitting by the Curie law of the magnetization curve at low temperature.

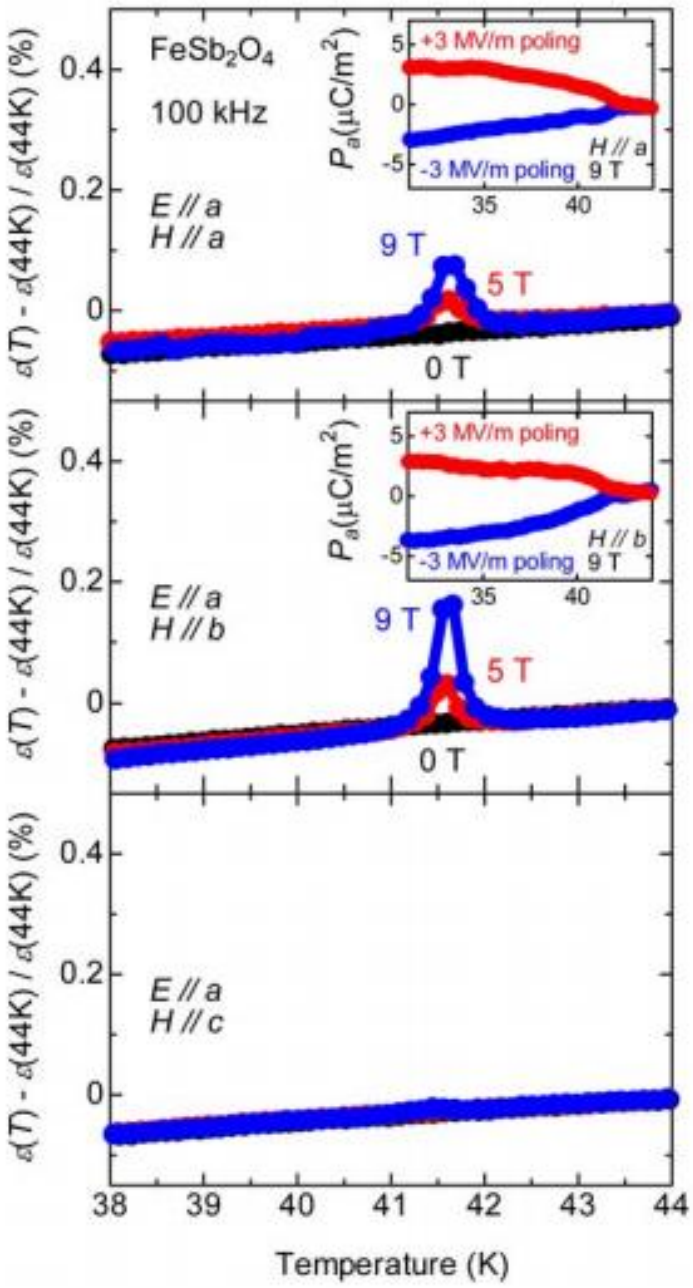

Figure 4-7: Dielectric constant and electric polarization along the *a* axis. The dielectric constant was measured with f = 100 kHz.

Next, ε and P along the a axis were measured which corresponds to the polar axis according to the proposed magnetic symmetry in the antiferromagnetic phase as depicted in Figure 4-7. ε has no anomaly in this temperature range in 0 T, indicating that there is no ferroelectric phase transition or ferroelectric polarization is negligibly small without magnetic field H although there are domains due to the lowering of the symmetry from the tetragonal to the orthorhombic structure. On the other hand, a sharp peak in ε appears with H normal to the c axis at T_N, and the peak becomes more significant with increasing H. Finite P was observed below T_N only when H was applied normal to the c axis, and the modulus is several $\mu C/m^2$. As will be discussed later, it is concluded that these signals are due to misalignment.

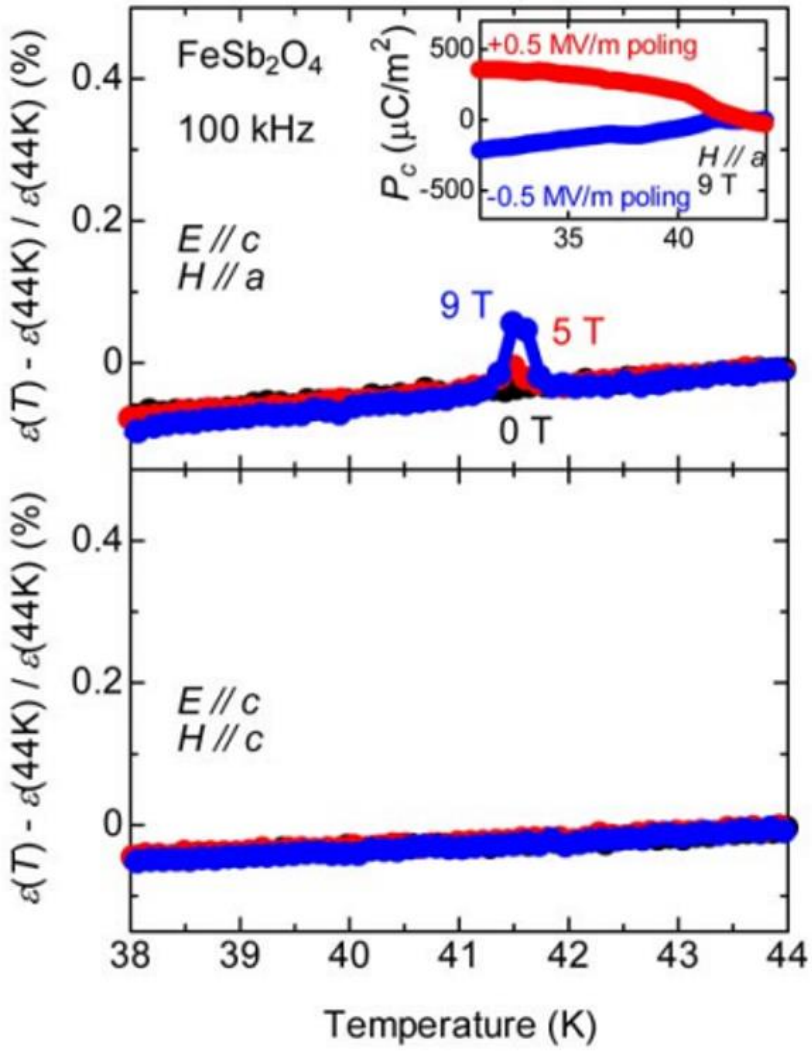

Figure 4-8: Dielectric constant and electric polarization along the c axis. The dielectric constant was measured with f = 100 kHz.

Finally, ε and P along the c axis were measured as shown in Figure 4-8. ε has no anomaly in this temperature range without H, however, a sharp peak in ε appears with H normal to the c axis. This type of anomaly in ε has been seen in some linear ME compounds, which suggests that P is finite with an applied H [9, 10]. Because the samples were needle-shaped with the longitudinal axis along c, the area of electrodes was small (90×90 μm^2) for the E // c measurements, raising concern that the anomalies might be underestimated. Reflecting the anomalies, finite P arises below T_N only when H is applied perpendicular to the c axis. The absolute value of P induced by H of 9 T was approximately 300 $\mu C/m^2$ which is some 100 times larger than P measured along the a axis, meaning that P_a was probably due to misalignment. The ME tensor is estimated to be 42.1 ps/m at 31 K, which is larger than typical linear ME materials [9, 11].

4.5 Discussion

The experimental results of this study revealed that P along the c axis is finite below T_N in an applied H normal to the c axis. This is consistent with the magnetic symmetry *m2m* with the ME tensor as [12]

$$P = \begin{pmatrix} 0 & 0 & \alpha_{13} \\ 0 & 0 & 0 \\ \alpha_{31} & 0 & 0 \end{pmatrix} H$$

with a tiny spontaneous P along the b axis. Naively, because the magnetic structure is commensurate, the microscopic origin of the spontaneous P is expected to be the exchange-striction mechanism which is independent of the spin-orbit interaction, inducing large P [13]. However, the distance between neighboring Fe^{2+} chains is relatively large (≈ 6 Å), and the magnetic coupling between the chains is mediated via Fe-O-O-Fe super-super exchange interaction. This means that large exchange striction cannot be expected within the *ab* plane, which is apparently related to the smallness of the spontaneous P. Figure 4-9 shows the schematic pictures of the super-super exchange path between the neighboring Fe^{2+} chains. As the main component is A_a, this super-super exchange interaction leads to a ferromagnetic coupling, which may be understood by considering that this super-super exchange path is mediated by the (almost) orthogonal e_g orbitals of the two Fe^{2+} ions (elongation direction of the octahedra is staggered in the *ab* plane, causing a staggered dz^2 orbitals, for example, which makes the super-super exchange interaction via the two dz^2 orbitals unlikely). As for the super-super exchange interaction, see for instance ref. 14. Then, as lowering the symmetry, position of the Fe^{2+} ions becomes general (x, y, z) from x = 1/4, y = 1/4, and z = 1/2 in the tetragonal phase [1]. Thus, Fe^{2+} ions can move in order to stabilize the magnetic interaction, including the super-super exchange interaction. However, it is difficult to stabilize the super-super exchange interaction further because move to one direction causes stabilization of one path and destabilization of the other paths by considering the overlap between Fe and O ions. Consequently, it is understood that the spontaneous P is tiny in this compound. This argument can also be applied to the small α_{13}. On the other hand, Fe^{2+} ions along the c axis are directly linked, and the distance between the neighboring Fe^{2+} ions is about 3 Å. When H is applied along the a axis, mirror symmetry between the two Fe^{2+} and the 2-fold

screw axis are broken, and *P* can appear along the *c* axis as depicted in Figure 4-10. Note that the microscopic origin can be explained with the same theory for Cr_2O_3 [15, 16] because the situation in $FeSb_2O_4$ is quite similar to that in the famous linear ME compound Cr_2O_3.

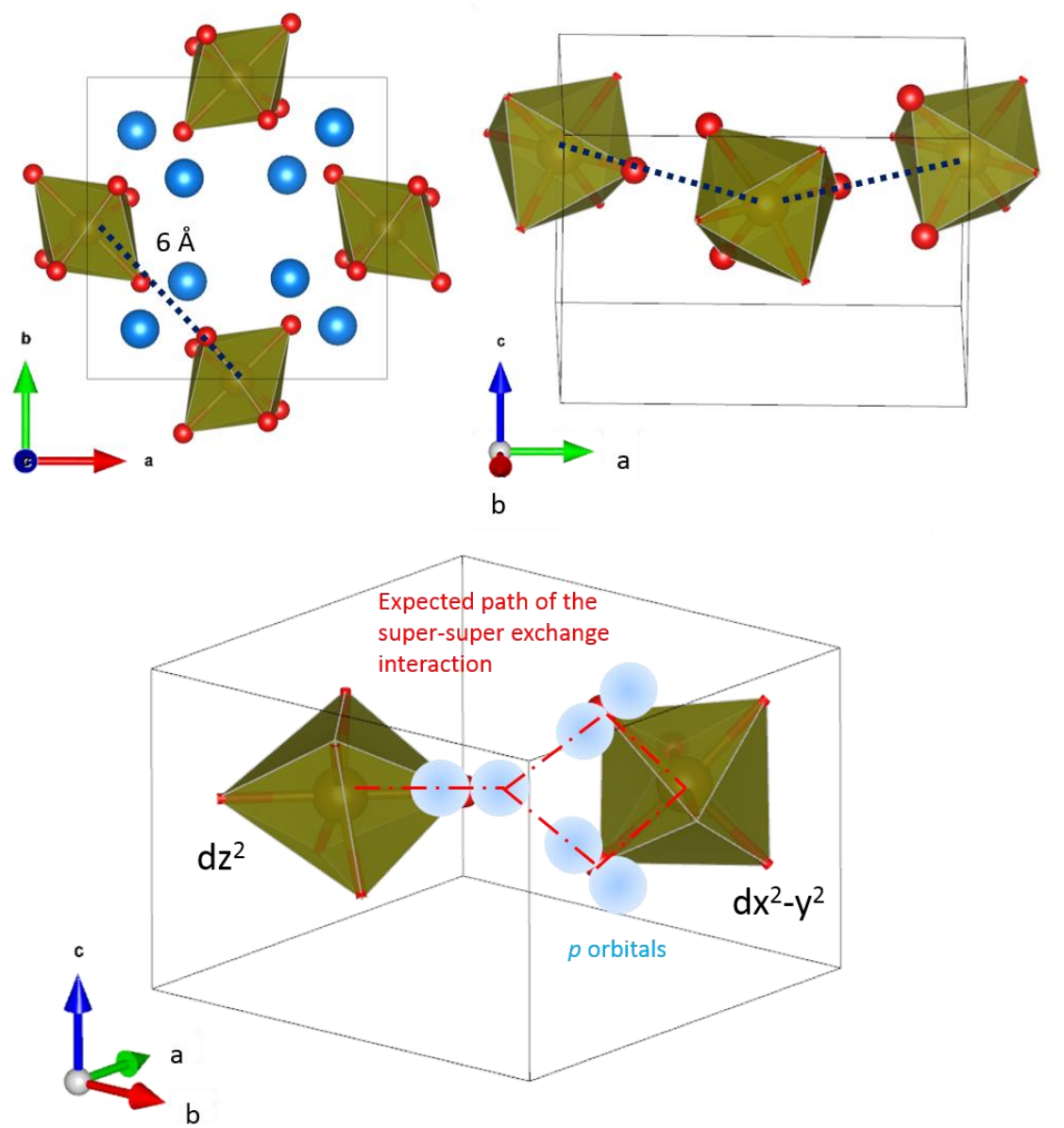

Figure 4-9: Super-super exchange interaction between Fe^{2+} neighboring chains. This path is the shortest one connecting the two Fe^{2+} ions in the *ab* plane.

$$P = \begin{pmatrix} 0 & 0 & \alpha_{13} \\ 0 & 0 & 0 \\ \alpha_{31} & 0 & 0 \end{pmatrix} H$$ (polar axis is b)

The spontaneous *P* was not detected.

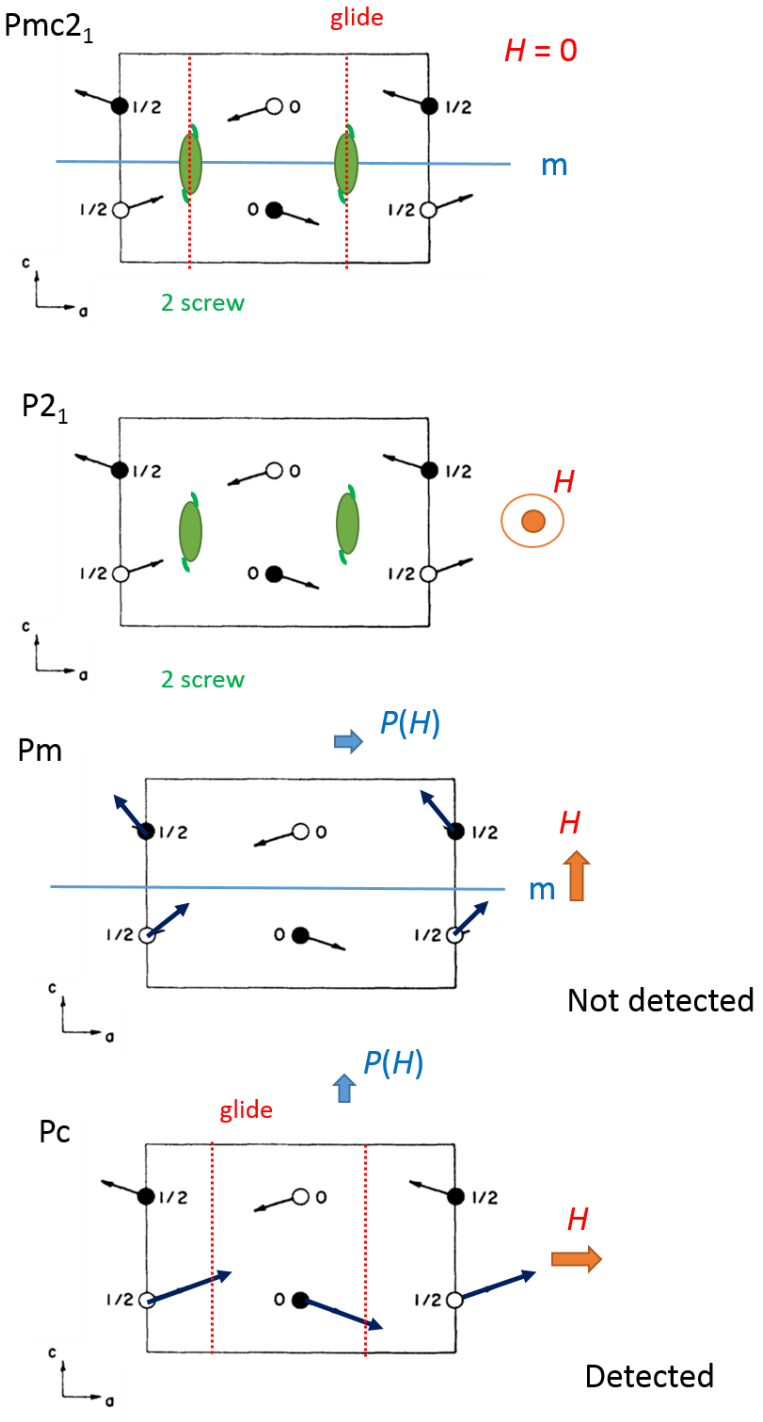

Figure 4-10: Symmetry consideration in the orthorhombic phase in $FeSb_2O_4$ with an applied magnetic field. (tetragonal setting)

4.6 Perspectives

Perspectives on this compound are mentioned. First, the magnetic point group *m2m* allows ferrotoroidal ordering with the toroidal moment *T* [18] along the *b* axis, which is parallel to the spontaneous *P* [12], which is a rare characteristic feature among the ME materials. This toroidal domain is identical by symmetry with the antiferromagnetic domain, which is also identical, therefore, to the ME domain and *P* domain. Thus, the toroidal moment can be switched by means of an electric field. In addition, 90° flop of *P* is possible in this compound by applying external *E* in association with a flop of the spins because the *b* axis in the tetragonal setting becomes the polar axis in the antiferromagnetic phase. Consequently, it is also possible to flop *T* by an external *E*. Putting the above discussions all together, not only 90° switching but also 180° switching of *T* by applying *E* is possible and would be interesting in $FeSb_2O_4$. Furthermore, related to the ferrotoroidal order, magneto-optic effects can be expected such as x-ray non-reciprocal directional dichroism [19] or non-reciprocal refraction [20], and it would be interesting to compare with ferrotoroidic $GaFeO_3$ which has a macroscopic magnetization in the absence of *H*.

Finally, this kind of the material AB_2O_4 where *A* is the transition metal and *B* = (Sb, As, Bi) can be synthesized by the hydrothermal method [7, 21], however, there are few reports [22, 23] on their properties so far, especially with using single-crystalline samples. Thus, there might be intriguing physical properties in this materials group.

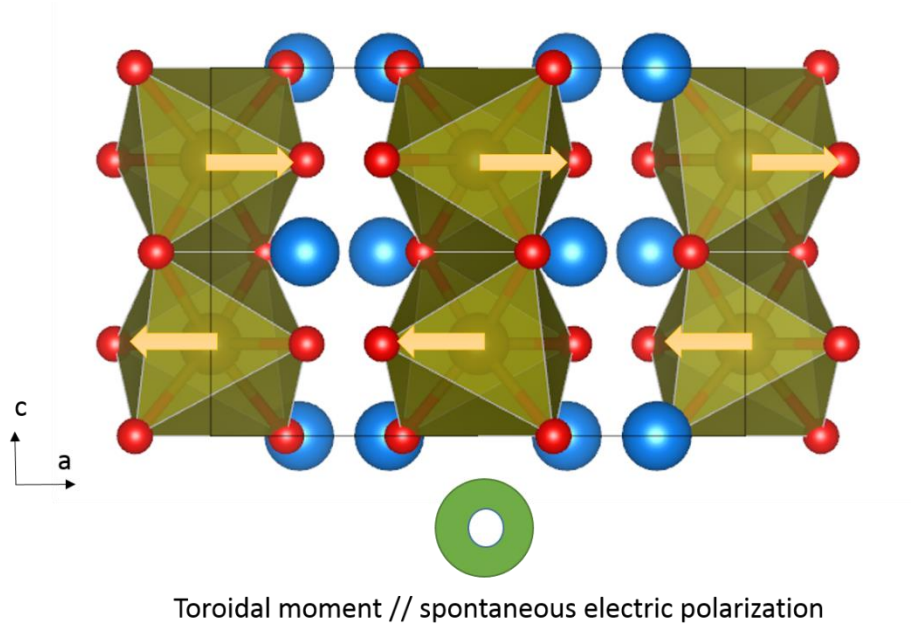

Figure 4-11: Toroidal moment parallel to the spontaneous electric polarization in $FeSb_2O_4$.

4.7 Summary

The magnetoelectric properties in single-crystalline $FeSb_2O_4$ were studied. Single crystals of $FeSb_2O_4$ were successfully grown by means of the hydrothermal method, and the anisotropy in the magnetization, the dielectric constant, and the magnetoelectric effect were measured. It was found that the experimental results are essentially explained by considering the magnetic space group $Pmc2_1$. The present results also demonstrate that the hydrothermal synthesis method can be useful to synthesize new magnetoelectric single crystals.

Acknowledgements

The author thanks N. Hanasaki, N. Sawai and T. Honda for their support in experiment for hydrothermal synthesis, and K. Kimura for fruitful discussions. This work was supported in part by Grants-in-Aid for Scientific Research (Grants No. 24244058) from the Japan Society for the Promotion of Science.

References

[1] J. A. Gonzalo, D. E. Cox, and G. Shirane, Phys. Rev. **147**, 415 (1966).

[2] R. M. Hornreich, Solid State Commun. **7**, 1081 (1969).

[3] G. Gorodetsky, M. Sayar, and S. Shtrikman, Mat. Res. Bull. **5**, 253 (1970).

[4] S. Goshen, D. Mukamel, H. Shaked, and S. Shtrikman, Phys. Rev. B **2**, 4679 (1970).

[5] S. Goshen, D. Mukamel, H. Shaked, and S. Shtrikman, J. Appl. Phys. **40**, 1590 (1969).

[6] A. Iyama, Y. Wakabayashi, N. Hanasaki, and T. Kimura, Submitted.

[7] E. Koyama, I. Nakai, and K. Nagashima, Nippon Kagaku Kaishi **6**, 793 (1979) [in Japanese].

[8] P. J. Sivardiére, Acta Cryst. A**26**, 101 (1970).

[9] A. Iyama and T. Kimura, Phys. Rev. B **87**, 180408(R) (2013).

[10] N. Mufti, G. R. Blake, M. Mostovoy, S. Riyadi, A. A. Nugroho, and T. T. M. Palstra, Phys. Rev. B **83**, 104416 (2011).

[11] T. Arima, D. Higashiyama, Y. Kaneko, J. P. He, T. Goto, S. Miyasaka, T. Kimura, K. Oikawa, T. Kamiyama, R. Kumai, and Y. Tokura, Phys. Rev. B **70**, 064426 (2004).

[12] H. Schmid, J. Phys.: Condens. Matter **20**, 434201 (2008).

[13] I. E. Sergienko, C. Sen, and E. Dagotto, Phys. Rev. Lett. **97**, 227204 (2006).

[14] M. Mochizuki and N. Furukawa, Phys. Rev. B **80**, 134416 (2009).

[15] M. Date, J. Kanamori, and M. Tachiki, J. Phys. Soc. Jpn. **16**, 2589 (1961).

[17] M. Mostovoy, A. Scaramucci, N. A. Spaldin, and K. T. Delaney, Phys. Rev. Lett. **105**, 087202 (2010).

[18] N. A. Spaldin, M. Fiebig, and M. Mostovoy, J. Phys.: Condens. Matter **20**, 434203 (2008).

[19] T. Arima, J. Phys.: Condens. Matter **20**, 434211 (2008).

[20] K. Sawada and N. Nagaosa, Phys. Rev. Lett. **95**, 237402 (2005).

[21] C. Henmi, Mineral. Mag. **59**, 545 (1995).

[22] H. T. Witteveen, Solid State Commun. **9**, 1313 (1971).

[23] J. R. Gavarri and A. W. Hewat, J. Solid State Chem. **49**, 14 (1983).

Chapter 5

High-field investigation on the magnetic and dielectric properties in $SmMnO_3$

5.1 Introduction

This chapter describes the high-magnetic-field investigation on the magnetic and dielectric properties in $SmMnO_3$ which shows a distinctive magnetodielectric effect. This chapter is organized as follows. First, previous studies on $SmMnO_3$ are given, including details on the magnetic and dielectric properties. After the purpose of this study is provided, the results of the high-field investigation are introduced. It is discussed how the behaviors in high magnetic fields of the magnetization and the dielectric constant are understood. Finally, perspectives on this material are mentioned.

5.2 Previous studies on $SmMnO_3$

RMnO$_3$ has a distorted perovskite structure with the space group *Pbnm* where R is a rare-earth ion [1-4]. The magnetic structure of RMnO$_3$ varies with the radius of each R ion r_R [5, 6]. The ground state of RMnO$_3$ with relatively small r_R (e.g., R = Tb, Dy, and so on) is cycloidal spin spiral and is famous for the ferroelectricity induced by the spiral magnetic ordering [7-15]. In this case, large coupling between the magnetic and electric properties have been reported, such as 90° flop of the electric polarization P by applying a magnetic field H, or divergence of the dielectric constant ε during the flop of P which is strongly correlated with the motion of the domain walls [7, 16-18]. On the other hand, the ground state of RMnO$_3$ with large r_R (e.g., R = La, Nd, Sm, and so on) is A-type antiferromagnetic and paraelectric [19-21]. Therefore, the coupling between magnetic

and dielectric properties in this phase is not expected. Nevertheless, large coupling between them was observed in one of such materials, $SmMnO_3$ [22].

$SmMnO_3$ is N-type ferrimagnetic, in which temperature T -induced magnetization M reversal occurs at compensation temperature $T_{comp} \approx 9$ K in low H [23], which is ascribed to be the different temperature dependence between the Sm and Mn sublattice magnetization. In H above ~ 1 T, first-order-like transition occurs around T_{comp} in M, and at the same temperature, ε shows an abrupt change, which is the magnetodielectric effect, as shown in Figure 5-1 where the lattice constants also change abruptly [24]. The above phenomena can be understood by considering the magnetic configurations of the Sm and Mn moments as follows. At high T and low H, weak ferromagnetic moments of the Mn ions are parallel to the applied H, and the Sm moments are oppositely polarized to the applied H by the Mn-Sm antiferromagnetic interaction. At low T, the polarized Sm moments become large, and the net magnetization becomes antiparallel to the applied H, which is the origin of the T-induced M reversal in low H.

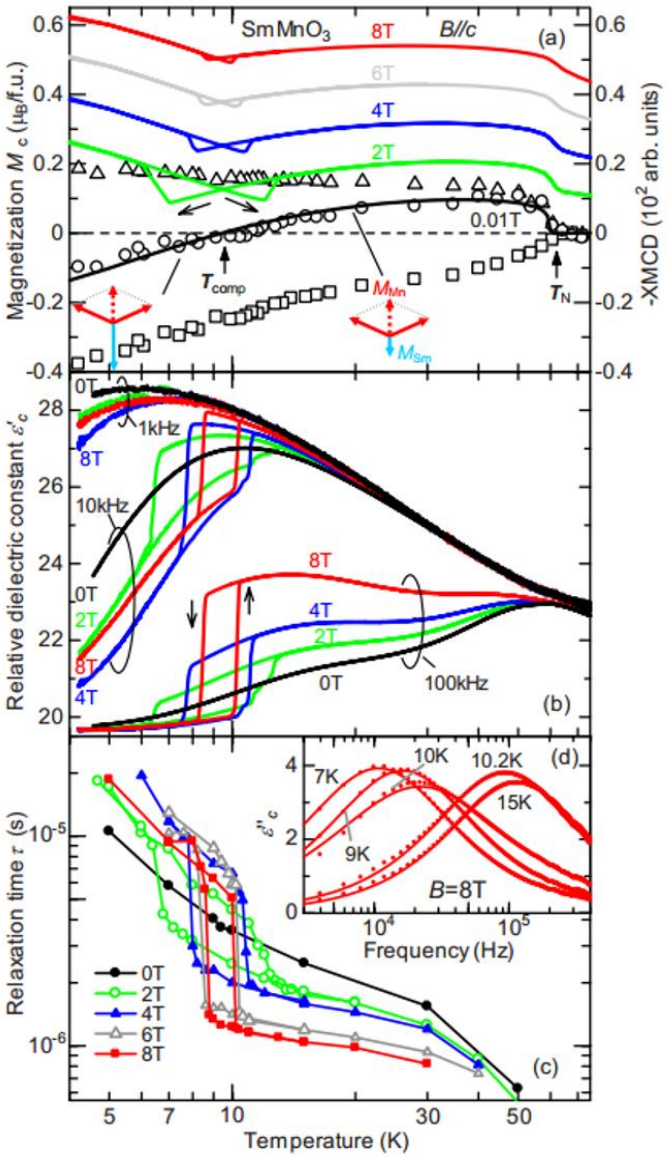

Figure 5-1: Magnetodielectric effect in A-type anti-ferromagnetic $SmMnO_3$ [22].

On the other hand, in relatively high H and at low T, the Sm moments become parallel to the applied H due to the stabilization by the Zeeman effect, and the weak-ferromagnetic Mn moments become antiparallel to the applied field. This is the origin of the first-order transition around T_{comp} in H above ~ 1 T.

Here, the abrupt change in ε is ascribed to a sudden change in the canting angles θ of the weakly ferromagnetic Mn moments due to the Dzyaloshinskii-Moriya interaction [25] because ε in $EuMnO_3$ increases by increasing H where the total magnetic moment J of Eu^{3+} is zero in the ground state, and therefore, the increase in ε originates from the increase in θ (The data will be shown later.). The microscopic origin of θ-dependence of ε is thought to be related to a subtle change in occupancy of each e_g orbital [24]. Then, during the 1st-order transition, the net magnetic moment reverses relative to an applied H, which leads to a sudden change in θ, and in ε.

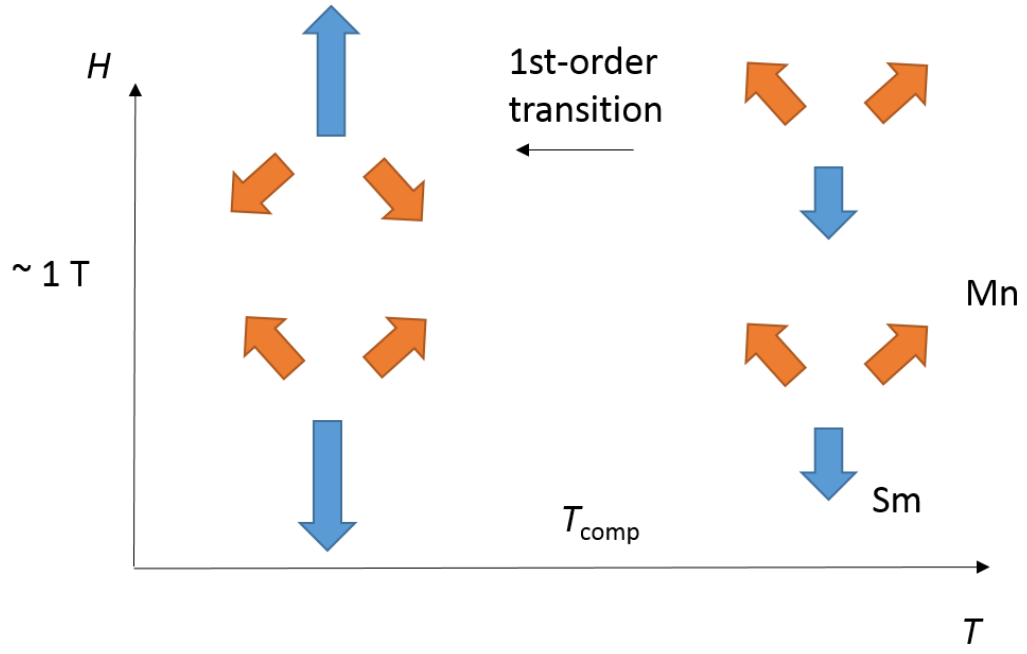

Figure 5-2: Plausible magnetic configurations in $SmMnO_3$.

5.3 The purpose of this study

Then, a question to naturally ask arises what happens in a higher magnetic field. Does the magnetodielectric effect become more remarkable in higher H? How is M which becomes more and more smooth around T_{comp} when an applied H becomes higher and higher? Does the first-order transition remain or disappear in higher H? Thus, the purpose of this study is to answer these questions.

Besides, Cheng and coworkers investigated an internal exchange field in $SmMnO_3$ by analyzing the specific heat data [26]. They observed an H-dependent Schottky-type contribution to the low-T specific heat, and interpreted that the contribution comes from the lifted degeneracy of Kramers doublet on the Sm^{3+} ions. The energy gap Δ at $H = 0$ was estimated at $\Delta/k_B \approx 8.6$ K, where k_B is the Boltzmann constant. Taking into account the antiparallel configuration between the polarized Sm and the weakly ferromagnetic Mn moments, Δ can be proportional to the internal exchange field H_{in} at the Sm^{3+} site, or the interaction between the Sm 4f and Mn 3d moments. Therefore, it is intriguing especially how the dielectric and magnetic properties in $SmMnO_3$ changes in H larger than H_{in}.

5.4 Experimental details

The experimental results are given in this section [27]. Single crystals of $SmMnO_3$ and $EuMnO_3$ for the reference system were grown by the floating-zone method [28]. The growth was carried out with the use of a halogen-lamp image furnace at a growth rate of 8 mm/h in a flow of Ar gas. The grown crystals were confirmed to be of a single phase by measurements of powder x-ray diffraction, oriented by Laue x-ray patterns, and cut into plates with the largest planes perpendicular to the *c* axis. For measurements of the dielectric constant, silver was evaporated to the planes as electrodes. The dielectric constant along the *c* axis at 100 kHz and the magnetization along the *c* axis were measured with capacitance bridges and a vibrating sample magnetometer, respectively. These measurements were done in magnetic fields up to 35 T with resistive magnets (Cell 8 and 12) at the National High Magnetic Field Laboratory, Tallahassee, FL, USA. In the present study, a magnetic field were applied only along the *c* axis in the *Pbnm* setting.

Figure 5-3(a) shows the *T*-dependence of ε_c at several *H* higher than 5 T. As *H* increases, ε_c becomes larger below $T_N \approx 60$ K, and exhibits a pronounced magnetodielectric effect around T_{comp}. In the high-field data at $H \gtrsim 15$ T, ε_c divergently increases with decreasing *T* below T_N and shows a discontinuous drop with a small hysteresis at T_t where the first-order transition occurs. In the previous low-field measurement [22], the hysteresis region of the 1st-order transition at T_t steeply shrank with increasing *H* but was always centered at T_{comp}. However, the present results show that the application of higher *H* lowers T_t, which is clearly seen as the shift of the discontinuous drop towards lower *T* with increasing *H*. This means that high *H* suppresses the low-*T* phase. Another notable feature in the present high-field data is the magnitude of ε_c beow T_t. Below 4 – 5 T, ε_c decreases with increasing *H* below T_t, however, ε_c at high *H* increases with increasing *H* even below T_t as seen in Figure 5-3(a).

Figure 5-3(b) represents the *T*-dependence of M_c in the same *H* as that of the dielectric measurements. As seen in the ε_c-*T* curves displayed in Figure 5-3(a), M_c-*T* curves also show distinct anomalies at T_t. One of the most noteworthy features in Figure 5-3(b) is that the M_c-*T* curves in low *H* ($\lesssim$ 15 T) show a different behavior from those in high *H* ($\gtrsim$ 15 T). That is to say, above T_t, the M_c-*T* curve at 5 T shows the suppression towards T_t while that at 35 T increases. Related to this difference, M_c at 5 T shows the minimum at T_t while that at 35 T shows a sudden drop at T_t towards lower *T*. It seems that these two distinct

features appear in H below and above ~ 15 T at which the M_c-T curve becomes nearly T-independent at $T > T_t$.

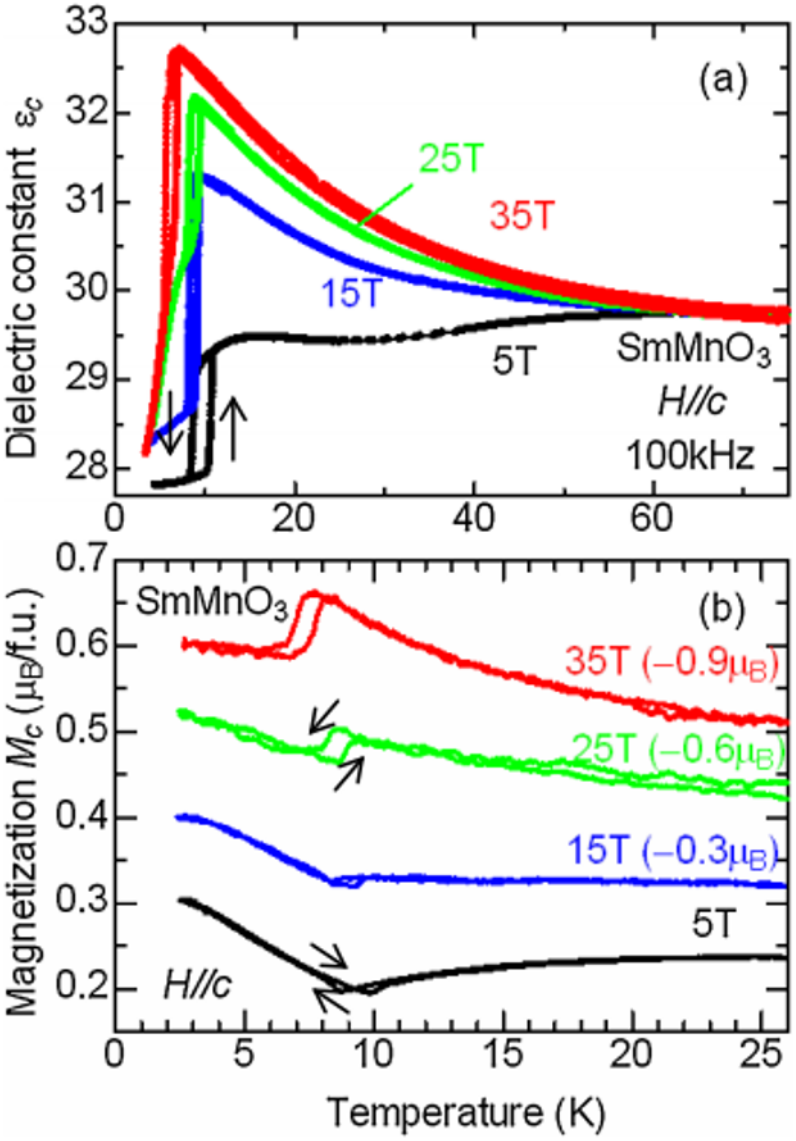

Figure 5-3: The temperature dependence of the dielectric constant and the magnetization along the c axis.

This difference between the low- and high-field data probably comes from whether applied H exceeds the internal exchange field H_{in} or not. Here, the magnitude of H_{in} can be interpreted as that of the antiferromagnetic interaction between the polarized Sm 4f and the weakly ferromagnetic Mn 3d moments. By using the energy gap ($\Delta/k_B \approx 8.6$ K) obtained by the specific heat measurement and the theoretical value of the effective moment for Sm^{3+} ion in the ground state (0.845 μ_B), H_{in} can be estimated at about 15 T.

Indeed, this value is equivalent to the magnetic field at which Δ obtained by the linear extrapolation of low-H ($\lesssim$ 9 T) data becomes zero [16]. When the applied H is smaller than H_{in}, the Sm moments are polarized in the direction antiparallel to H because the antiferromagnetic coupling between the Sm and Mn moments s stronger than H. Therefore, M_c at 5 T and just above T_t becomes smaller with decreasing T. When the applied H is larger than H_{in}, however, the Sm moments are polarized parallel to H because the applied H overcomes H_{in}. Then, M_c becomes larger when the polarization of the Sm moments increases by lowering T towards T_t [see the data at H > 15 T in Figure 5-3(b)]. In addition, M_c at high H shows a sudden drop at T_t towards low T, which means that there is no gain of the Zeeman energy at the transition. This result indicates that the transition at high H does not originate from the simultaneous magnetization reversal for the Sm and Mn moments, as previously discussed for the data at low H ($H \lesssim 8$ T). Thus, the magnetic states at $H > H_{in}$ may be distinct from those at $H < H_{in}$.

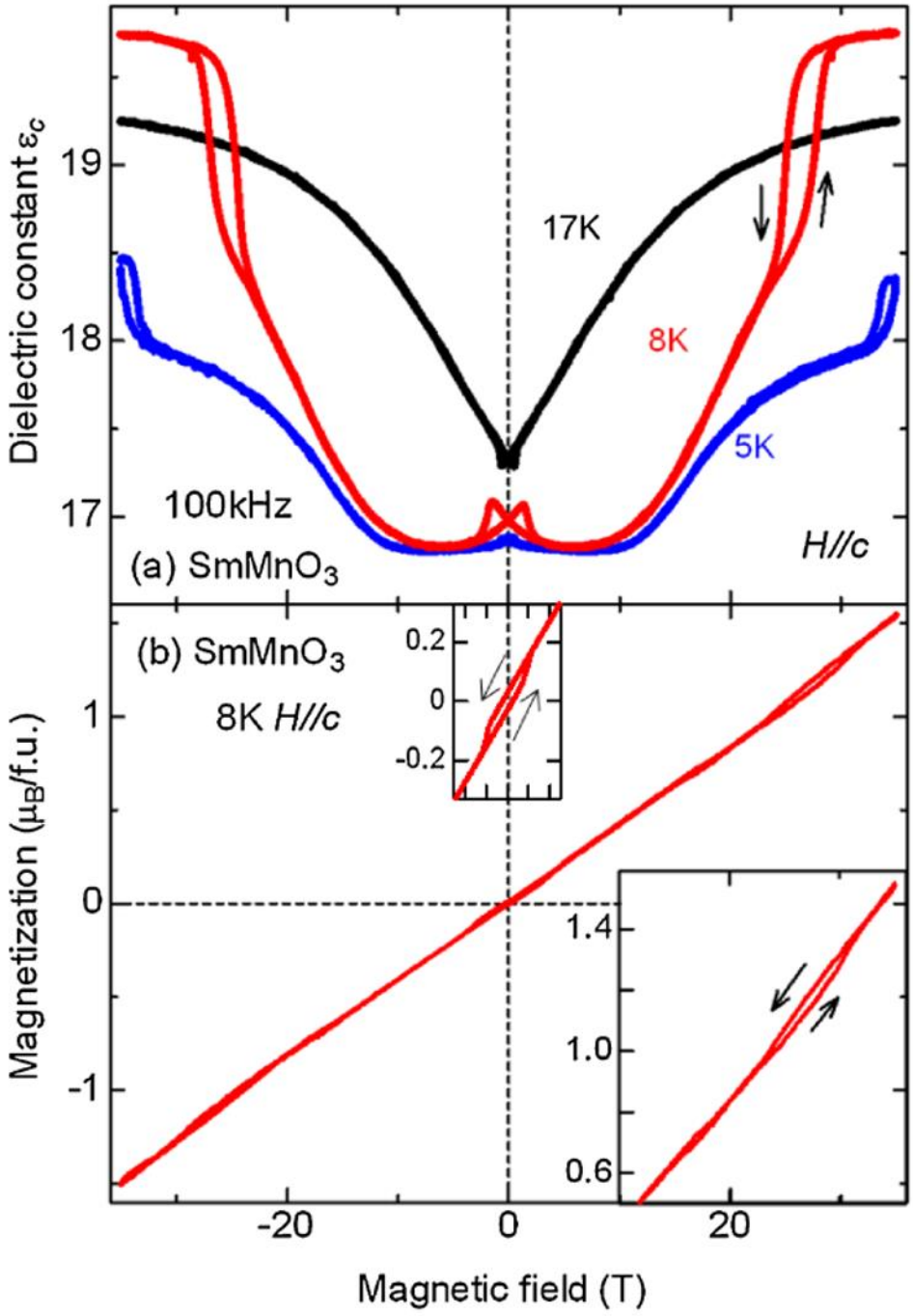

Figure 5-4: Magnetic field dependence of the dielectric constant and the magnetization.

To further examine the magnetic and dielectric anomalies around T_{comp}, we measured the isothermal ε_c and M_c as functions of H. The H profiles of ε_c and M_c are shown in Figure 5-4(a) and 5-4(b), respectively. As seen in Figure 5-4(a), the isothermal ε_c-H curves were taken at T above (17 K) and below (8 and 5 K) T_{comp}. In the low-H region (H

< ~ 3T), all the data show sudden jumps which are attributed to ferromagnetic spin reversal [5]. [Compare the 8 K data with the M_c-H data shown in the top middle inset of Figure 5-4(b).] Apart from the low-H hysteresis region, at 17 K (> T_{comp}), ε_c monotonically increases as the magnitude of H increases. By considering the interpretation of the previous study [5], this behavior can be related to a monotonic increase of the canting angles θ of Mn moments with increasing H. Below T_{comp}, however, another discontinuous jump with hysteresis was observed in ε_c (25-28 T and 33-35 T at 8 K and 5 K, respectively). This high-H dielectric jump also accompanies a magnetic anomaly with hysteresis. As seen in the M_c-H curve at 8 K [Figure 5-4(b)], M_c linearly increases up to ~ 27 T, slightly deviates from the linear H-dependence around 25-28 T at which hysteretic behavior is observed [lower right inset of Figure 5-4(b)].

Another remarkable feature in the ε_c-H curves is obtained at around ~ 10 T in the data below T_{comp}. Though ε_c at 5 and 8 K monotonically decreases with increasing H up to ~ 10 T, it starts to increase at around 10 T. Considering the close relationship between the magnitude of ε_c and θ, the ε_c-H curves suggest that θ decreases towards ~ 10 T, becomes 0 around 10 T, and then increases above ~ 10 T. This interpretation is plausible because the magnetic field (~ 10 T) is the same order with that of H_{in} which corresponds to the magnitude of the Sm-Mn antiferromagnetic interaction.

For the reference system, ε_c of $EuMnO_3$ was measured as shown in Figures 5-6 and 5-7. Because Eu^{3+} has no magnetic moment in the ground state, the change in ε_c by applying H reflects only the Mn moments. Below $T_N \approx 55$ K, ε_c monotonically increases with increasing H, which is the consequence of increase in θ. At low T, the H-dependence becomes small, compared with the intermediate T as 20 K, which might be related to freezing of phonons at low T.

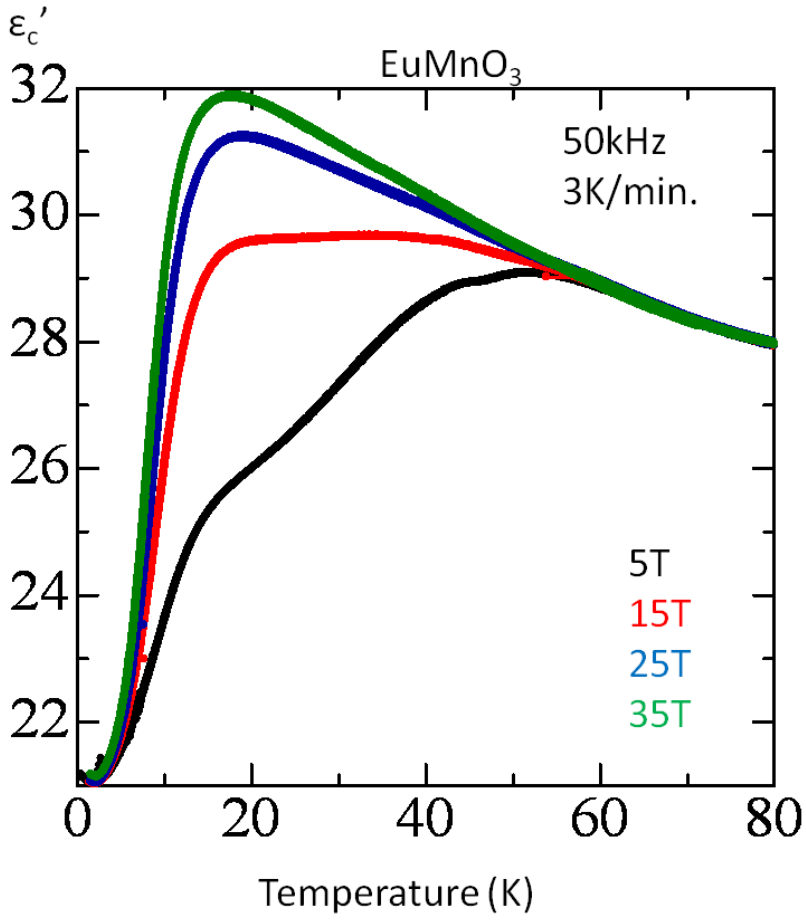

Figure 5-6: Temperature dependence of the dielectric constant in $EuMnO_3$.

Figure 5-7 shows *H*-dependence of ε_c at several *T*. Contrast to $SmMnO_3$, ε_c of $EuMnO_3$ monotonically increases at all *T* investigated, apart from around 0 T which is a result of the ferrimagnetic reversal. This is consistent with the scenario that increase in ε_c is the result of the increase in θ because weakly ferromagnetic Mn moments are always parallel to the applied *H* in this compound except around 0 T. Thus, it clearly suggests that ε_c reflects only the Mn moments, and it is not related to 4f moments.

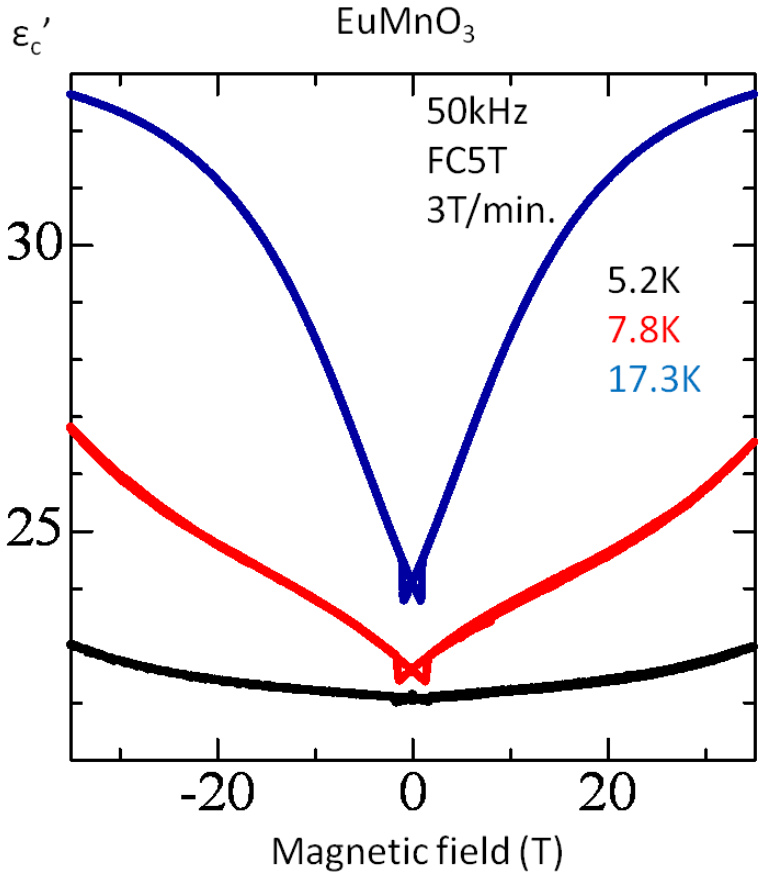

Figure 5-7: Magnetic field dependence of the dielectric constant in $EuMnO_3$.

5.5 Discussion

The experimental results are summarized in Figure 5-8 as the H-T phase diagram in which the gray area corresponds to the hysteresis region. The phase boundaries are determined by T_t observed in M_c-T and ε_c-T curves. As one can see, the low-T phase is suppressed by the application of high H, meaning that the high-T phase is more stable in higher H. It is considered that the configurations of the polarized Sm and the weakly ferromagnetic Mn moments in the phase diagram can be classified into roughly four states, as depicted in the insets of Figure 5-8. These four states can be understood in terms of the competition among thermal energy, the Zeeman energy, and the Sm-Mn antiferromagnetic interaction. In a weak magnetic field below ~ 15 T, which is comparable to the internal exchange field H_{in}, the Sm moments are polarized antiparallel to the net Mn moments because H_{in} is larger than the applied H. Besides, the Sm moments are polarized parallel to H at $T < T_t$ (left lower inset of Figure 5-8) while antiparallel at $T > T_t$ (right lower inset of Figure 5-8) in weak magnetic fields, as indicated by the specific heat measurement [26]. This is because the magnitude of polarized Sm moments becomes larger with decreasing T, exceeds that of net Mn moments, and then it is more stable for the Sm moments to be parallel to the applied H due to the gain from the Zeeman energy. In a high H above ~ 15 T, on the contrary, the Sm moments are polarized parallel to the direction of the net Mn moments as well as that of H at any temperatures because H_{in} is weaker than the applied H. Considering the sudden suppression of ε_c towards low T at the high-H transition, it is inferred that the high-H transition is also ascribed to a sudden decrease of the canting angles of the Mn moments. However, unlike the case at low H, the simultaneous reversal of the Sm and the Mn moments may not occur because both the Sm and the net Mn moments are aligned in the direction of H at high H. The transition temperature is below 10 K whose energy is close to that of H_{in}, indicating that the Sm-Mn antiferromagnetic interaction plays an important role against the Zeeman energy. Therefore, as illustrated in the upper insets of Figure 5-8, it is expected that the sudden decrease in the canting angles at T_t occurs to gain the Sm-Mn interaction. In this manner, it is concluded that the observed transition is triggered by keen competition among thermal energy, the Zeeman energy, and the Sm-Mn antiferromagnetic interaction.

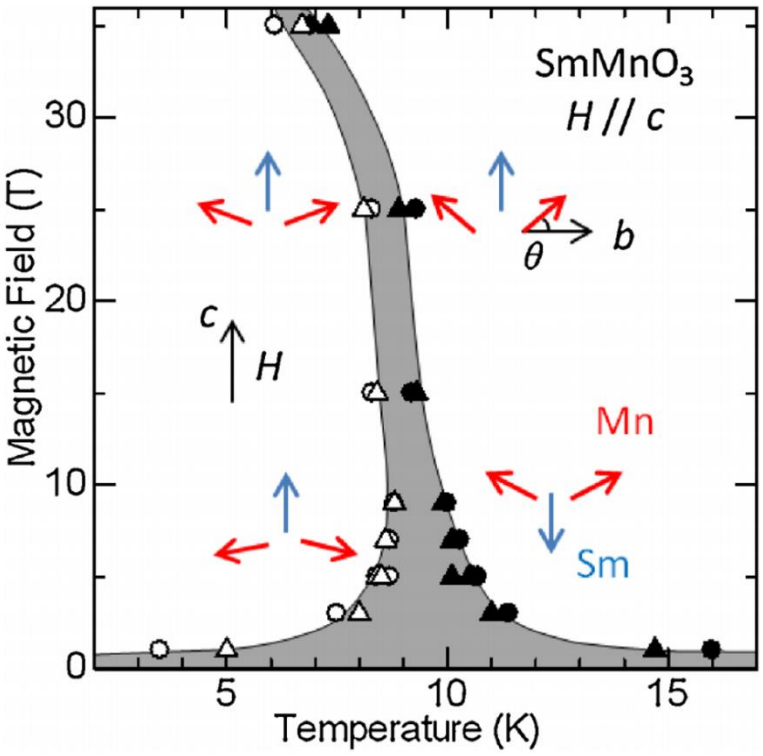

Figure 5-8: Magnetic phase diagram of $SmMnO_3$ up to 35 T. Circles and triangles represent T_t obtained from the ε_c-T and the M_c-T curves, respectively. Open and closed marls represent T_t in the cooling and heating runs, respectively. The gray rea represents the hysteresis region. Illustrations in the inset depict possible configurations of polarized Sm (blue arrows) and canted Mn (red arrows) moments in the respective T-H regions. The length of the arrows indicates the magnitude of the moments.

5.6 Perspectives

One question remains open. Why does the first-order-like transition occurs especially in high H in $SmMnO_3$? In low H, it is plausible that the transition occurs because of the simultaneous reversal of the Sm and Mn moments in order to gain the Zeeman energy. On the other hand, in high H, the Zeeman energy gain decreases during the phase transition because the total M decreases at low-T phase in high H. Therefore, another energy gain must be considered other than the Sm-Mn antiferromagnetic interaction, which is not the sufficient condition for the phase transition to occur. Then, the natural answer seems to be the ordering of the Sm moments at low T. However, in this case in a high H, the crossover is more likely than the phase transition because the magnetic symmetry at low T is probably the same with that of the high T phase [29], although the experiment clearly indicates the phase transition, not the crossover. Hence, the investigation of the nature of this phase transition would be interesting. One possibility is the ordering of other components –the a and b components– of the Sm moments. This is for the future investigation.

5.7 Summary

Magnetic and magnetodielectric properties of *Pbnm* orthorhombic $SmMnO_3$ in high magnetic fields up to 35 T applied along the c axis has been investigated. A first-order-like transition was observed in both the dielectric constant and the magnetization for in-field data studied here. The transition nature is found to be different between the data taken in magnetic fields smaller and larger than the internal exchange field equivalent to the Sm 4*f* - Mn 3*d* antiferromagnetic interaction. Considering such a difference, it is concluded that the transition observed in $SmMnO_3$ is ascribed to keen competition among the thermal energy, the Zeeman energy, and the Sm 4*f* - Mn 3*d* antiferromagnetic interaction.

Acknowledgements

The author thanks V. Yu Ivanov, A. A. Mukhin, and M. Hagiwara for fruitful discussions, and also thanks J.-S. Jung, E. S. Choi, J. Hwang, T. Takeuchi and T. Nakano for their help with experiments. High-field experiments were performed at the National High Magnetic Field Laboratory, which is supported by the US DOE, the National Science Foundation, and the State of Florida. This work was in part supported by the Institutional Program for Young Researcher Overseas Visits, Grand-in-Aid for Scientific Research (20674005 and 20001004), and the Global COE Program (G10) from the Japan Society for the Promotion of Science.

References

[1] T. Kimura, Annu. Rev. Mat. Res. **37**, 387 (2007).

[2] J. R.-Carvajal, M. Hennion, F. Moussa, A. M. Moudden, L. Pinsard, and A. Revcolevschi, Phys. Rev. B **57**, 3189(R) (1998).

[3] W.-G. Yin, D. Volja, and W. Ku, Phys. Rev. Lett. **96**, 116405 (2006).

[4] E. Pavarini and E. Koch, Phys. Rev. Lett. **104**, 086402 (2010).

[5] T. Goto, T. Kimura, G. Lawes, A. P. Ramirez, and Y. Tokura, Phys. Rev. Lett. **92**, 257201 (2004).

[6] M. Mochizuki, N. Furukawa, and N. Nagaosa, Phys. Rev. B **84**, 144409 (2011).

[7] T. Kimura, T. Goto, H. Shintani, K. Ishizuka, T. Arima, and Y. Tokura, Nature **426**, 55 (2003).

[8] M. Kenzelmann, A. B. Harris, S. Jonas, C. Broholm, J. Schefer, S. B. Kim, C. L. Zhang, S.-W. Cheong, O. P. Vajk, and J. W. Lynn, Phys. Rev. Lett. **95**, 087206 (2005).

[9] H. Katsura, N. Nagaosa, A. V. Balatsky, Phys. Rev. Lett. **95**, 057205 (2005).

[10] M. Mostovoy, Phys. Rev. Lett. **96**, 207204 (2006).

[11] I. A. Sergienko and E. Dagotto, Phys. Rev. B **73**, 094434 (2006).

[12] H. J. Xiang, E. J. Kan, Y. Zhang, M.-H. Whangbo, and X. G. Gong, Phys. Rev. Lett. **107**, 157202 (2011).

[13] T. A. Kaplan and S. D. Mahanti, Phys. Rev. B **83**, 174432 (2011).

[14] A. B. Harris, Phys. Rev. B **76**, 054447 (2007).

[15] A. Raeliarijaona, S. Singh, H. Fu, and L. Bellaiche, Phys. Rev. Lett. **110**, 137205 (2013).

[16] T. Kimura, G. Lawes, T. Goto, Y. Tokura, and A. P. Ramirez, Phys. Rev. B **71**, 224425 (2005).

[17] F. Kagawa, M. Mochizuki, Y. Onose, H. Murakawa, Y. Kaneko, N. Furukawa, and Y. Tokura, Phys. Rev. Lett. **102**, 057604 (2009).

[18] M. Mochizuki and N. Furukawa, Phys. Rev. Lett. **105**, 187601 (2010).

[19] G. Matsumoto, J. Phys. Soc. Jpn. **29**, 606 (1970).

[20] I. Solovyev, N. Hamada, and K. Terakura, Phys. Rev. Lett. **76**, 4825 (1996).

[21] M. Mochizuki and N. Furukawa, Phys. Rev. B **80**, 134416 (2009).

[22] J.-S. Jung, A. Iyama, H. Nakamura, M. Mizumaki, N. Kawamura, Y. Wakabayashi, and T. Kimura, Phys. Rev. B **82**, 212403 (2010).

[23] V. Y. Ivanov, A. A. Mukhin, A. S. Prokhorov, and A. M. Balbashov, Phys. Stat. Solidi B **236**, 445 (2003).

[24] J.-S. Jung, A. Iyama, H. Nakamura, Y. Wakabayashi, and T. Kimura, Phys. Rev. B **85**, 174414 (2012).

[25] V. Skumryev, F. Ott, J. M. D. Coey, A. Anane, J.-P. Renard, L. P.-Gaudart, and A. Revcolevschi, Eur. Phys. J. B **11**, 401 (1999).

[26] J.-G. Cheng, J.-S. Zhou, J. B. Gooednough, Y. T. Su, Y. Sui, and Y. Ren. Phys. Rev. B **84**, 104415 (2011).

[27] A. Iyama, J.-S. Jung, E. S. Choi, J. Hwang, and T. Kimura, J. Phys. Soc. Jpn. **81**, 013703 (2012).

[28] T. Mori, N. Kamegashira, K. Aoki, T. Shishido, and T. Fukuda, Mater. Lett. **54**, 238 (2002).

[29] E. F. Bertaut, Acta Crystallogr., Sect. A **24**, 217 (1968).

Chapter 6

Neutron scattering study in $SmMnO_3$

6.1 Introduction

This chapter describes the results on neutron scattering experiment in $SmMnO_3$ single crystals which show a distinctive magnetodielectric effect. This chapter is organized as follows. First, previous studies on $SmMnO_3$ are briefly given. After the purpose of this study is mentioned, the results of the neutron scattering experiment are introduced. It is discussed how the Sm and Mn magnetic moments behave when the magnetodielectric effect is observed.

6.2 Previous studies

$SmMnO_3$ shows a remarkable magnetodielectric effect as described in ref. 1-3 and chapter 5. Here, the magnetic structure is focused on. Figure 6-1 depicts temperature T dependence of the dielectric constant along the c axis (ε) and the magnetization along the c axis M in the *Pbnm* notation. Below T_N ~ 60 K, a net M arises due to weakly ferromagnetic Mn moments induced by the Dzyaloshinskii-Moriya (DM) interaction [4, 5]. Below ~ 30 K in a weak magnetic field H, M decreases towards low T, and eventually becomes negative below T_{comp} ~ 9 K. This is attributed to development of the Sm magnetic moments which are polarized antiparallel to H due to Sm-Mn antiferromagnetic interaction. In a weak H, no anomaly is observed at low T, and T-dependence of ε is a smooth curve. However, in a relatively high H, M shows a first-order-like transition around T_{comp}, and at the same point, ε has a clear jump which is the magnetodielectric effect. This has been considered as a result of simultaneous reversal of the Sm and Mn moments in order to gain Zeeman energy because the net Sm moment is larger than the

net Mn moment at low *T*, and hence larger gain from Zeeman energy is obtained when the Sm moment becomes parallel to *H* as schematically illustrated in Figure 6-2.

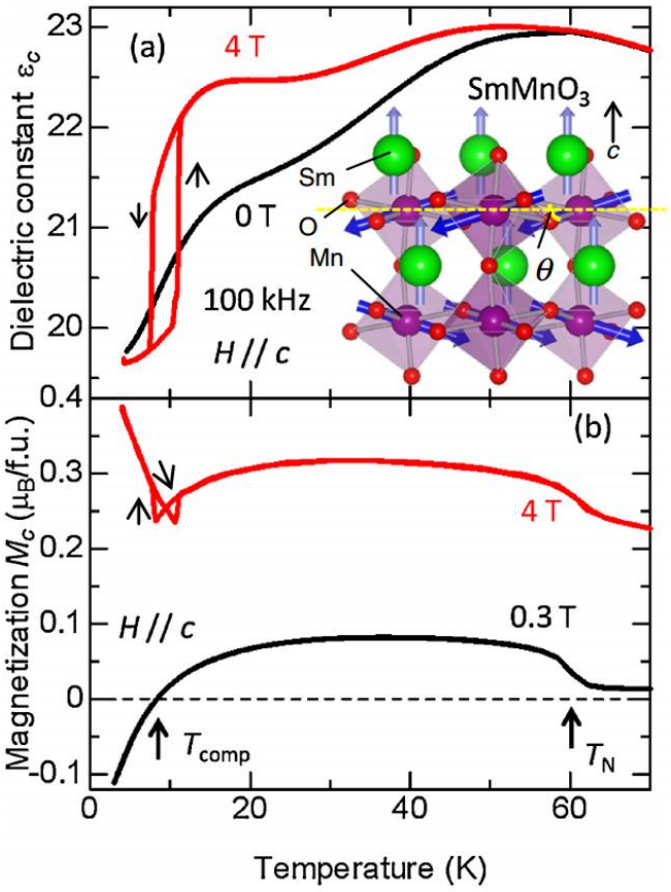

Figure 6-1: Temperature dependence of dielectric constant and magnetization [2].

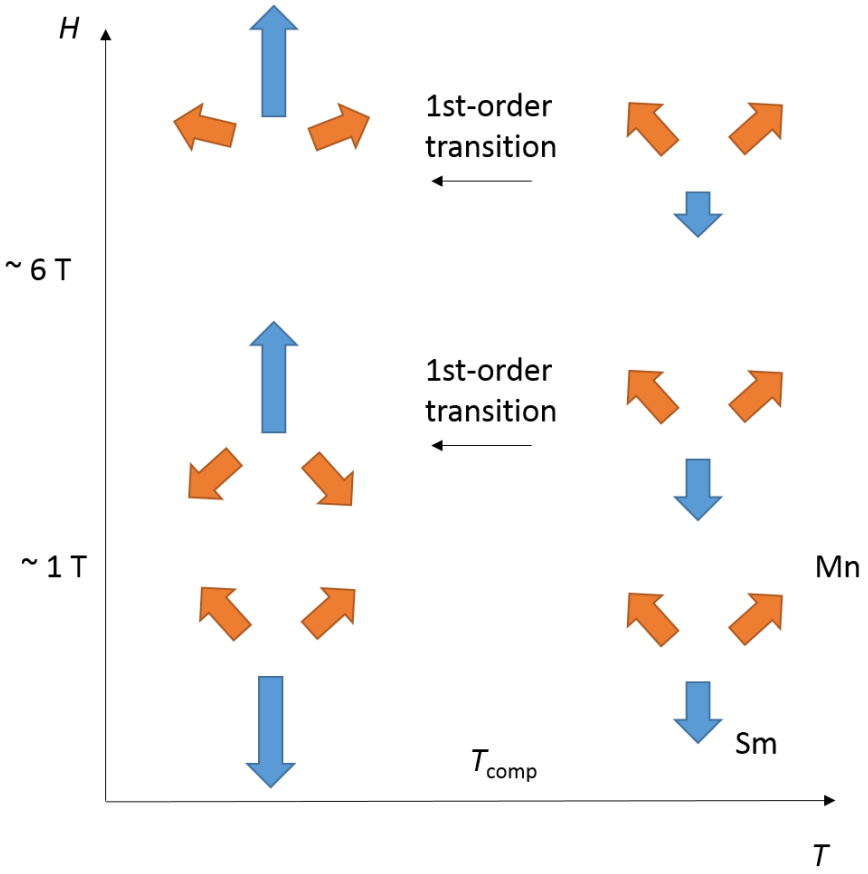

Figure 6-2: Plausible magnetic configurations in $SmMnO_3$.

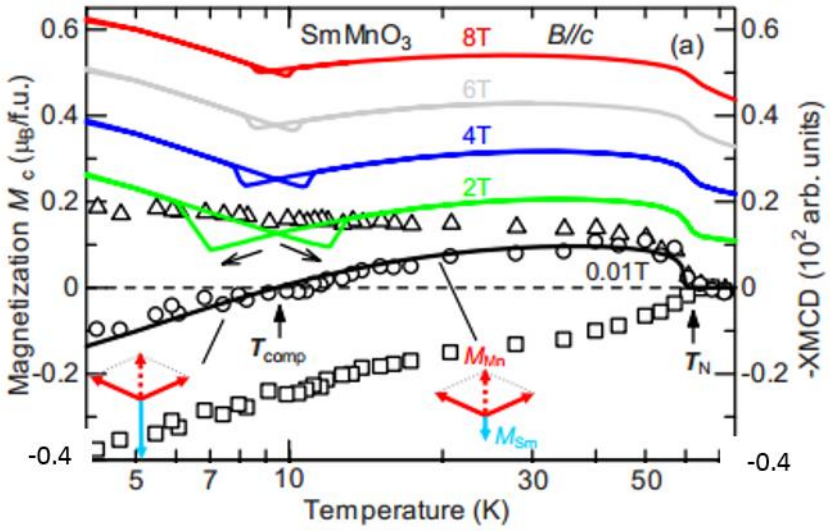

Figure 6-3: Temperature dependence of magnetization and XMCD signal [1].

It is necessary to confirm the magnetic structure by means of some probes whether the deduced structure is correct or not. Previously, x-ray magnetic circular dichroism (XMCD) was performed with single crystalline specimens [1].

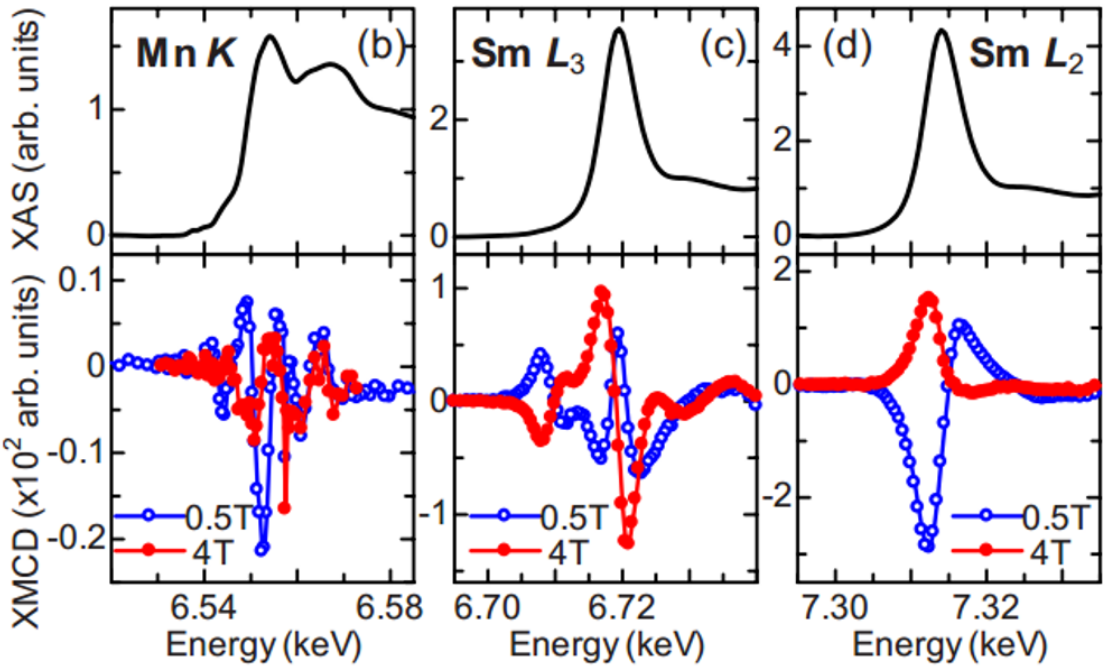

Figure 6-4: Energy dependence of XMCD signals with Mn *K* edge (1s to 4p) and Sm *L* edge (2p to 5d) [1].

XMCD can detect element-specific magnetization by the use of each resonance as Figure 6-4 [6, 7]. However, the previous measurement [1] was performed with hard x-rays around a range of Mn *K* edge (1s to 4p) and Sm *L* edge (2p to 5d). Thus, XMCD signal originates from indirect coupling to Mn 3d and Sm 4f states, which disable to quantitatively analyze the XMCD signals.

6.3 The purpose of this study

Then, as an alternative approach, neutron scattering experiment was employed in order to survey the magnetic structure. Neutron scattering technique is a powerful tool to investigate magnetic structures in a material because neutrons have spin degree of freedom. Although natural isotope of Sm is a large absorber of neutrons, this problem can be overcome using hot neutrons which have shorter wavelength than usual thermal neutrons, as mentioned in detail in the section 2.4. Therefore, the purpose of this study is to investigate the magnetic structure by means of neutron scattering technique with hot neutrons.

6.4 Experimental details

In this section, experimental results are shown. Neutron scattering experiment was carried out at D9 and D3 in Institute Laue-Langevin with a single crystal of $SmMnO_3$ grown by the floating-zone method. The dimension of the single crystal was ~ 2 × 2 × 1 mm^3. The wavelength of neutrons was 0.511 Å.

First, Bragg reflections corresponding to *Pmmm* (at small-*q* region) and *Pbnm* (at large-*q* region) were collected at 40 K (below T_N ~ 60 K). The results are shown in Table 6-1.

Table 6-1 Crystallographic data of $SmMnO_3$ at 40 K.

Formula	$SmMnO_3$
Crystal system	Orthorhombic
Space group	*Pbnm*
Lattice parameters	a = 5.3432 Å
	b = 5.8451 Å
	c = 7.4669 Å
	V = 233.2027 $Å^3$

Atomic coordinates

site	*x*	*y*	*z*	*B*
Sm	0.9584(10)	0.0747(5)	0.25	0.024(2)
Mn	0.5	0	0	0.004(3)
O1	0.0961(10)	0.4726(5)	0.25	0.0077(19)
O2	0.7088(7)	0.3231(4)	0.0473(2)	0.0061(13)

Anisotropic displacement parameters

site	U_{11}	U_{22}	U_{33}	U_{12}	U_{13}	U_{23}
Sm	0.051(4)	0.0109(10)	0.0106(9)	-0.0010(14)	0	0
Mn	0.007(6)	0.0036(14)	0.0012(11)	0.0027(18)	0.0002(15)	0.0004(11)
O1	0.018(4)	0.0036(10)	0.0019(8)	-0.0037(13)	0	0
O2	0.011(3)	0.0040(7)	0.0031(6)	-0.0006(9)	0.0002(8)	-0.0001(5)

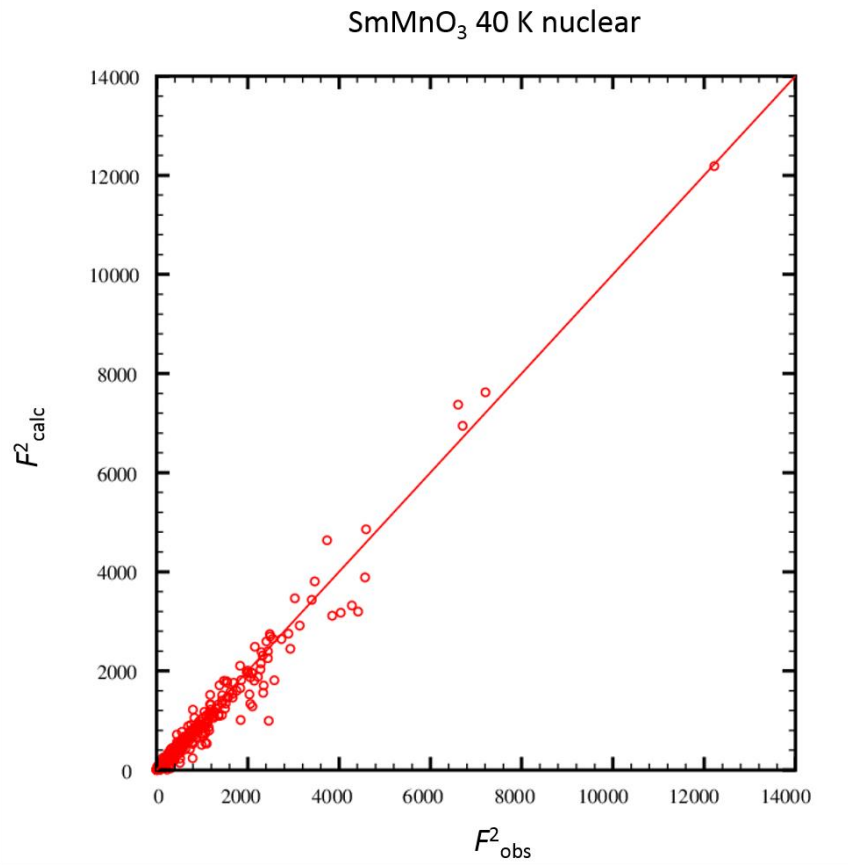

Figure 6-1: Calculated versus observed values of the squared intensities for data collected at 40 K.

The number of reflections was 363, and the χ^2 was 14.53.

Although the goodness of fit is not sufficient possibly due to still large absorption, the lattice parameters show good agreement with previous measurements [8-10]. Because the crystal structure was properly determined in spite of a material including natural isotope of Sm, next, the magnetic properties were investigated.

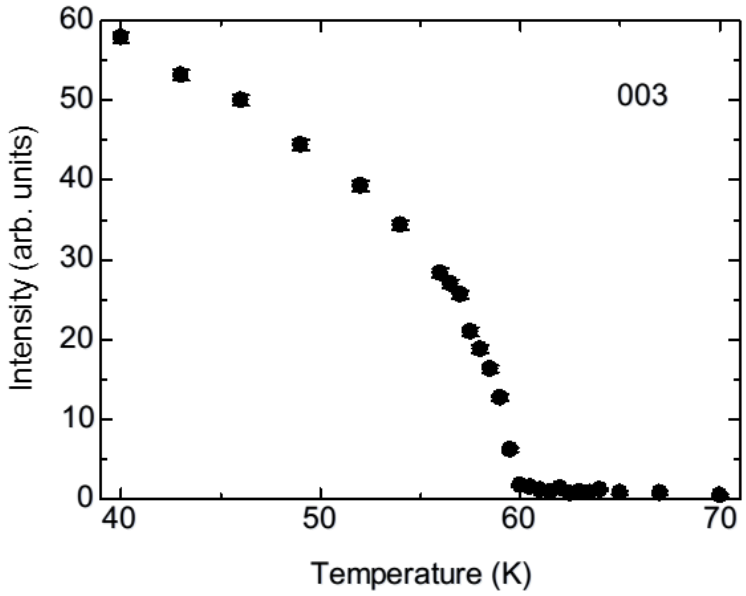

Figure 6-2: Temperature dependence of 003 Bragg intensity.

Figure 6-2 depicts *T*-dependence of 003 Bragg intensity measured in 0 T which reflects Mn magnetic moments mainly along the *b* axis because 003 is a forbidden reflection from nuclear scattering. Below $T_N \sim 60$ K, antiferromagnetic magnetic structure develops with the main component of *b*, which is a common feature of $R\mathrm{MnO_3}$ (*R* = La – Sm) with A-type antiferromagnetic structure. This Bragg intensity is proportional to squared order parameter (= staggered magnetization with the *b* component) because the intensity is almost null at $T > T_N$ [11].

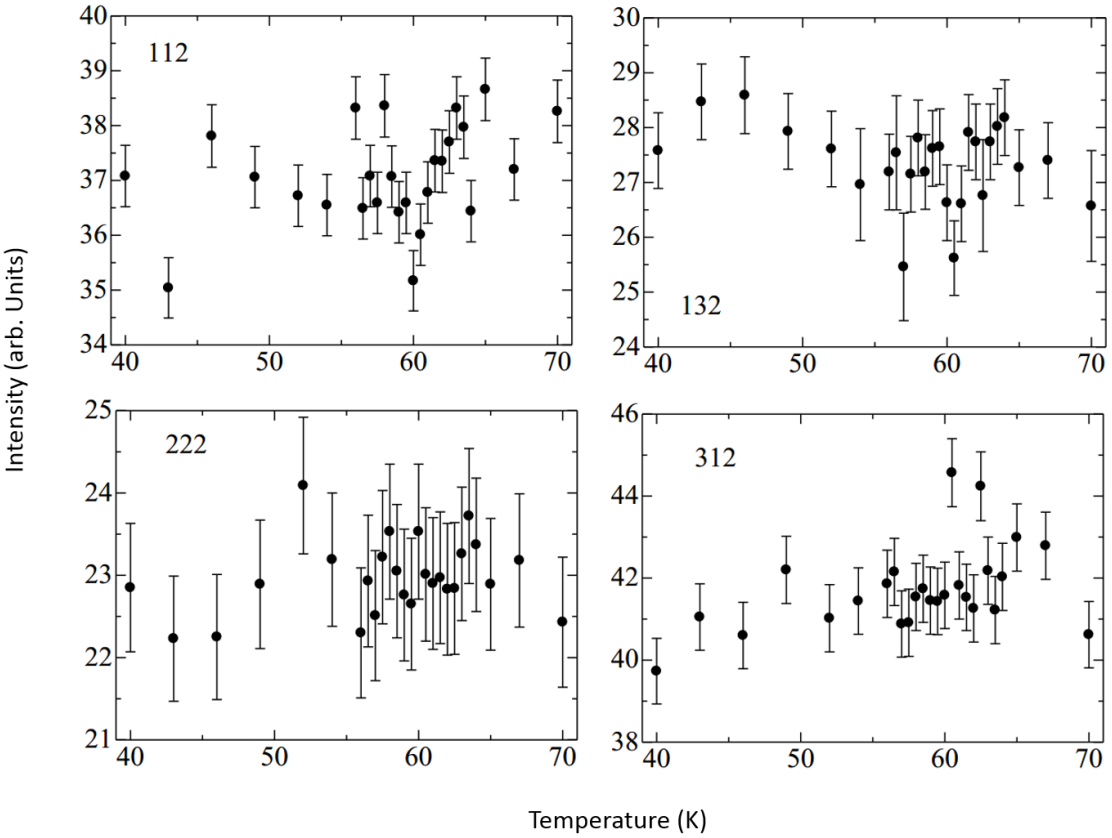

Figure 6-3: Bragg intensity profiles which can detect weakly ferromagnetic component of Mn magnetic moments along the *c* axis.

Next, *T*-dependence of Bragg reflections which can detect weakly ferromagnetic component along the *c* axis are described in Figure 6-3. The measurement condition was the same with that of the experiment shown in Figure 6-2. Although the development of (003) reflection below 60 K (Figure 6-2) obviously show the antiferromagnetic structure, these profiles in Figure 6-3 show no clear signals of weakly ferromagnetic component along the *c* axis. The presumable reasons are that these reflections are not forbidden from nuclear scattering and the weakly ferromagnetic component is small.

Since zero-field measurement could not detect the weakly ferromagnetic component, in-field measurement was done with the use of polarized hot neutrons at D3 in Institute Laue-Langevin. The same sample used in the above-mentioned measurements was set so that the *ab* plane becomes horizontal. A vertical magnetic field was applied to the *c* axis. Incident beam polarization was 0.90.

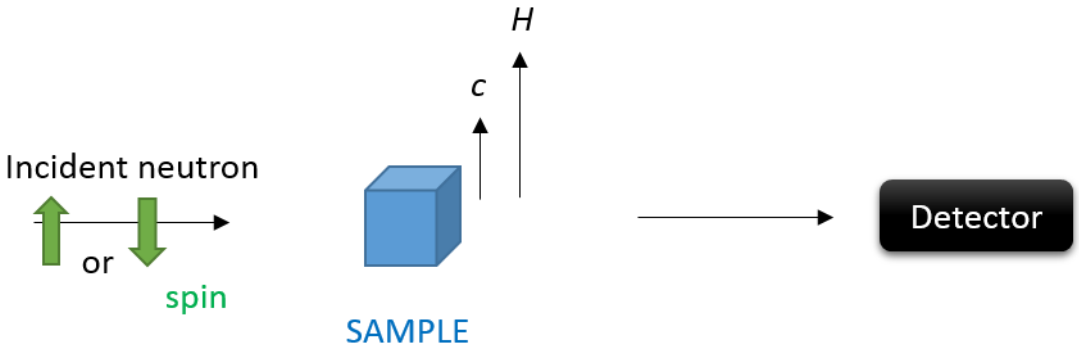

Figure 6-4: Measurement setup for flipping ratios.

The flipping ratios of (200) and (110) reflections in a magnetic field along the *c* axis were measured. (200) and (110) reflections are chosen to determine the Sm and Mn ferromagnetic moments because antiferromagnetic contributions to their magnetic structure factor are null. Since the two peaks are in the horizontal scattering plane, flipping ratios are

$$R = \frac{F_N^2 + F_M^2 + 0.90 \cdot 2 \cdot F_N \cdot F_M}{F_N^2 + F_M^2 - 0.90 \cdot 2 \cdot F_N \cdot F_M}$$

Nuclear structure factors, Q, and form factors in dipolar approximation are

F_N (110) = 0.28566 × 10^{-12} cm, Q = 1.591 Å^{-1}, $f_{Mn}(Q)$ = 0.863, $f_{Sm}(Q)$ = 1.140,
F_N (200) = -2.0206 × 10^{-12} cm, Q = 2.348 Å^{-1}, $f_{Mn}(Q)$ = 0.730, $f_{Sm}(Q)$ = 1.261,

and magnetic structure factors are

F_M (110) = 0.2695 × (-4f_{Mn}(110) × M_{Mn} + 3.553f_{Sm}(110) × M_{Sm}) ×10^{-12} cm,
F_M (200) = 0.2695 × (4f_{Mn}(200) × M_{Mn} + 3.932f_{Sm}(200) × M_{Sm}) ×10^{-12} cm.

One can obtain the magnetic moments from the two equations as

$M_{Sm} = (0.787 \times F_M(110) + 0.930 \times F_M(200)) / 2.101$

$M_{Mn} = (F_M(200) - 1.336 M_{Sm}) / 0.787$

The obtained results are shown in Figures 6-6 and 6-7.

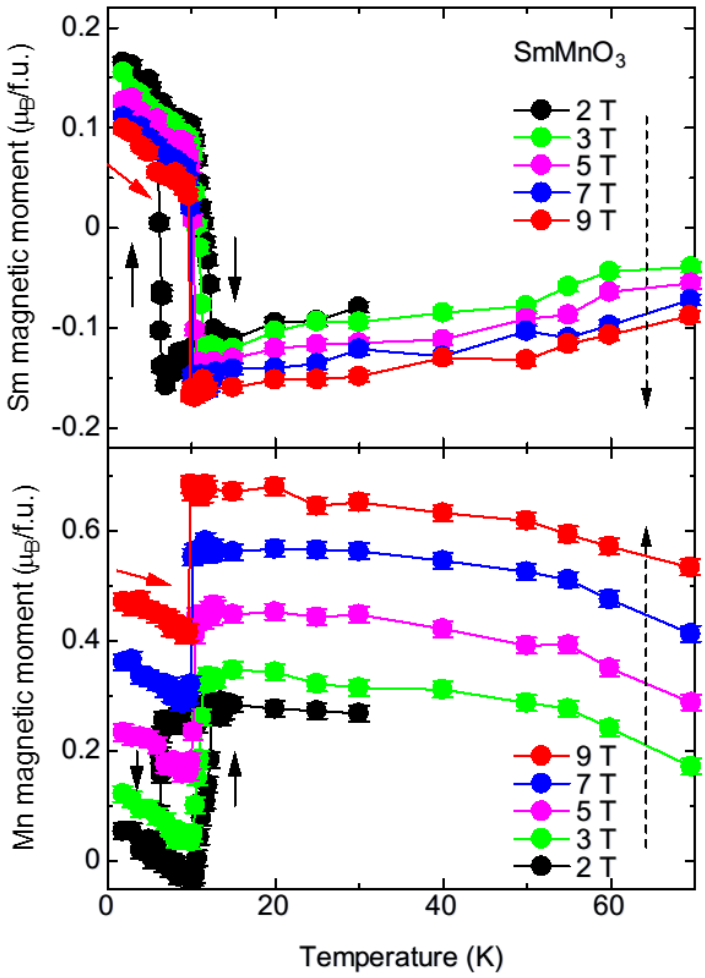

Figure 6-6: Temperature dependence of magnetic moments of Sm and Mn in a magnetic field along the *c* axis.

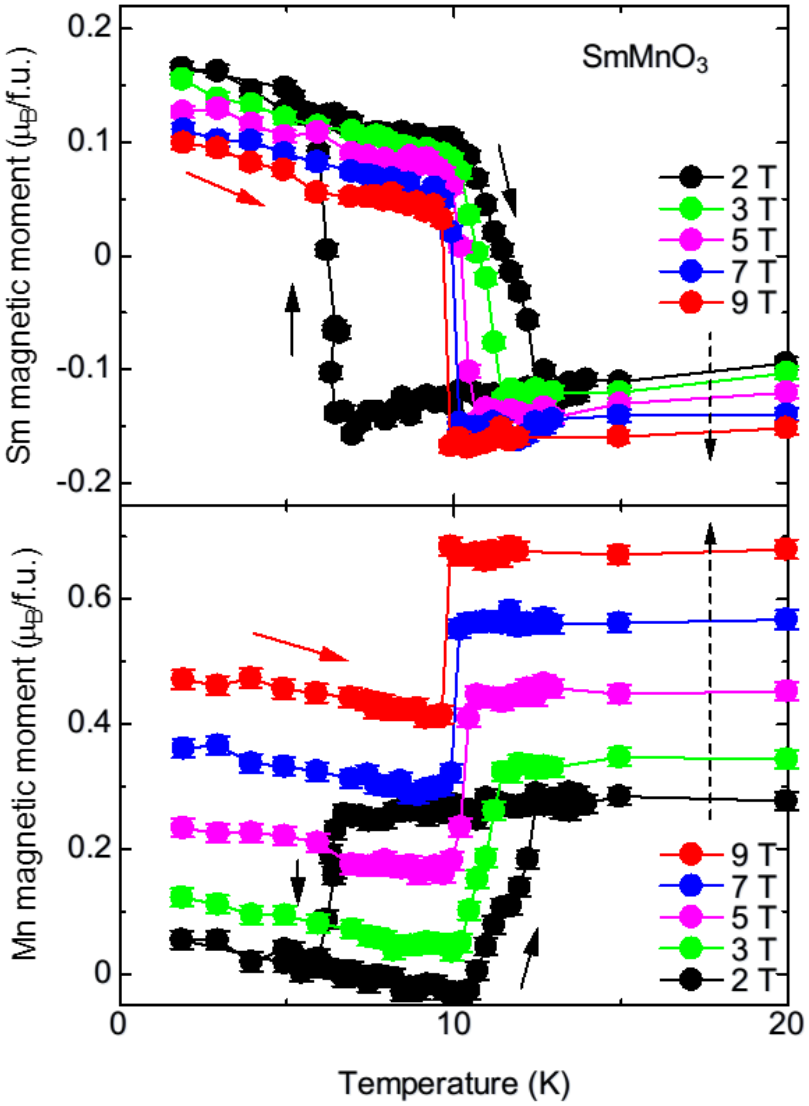

Figure 6-7: Enlarged view of Figure 6-6.

As in Figures 6-6 and 6-7, above 10 K, the Mn moments M_{Mn} increase by increasing H as expected, and the Sm moments M_{Sm} are negative which is consistent with the fact that this material is ferrimagnetic showing T-induced M reversal. At around T_{comp}, a sudden change in Sm and Mn magnetic moments was clearly observed. As lowering T, M_{Sm} become positive from negative and M_{Mn} drops, which is also consistent with the previous considerations [1-3].

6.5 Discussion

From the neutron scattering experiments with polarized hot neutrons, T profiles of M_{Sm} and M_{Mn} were obtained. First, let us compare the result with a bulk measurement.

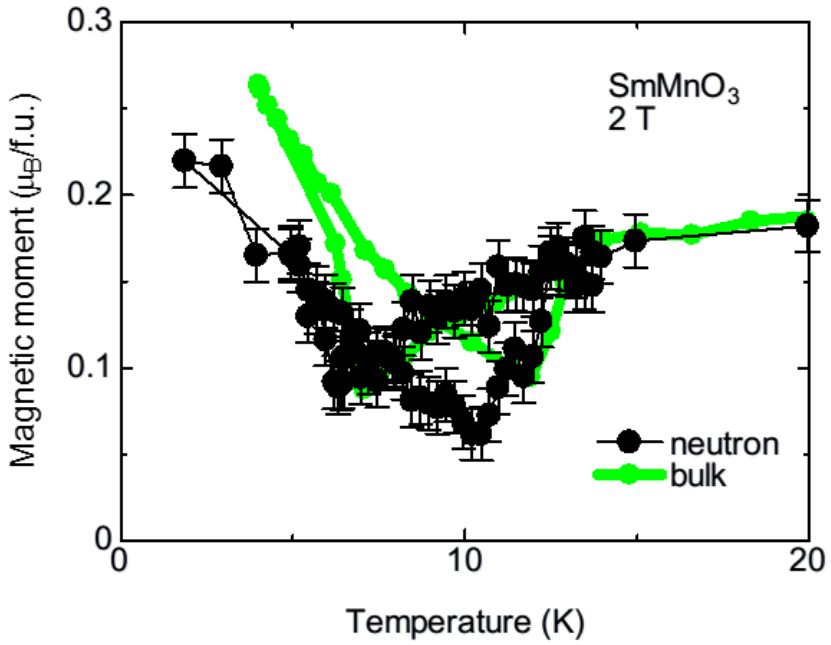

Figure 6-8: Temperature dependence of magnetization obtained from a bulk measurement and neutron scattering experiment. The bulk magnetization is drawn from [1].

Figure 6-8 represents T-dependence of magnetization M obtained from a bulk measurement and neutron scattering experiment ($M_{Sm} + M_{Mn}$). The T-dependence is fairly consistent with the bulk M. Consequently, it is concluded that the neutron scattering experiment faithfully detected the ferromagnetic component of the Sm and Mn moments along the c axis.

Next, because the Mn contribution was successfully separated from the Sm contribution, canting angles of the Mn moments are estimated from the result in Figure 6-6. Assuming that Mn^{3+} has a full moment of 4.899 μ_B, the canting angles θ are estimated to be

$$\vartheta = sin^{-1}(\frac{M_{Mn}}{4.899})$$

Then, the obtained result is plotted in Figure 6-9. As clearly seen in Figure 6-9, the canting angles of the Mn magnetic moments suddenly change in the vicinity of T_{comp} in H, therefore, the abrupt change in the dielectric constant in H originates from the abrupt change in the canting angles which is consistent with the previous considerations [1-3].

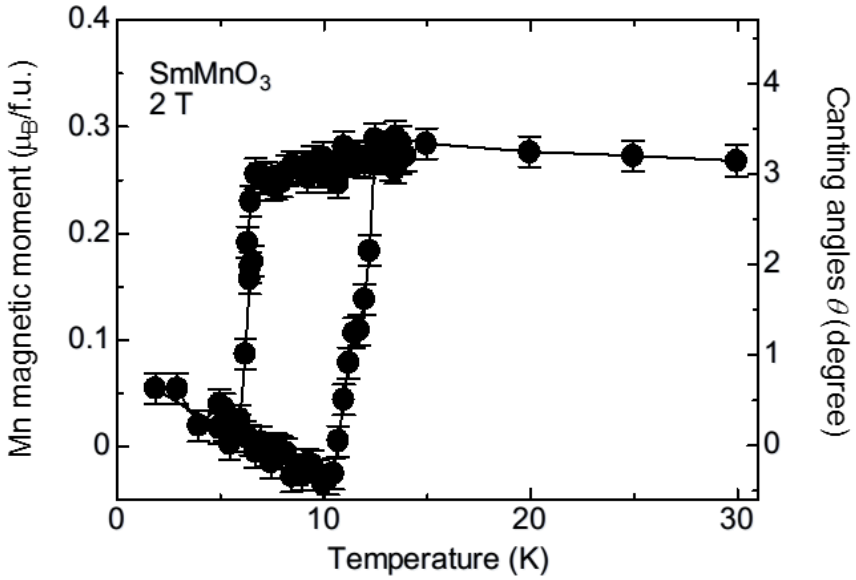

Figure 6-9: Estimation of temperature-dependence of the canting angles of Mn magnetic moments.

As an order of magnitude argument, the canting angles can be estimated by the ratio of exchange constant and the so-called D vector. Consider the exchange path along the c axis as in Figure 6-10. Antiferromagnetic exchange constant along the c axis was estimated by the first-principles calculation as J_c ~ 1.27 meV, and the D vector which causes canting towards the c axis was estimated to be 0.30 meV [12]. Then, the canting angles are estimated by the following equation.

$$tan\theta = \frac{D}{2J_c}$$

Consequently, θ is calculated to be 6.74° which is consistent as an order of magnitude with the experimental result.

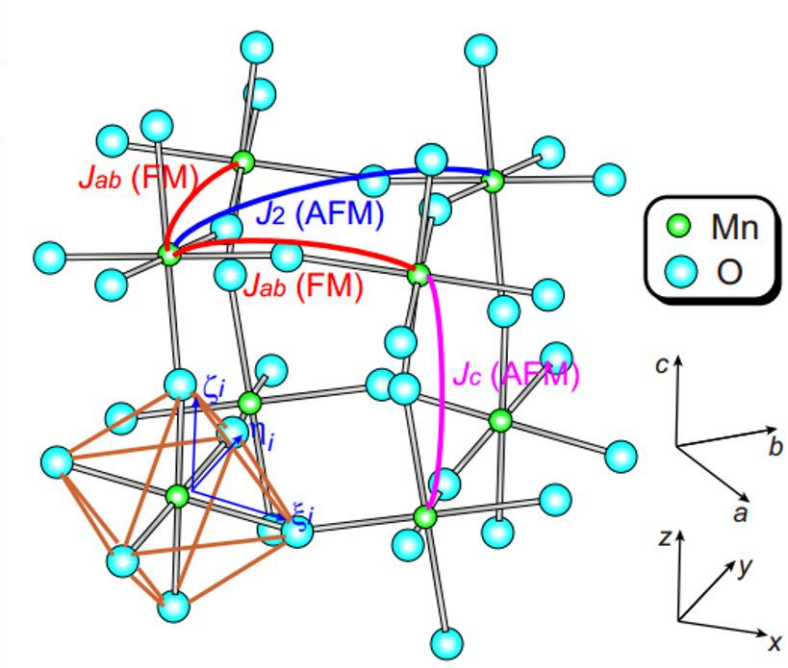

Figure 6-10: Crystal structure and exchange paths in RMnO$_3$ [12].

As for M_{Sm}, the absolute value is substantially smaller than 0.845 μ_B which is an effective moment in the ground state of isolated Sm^{3+}. This reduction of the moments has often been observed in 4*f* elements due to crystal-field effects. Furthermore, because the total angular momentum of Sm^{3+} is small, quantum effect is expected to be larger than other 4*f* elements except Eu^{3+}, which may be an additional factor for the reduction. As a matter of fact, modulus of Sm magnetic moment is frequently ~ 0.1 – 0.3 μ_B in materials containing Sm [13-15]. Note that the Sm magnetic moments obtained in this study are smaller than the value previously obtained by specific heat measurement ~ 0.36 μ_B [16]. However, neutron scattering experiment is a direct method to evaluate the magnetic moment, the experiment in this study is probably more accurate. Finally, M_{Sm} decreases by increasing H in both high-T and low-T phases as in Figures 6-6 and 6-7. At present, the origin is unclear and it is necessary to check whether this behavior is intrinsic or not.

In this way, it is concluded that the experimental results provide the correct information on the magnetic structure of SmMnO$_3$. According to the experiments, it is confirmed that as previously thought [1-3], the reversal of the Sm moments occurs at the transition point, and the magnetodielectric effect in this compound can be understood by considering the canting angles of Mn moments.

6.6 Summary

Crystal and magnetic structures in $SmMnO_3$ have been investigated by neutron scattering experiments with the use of hot neutrons in order to suppress neutron absorption. The crystal structure is in good agreement with previous studies. An antiferromagnetic order of the Mn moments was observed in zero-field experiment. However, Mn weakly ferromagnetic component was not detected. With polarized hot neutrons, the weakly ferromagnetic component of the Mn moments and the polarized Sm moments were clearly observed by measuring flipping ratios in a magnetic field. It is concluded that the first-order-like transition comes from the reversal of the Sm moments and the drop of the weakly ferromagnetic Mn moments in a magnetic field. The magnetodielectric effect can be understood as previously thought by considering the canting angles of the Mn moments. This work suggests that neutron scattering experiment with hot neutrons is a powerful means and can be applicable to other materials even including large absorber of neutrons.

Acknowledgements

The author thanks G. Nénert, L. C. Chapon, and T. Aoyama for their help in experiments.

References

[1] J.-S. Jung, A. Iyama, H. Nakamura, M. Mizumaki, N. Kawamura, Y. Wakabayashi, and T. Kimura, Phys. Rev. B **82**, 212403 (2010).

[2] A. Iyama, J.-S. Jung, E. S. Choi, J. Hwang, and T. Kimura, J. Phys. Soc. Jpn. **81**, 013703 (2012).

[3] J.-S. Jung, A. Iyama, H. Nakamura, Y. Wakabayashi, and T. Kimura, Phys. Rev. B **85**, 174414 (2012).

[4] V. Yu Ivanov, A. A. Mukhin, A. S. Prokhorov, and A. M. Balbashov, Phys. Stat. Sol. (b) **236**, 445 (2003).

[5] V. Skumryev, F. Ott, J. M. D. Coey, A. Anane, J.-P. Renard, L. P.-Gaudart, and A. Revcolevschi, Eur. Phys. J. B **11**, 401 (1999).

[6] J. Stöhr, J. Magn. Magn. Mater. **200**, 470 (1999).

[7] T. Koide, H. Miyauchi, J. Okamoto, T. Shidara, T. Sekine, T. Saitoh, A. Fujimori, H. Fukutani, M. Takano, Y. Takeda, Phys. Rev. Lett. **87**, 246404 (2001).

[8] T. Mori, N. Kamegashira, K. Aoki, T. Shishido, and T. Fukuda, Mater. Lett. **54**, 238 (2002).

[9] D. O'Flynn, C. V. Tomy, M. R. Lees, A. D.-Aladine, and G. Balakrishnan, Phys. Rev. B **83**, 174426 (2011).

[10] H. Maeda, Y. Ishiguro, T. Honda, J.-S. Jung, S. Michimura, T. Imai, T. Kimura, and Y. Wakabayashi, J. Ceram. Soc. Jpn. **121**, 265 (2013).

[11] F. Moussa, M. Hennion, J. R.-Carvajal, H. Moudden, L. Pinsard, and A. Revcolevschi, Phys. Rev. B **54**, 15149 (1996).

[12] M. Mochizuki and H. Furukawa, Phys. Rev. B **80**, 134416 (2009).

[13] K. H. J. Buschow, A. M. van Diepen, and H. W. de Wijn, Phys. Rev. B **8**, 5134 (1973).

[14] J.-X. Boucherle, F. Givord, J. Schweizer, A. Gukasov, J.-M. Mignot, E. L.-Berna, H. Aoki, and A. Ochiai, Physica B **281&282**, 139 (2000).

[15] J. Pospíšil, G. Nénert, S. Miyashita, H. Kitazawa, Y. Skourski, M. Diviš, J. Prokleška, and V. Sechovský, Phys. Rev. B **87**, 214405 (2013).

[16] L. G. Marshall, J.-G. Cheng, J.-S. Zhou, J. B. Goodenough, J.-Q. Yan, and D. G. Mandrus, Phys. Rev. B **86**, 064417 (2012).

Chapter 7 Conclusion

One of the purposes of this study is to investigate not only electric polarization or magnetization but also dielectric constant in the linear magnetoelectric (ME) coupling, and clarify the relation between the linear ME effect and ME multiferroics. First, by studying the most famous linear ME compound Cr_2O_3, it has been revealed that Cr_2O_3 behaves as a ferroelectric (ferromagnet) in a magnetic (electric) field because of the observation of not only *P*-*E* (*M*-*H*) hysteresis curves but also a divergence-type anomaly in the dielectric constant at the transition point. By symmetry consideration, it has been clarified that the in-field ferroelectric behavior in Cr_2O_3 can be understood in the same way with pseudo-proper ferroelectric $TbMnO_3$. Second, the linear ME effect in $FeSb_2O_4$ has been revisited by investigating the ME property with single crystalline samples grown by the hydrothermal method for the first time. It has been observed that the dielectric constant shows a divergence-type anomaly at the transition point and an electric polarization arises below the transition temperature in a magnetic field, as observed in Cr_2O_3. Furthermore, the magnetic symmetry in $FeSb_2O_4$ allows the spontaneous electric polarization by the spin ordering, however, it has not been observed experimentally. These results can be understood by considering the peculiar quasi-one-dimensional crystal structure of this compound.

The other purpose of this study is to further study the unusual magnetodielectric effect in $SmMnO_3$. Thus, high-field investigation and neutron scattering experiment have been carried out. In the high-field study up to 35 T, it has been observed that the dielectric constant behaves in a similar way between low-field and high-field, however, the magnetization in high field behaves differently from that in low field. This behavior in the magnetization can be understood by an evidence that the internal field by the Sm-Mn antiferromagnetic interaction is ~ 15 T, and thus the Sm moments become parallel to the net Mn moments in a high magnetic field larger than the internal field. It has been indicated that the origin of the first-order-like transition may not be just the Zeeman effect. Then, the deduced magnetic structure has been confirmed by means of neutron scattering experiment with the use of hot neutrons to suppress neutron absorption by natural isotope of Sm. By using polarized hot neutrons, temperature dependence of weakly ferromagnetic Mn moments and polarized Sm moments have been measured with the reasonable absolute magnitudes. Therefore, the magnetodielectric effect in this compound can be understood by considering canting angles of Mn moments as previously discussed.

Acknowledgement

This thesis has never been achieved without a lot of supports. First of all, I feel truly grateful to Prof. T. Kimura for giving me the opportunity to pursue my PhD within his group. His incredibly deep insights and considerate teaching have been indispensable for me to qualify as a PhD and to keep studying physics in the future. I thank Associate Prof. Y. Wakabayashi especially for his supports on diffraction experiments in this thesis. His supports have enabled me to be confident in the results obtained by x-ray and neutron diffraction techniques. I also thank Assistant Prof. H. Nakamura and K. Kimura for their inspiring discussions. Their openhearted discussions on the ideas about physics have been attractive and stimulating.

I thank Dr. E. S. Choi, Dr. J. Hwang, Dr. T. Tokumoto, and Prof. Y. Takano for their help during my stay in Florida, USA. I also thank financial supports from Global COE Program led by Prof. Kitaoka. I appreciate all the members and secretaries in Kimura Lab. and Mr. N. Moritsch for his proofreading and teaching of English presentation.

Finally, I express my sincere gratitude to my family, especially my parents and my wife for all the supports.

Publication list

[1] “Magnetocapacitive effects in the Neel N-type ferrimagnet $SmMnO_3$”
J.-S. Jung, A. Iyama, H. Nakamura, M. Mizumaki, N. Kawamura, Y. Wakabayashi, and T. Kimura,
Phys. Rev. B **82**, 212403 (2010).

[2] “High-Magnetic-Field Effect on Interplay between Sm 4f and Mn 3d Moments in $SmMnO_3$”
A. Iyama, J.-S. Jung, E. S. Choi, J. Hwang, and T. Kimura,
J. Phys. Soc. Jpn. **81**, 013703 (2012).

[3] “Lattice distortion accompanied by magnetization reversal in A-type antiferromagnetic manganites”
J.-S. Jung, A. Iyama, H. Nakamura, Y. Wakabayashi, and T. Kimura,
Phys. Rev. B **85**, 174414 (2012).

[4] “Magnetoelectric hysteresis loops in Cr_2O_3 at room temperature”
A. Iyama and T. Kimura,
Phys. Rev. B **87**, 180408(R) (2013).

[5] “The Magnetoelectric Effect in $FeSb_2O_4$ Single Crystals”
A. Iyama, Y. Wakabayashi, N. Hanasaki, and T. Kimura,
To be published in Jpn. J. Appl. Phys. (2014).